A GEOLOGICAL EVALUATION OF DISTINCT INTRUSION-RELATED MINERALIZATION STYLES AT THE ÇUBUKLU PROSPECT (YAHYALI, CENTRAL ANATOLIA)

A THESIS SUBMITTED TO
THE GRADUATE SCHOOL OF NATURAL AND APPLIED SCIENCES
OF
MIDDLE EAST TECHNICAL UNIVERSITY

BY

MÜGE GÜRGEN

IN PARTIAL FULFILLMENT OF THE REQUIREMENTS
FOR
THE DEGREE OF MASTER OF SCIENCE
IN
GEOLOGICAL ENGINEERING

JANUARY 2024

Approval of the thesis:

A GEOLOGICAL EVALUATION OF DISTINCT INTRUSION-RELATED MINERALIZATION STYLES AT THE ÇUBUKLU PROSPECT (YAHYALI, CENTRAL ANATOLIA)

submitted by **MÜGE GÜRGEN** in partial fulfillment of the requirements for the degree of **Master of Science** i**n Geological Engineering, Middle East Technical University** by,

Prof. Dr. Halil Kalıpçılar
Dean, **Graduate School of Natural and Applied Sciences** _____

Prof. Dr. Erdin Bozkurt
Head of the Department, **Geological Engineering** _____

Assist. Prof. Dr. Ali İmer
Supervisor, **Geological Engineering, METU** _____

Examining Committee Members:

Prof. Dr. Kaan Sayıt
Geological Eng, METU _____

Assist. Prof. Dr. Ali İmer
Geological Eng, METU _____

Assoc. Prof. Dr. Fatma Toksoy Köksal
Geological Eng, METU _____

Assoc. Prof. Dr. Sinan Akıska
Geological Eng, Ankara University _____

Assist. Prof. Dr. Erkan Yılmazer
Geological Eng, Aksaray University _____

Date: 25.01.2024

I hereby declare that all information in this document has been obtained and presented in accordance with academic rules and ethical conduct. I also declare that, as required by these rules and conduct, I have fully cited and referenced all material and results that are not original to this work.

Name Last name : Müge Gürgen

Signature :

ABSTRACT

A GEOLOGICAL EVALUATION OF DISTINCT INTRUSION-RELATED MINERALIZATION STYLES AT THE ÇUBUKLU PROSPECT (YAHYALI, CENTRAL ANATOLIA)

Gürgen, Müge
Master of Science, Geological Engineering
Supervisor: Assist. Prof. Dr. Ali İmer

January 2024, 129 pages

The Çubuklu prospect is situated within the Yahyalı Nappe of the Taurides in Central Anatolia. At Çubuklu, Paleozoic-Mesozoic carbonate rocks have been intruded by the Eocene Karamadazı Granitoid, which resulted in formation of distinct intrusion-related mineralization styles.

The NE part of the study area comprises porphyry Cu-Mo mineralization centered around a granodiorite porphyry intrusion. Porphyry mineralization is observed in a narrow zone of potassic alteration comprising secondary biotite and lesser K-feldspar. Chalcopyrite, molybdenite, and pyrite occurs either as weak disseminations or along sheeted B-type quartz-sulfide veinlets. The adjacent Cu-Fe skarn mineralization extends farther towards SW along narrow dikes and occurs within dolomitic carbonates dominated by magnesian exoskarn comprising forsterite-serpentinite-chlorite-calcite. Rare calcic exoskarn and endoskarn are characterized by garnet-pyroxene-chlorite-epidote-carbonate. The SW part of the study area contains carbonate-replacement Pb-Zn ores, which have been mostly oxidized into

secondary Pb-Zn minerals. Where preserved, sulfidic ore contains abundant pyrite alongside sphalerite, chalcopyrite, lesser tetrahedrite, covellite, and galena. Carbonate-replacement ores are best developed in organic-rich carbonate rocks, which have undergone intense dolomitization and silicification.

The spatial distribution of mineralization types as well as metal zonation at Çubuklu are mainly controlled by the architecture of the igneous system and the nature of the wall-rocks. Porphyry Cu-Mo mineralization is associated with the core of the igneous complex in the NE, and transitions first into proximal Fe-Cu skarn and later into stratabound Pb-Zn mineralization towards SW. Recognition of a porphyry-system at Çubuklu bears significant importance for porphyry prospectivity for the Karamadazı district, as well as potential porphyry fertility of other Eocene magmatic systems in south Central Anatolia.

Keywords: Karamadazı, Eocene magmatism, Porphyry, Skarn

ÖZ

ÇUBUKLU PROSPEKTİNDE (YAHYALI, ORTA ANADOLU) SOKULUMLA İLİŞKİLİ FARKLI CEVHERLEŞME TİPLERİNİN JEOLOJİK BİR DEĞERLENDİRMESİ

Gürgen, Müge
Yüksek Lisans, Jeoloji Mühendisliği
Tez Yöneticisi: Dr.Öğr. Üyesi Ali İmer

Ocak 2024, 129 sayfa

Çubuklu prospekti Orta Anadolu'da, Toroslara ait Yahyalı Napı içerisinde yer alır. Çubuklu'da Paleozoyik-Mesozoyik karbonat kayaçların içerisine Eosen yaşlı Karamadazı Granitoyidi'nin yerleşmesi sonucunda farklı tipte sokulumla-ilişkili farklı tipte cevherleşmeler ortaya çıkmıştır.

Çalışma alanının KD'sunda bulunan porfiri Cu-Mo cevherleşmesi bir granodiyorit porfiri sokulumunun çevresinde gelişmiştir. Burada porfiri cevherleşmesi ikincil biyotit ve K-feldspat ile temsil edilen dar bir potasik alterasyon zonunun içerisinde gözlenmektedir. Kalkopirit, molibdenit ve pirit zayıf saçınımlar halinde veya birbirine paralel B-tipi kuvars-sülfit damarları boyunca yer alır. Cu-Fe skarn cevherleşmesi porfiri sistemiyle yan yana gelişmiş olup dayk zonları boyunca GB'ya doğru uzanmaktadır. Dolomitik karbonatlarda bulunan magnezyen ekzoskarn ağırlıklı olarak forsterit-serpantinit-klorit-kalsit içermektedir. Daha ender gözlenen kalsik ekzoskarn ve endoskarn ise granat-piroksen-klorit-epidot-karbonat ile karakterizedir. Çalışma alanının GB'sı genelde ikincil Pb-Zn minerallerine

oksitlenmiş karbonat-ornatma-tipi Pb-Zn cevherleşmesi içermektedir. Korunan sülfitli cevherde çokça pirit ile sfalerit, kalkopirit ve daha az tetrahedrit, kovelin ve galen gözlenmektedir. Karbonat-ornatma tip cevherleşme yoğun dolomitleşme ve silisleşmeye maruz kalmış organikçe-zengin karbonat birimleri içerisinde gelişmiştir.

Çubuklu sahasında cevherleşmelerin konumsal dağılımı ile metal zonlanması temelde magmatik sistemin yapısı ve cevher yankayacının kimyası tarafından kontrol edilmektedir. Porfiri Cu-Mo cevherleşmesi KD'da magmatik kompleksin merkeziyle ilişkili olup GB'ya doğru önce Fe-Cu skarn ve daha sonra stratigrafik olarak sınırlı Pb-Zn cevherleşmesine geçiş yapmaktadır. Çubuklu'daki porfiri keşfi Karamadazı bölgesinde porfiri aramacılığı çalışmaları ve ayrıca Orta Anadolu'nun güneyindeki diğer Eosen yaşlı magmatiklerin porfiri üretkenliği açısından büyük önem taşımaktadır.

Anahtar Kelimeler: Karamadazı, Porfiri, Eosen magmatizma, Skarn

ACKNOWLEDGMENTS

I would like to express my deepest appreciation to my supervisor, Assist. Prof. Dr. Ali İmer, for his mentorship, constructive criticism, and advice, as well as for his insightful suggestions and invaluable contributions at every step of this study.

I extend my sincere thanks to my defense committee for generously sharing their knowledge and expertise. Additionally, I am grateful to Dr. Mustafa Yücel Kaya for providing background petrographic knowledge on carbonate rocks.

I am deeply thankful to Centerra Madencilik A.Ş for both their moral and financial support, which has made this study possible. I express my appreciation to Exploration Manager Tolga Tosun for his unwavering support, Principal Geologist Deniz Can Serçe for sharing his expertise, and GIS Geologist İrem Çakır for her assistance and emotional support.

I am extremely grateful to İrem Işık and Barış Can Baysal for their invaluable assistance, unwavering moral support, encouragement, and belief in me that have kept my spirits and motivation high from the beginning to the end of this journey.

Special thanks to Göksu Karataş, Atilla Kılıç, Taner Tekin, Melike Aslan, and Berivan Çelik for their practical suggestions, helpful advice, alongside providing entertainment and emotional support.

I want to express my deepest appreciation to my family for their encouragement, which has been instrumental in motivating me to overcome challenges throughout my life.

TABLE OF CONTENTS

ABSTRACT v

ÖZ vii

ACKNOWLEDGMENTS ix

TABLE OF CONTENTS x

LIST OF TABLES xii

LIST OF FIGURES xiii

CHAPTERS

1 INTRODUCTION 1

1.1 Purpose and Scope 1

1.2 Methodology 3

1.3 Location of the Study Area 4

1.4 Overview of Intrusion-Related Base Metal Deposits 5

1.4.1 Porphyry Deposits 7

1.4.2 Skarn Deposits 8

1.4.3 Carbonate Replacement Deposits 10

2 LITERATURE REVIEW 11

2.1 Regional Setting 11

2.1.1 Geodynamic/Tectonic Evolution of Anatolide-Taurides 12

2.1.2 Geology of the Karamadazı District 21

3 GEOLOGY OF ÇUBUKLU DISTRICT 29

3.1 Carboniferous Metamorphic Rocks 32

3.2 Paleozoic Mesozoic Carbonate Rocks 34

3.3 Eocene Karamadazı Granitoid 38

3.4 Quaternary Cover Unit 44
3.5 Structure 45
4 ALTERATION AND MINERALIZATION STYLES AT ÇUBUKLU 49
4.1 Skarn-Type Alteration and Mineralization 57
4.1.1 Endoskarn 59
4.1.2 Exoskarn 62
4.2 Carbonate-Replacement-Style Alteration and Mineralization 73
4.3 Porphyry-Style Alteration and Mineralization 84
4.3.1 Re-Os Molybdenite Geochronology 93
5 DISCUSSION AND CONCLUSION 95
5.1 Discussion 95
5.1.1 Formation of Skarn-Type Alteration and Mineralization 95
5.1.2 Metal Zonation 98
5.1.3 Regional Significance 99
5.2 Conclusion 106
REFERENCES 109

LIST OF TABLES

TABLES

Table 1. Significant intercepts of drill hole: PSD-6. 71
Table 2. Significant intercepts of drill hole: PSD-16. 78
Table 3. Significant intercepts of drill hole: PSD-14. 83
Table 4. Significant intercepts of drill hole: PSD-8. 90
Table 5. The result of the Re-Os geochronology (drill hole: PSD-8, from 166.70 m). 93
Table 6. Summary of the Eocene magmatism associated deposits and prospects in Eastern and Central Anatolia. 104

LIST OF FIGURES

FIGURES

Figure 1.1. a) Eastern Anatolia geological map showing Cretaceous ophiolite, Cretaceous to Eocene plutonic and volcanic complexes, Paleozoic to Mesozoic basement and Tertiary sedimentary and/or volcanic cover represented by white areas (modified after MTA, 1989; Bozkurt, 2001; İmer et al., 2013), b) The major tectonic units of Turkey (modified after Okan and Tüysüz, 1999; İmer et al., 2013). Abbreviations: Bornova Flysch Zone, BSZ=Bitlis Suture Zone, CAFZ=Central Anatolian Fault Zone, CATB=Central Anatolian Thrust Belt, DFZ=Dumlu Fault Zone, DSFZ=Dead Sea Fault Zone, EAFZ=East Anatolian Fault Zone, GYFZ=Göksu–Yazyurdu Fault Zone; İAESZ=İzmir–Ankara–Erzincan Suture Zone, IPSZ=Intra-Pontide Suture Zone, MOFZ=Malatya–Ovacık Fault Zone, NAFZ=North Anatolian Fault Zone, NEAFZ=North East Anatolian Fault Zone.... 2
Figure 1.2. Location map of the Çubuklu prospect in Yahyalı District, Central Anatolia (retrieved from Google Earth). 5
Figure 1.3. The model of porphyry Cu system that illustrates spatial association of central porphyry Cu (± Au ± Mo) deposit in a multiphase intrusion stock and proximal and distal skarn, carbonate-replacement, and sediment-hosted deposits (modified from Sillitoe, 1995, 1999, 2000, 2010). 7
Figure 1.4. The formation of intrusion-related skarn deposits as result of prograde stage (a) and retrograde stage (b) (Corbett and Leach, 1998; Robb, 2005). 9
Figure 2.1. The tectonic map illustrating continental blocks and major sutures of Anatolia and the surrounding regions (Okay and Tüysüz, 1999). 12
Figure 2.2. The major geological features of Central Anatolia including Karamadazı region, situated within the Yahyalı metamorphics and bounded by the Ecemiş Fault (modified after Radwany et al., 2017) 16
Figure 2.3. Map showing the main units of the Aladağ region to the east of the Ecemiş Fault (after Tekeli et al., 1984). 20

Figure 2.4. The location and regional geologic map of Karamadazı Area modified from Ulakoğlu (1983) after Kuşcu et al. (2001). 22
Figure 2.5. The generalized stratigraphic columnar section of Karamadazı area simplified after Ulakoğlu (1983). 23
Figure 3.1. Map showing the study area (Postallı Madencilik license), located nearly 11 km northwest of Yahyalı Town. The boundaries of the Postallı license are highlighted in red. 30
Figure 3.2. Geological map of the Çubuklu prospect showing distribution of main lithological units, structures, and the locations of the Postallı underground galleries. 31
Figure 3.3. a) Outcrop photograph of chlorite-calcite schist, b) Microphotograph (PPL, TL image) of deformed chlorite layers, c) Microphotograph of (XPL, TL image) sericite-chlorite layer and fine to coarse grains of calcite. Abbreviations: chl = chlorite, ser = sericite, ca = calcite, XPL = cross-polarized light, PPL = plane-polarized light, TL = transmitted light. 33
Figure 3.4. Drill core photograph of black limestone with clay and silt interlayers (drill hole: PSD-16, from 110.40 m to 114.20 m), b) Macrophotograph of black limestone (drill hole: PSD-16, from 111.50 m), c) Microphotograph (XPL, TL image) of elongated interlayers of dolomite and organic matter (drill hole: PSD-16, from 111.50 m). Abbreviations: dol=dolomite, XPL= cross-polarized light, TL = transmitted light. 35
Figure 3.5. Outcrop photograph showing an alternating sequence of gray and black limestone in the Keybet Hill. Organic- and clay-rich layers display a recessive topography compared to gray limestones. Minor strike-slip fault offsets of a few meters can be traced through this sequence. 36
Figure 3.6. Drill core photograph of clast-supported breccia composed of angular to subangular black limestone clasts with calcite matrix (drill hole: PSD-16, from 152.00 to 155.70 m) 37
Figure 3.7. a) Macrophotograph of fine- to coarse-grained, clast-supported, monomictic conglomerate with calcite-smithsonite matrix (drill hole: PSD-16, from

228.30 m), b) Microphotograph (XPL, TL image) of calcite matrix and micritic limestone clasts (drill hole: PSD-16, from 228.30 m). Abbreviations: ca = calcite, mtc = micritic limestone, XPL= cross-polarized light, TL = transmitted light. 37
Figure 3.8. Ground magnetic map of the Çubuklu license (reduced to pole magnetic anomaly map), red lines and black dashed lines represent tenement boundaries and magnetic-high zones, respectively. 39
Figure 3.9. Outcrop photograph of the faulted contact between limestone and weathered intrusion from a) dike exposed at northeast part of the tenement b) stock covering southwestern part of the study area. 40
Figure 3.10. a) Drill core photograph of granodiorite porphyry (drill hole: PSD-6, from 78.50 m), b) Microphotograph (XPL, TL image) of clay-altered plagioclase, chloritized hornblende, quartz and epidote (drill hole: PSD-6, from 78.50 m), c) Drill core photograph of quartz diorite (drill hole: PSD-6, from 154.70 m), d) Microphotograph of (XPL, TL image) fine to coarse grained sericite altered plagioclase, chloritized biotite, and quartz (drill hole: PSD-6, from 154.70 m), e) Drill core photograph of dacite porphyry (drill hole: PSD-16, from 535.80 m), f) Microphotograph (XPL, TL image) of coarse quartz and biotite phenocrystals in fine grained groundmass (drill hole: PSD-16, from 535.80 m), g) Drill core photograph of andesitic dike (drill hole: PSD-6, from 85.50 m), h) Microphotograph (XPL, TL image) of plagioclase phenocryst replaced by chlorite in chloritized groundmass (drill hole: PSD-6, from 85.50 m). Abbreviations: qtz = quartz, bio = biotite, ep =e pidote, plg = plagioclase, hb = hornblende, ser = sericite, chl = chlorite, cl = clay, XPL= cross-polarized light, TL = transmitted light. 43
Figure 3.11. Transition between the Quaternary alluvium and the underlying granodiorite porphyry (drill hole: PSD-8; 105.70 to 111.20 m). 45
Figure 3.12. a) Outcrop photograph of strongly-deformed limestone with fracture-fill limonite and calcite, b) Microphotograph (XPL, TL image) of micritic limestone including fine-grained quartz cut by late, fine-grained calcite veinlets. Opaque minerals are possibly pyrite or Fe-oxides formed after pyrite.

Abbreviations: ca = calcite, mtc = micritic limestone, XPL= cross-polarized light, TL = transmitted light. 46
Figure 3.13. a) Outcrop photograph of cream, pale white marble with whitish sugary-textured, coarse-grained calcite bands, b) Microphotograph (XPL, TL image) of fine- to medium-grained, foliated calcite cut by late, narrow calcite veinlets and quartz. Abbreviations: ca = calcite, qtz = quartz, XPL= cross-polarized light, TL = transmitted light. 47
Figure 3.14. a) Drill core photograph of gray, yellowish brown, fine to coarse grained, polymictic, clast supported, fault breccia with carbonate matrix, strongly silicified gray limestone, calcite clasts, and limonite veinlets (drill hole: PSD-16 from 460.80 m) b) Microphotograph of (XPL, TL image) angular to subangular dolomitic clast surrounded by deformed dolomite matrix (drill hole: PSD-16 from 460.80 m). Abbreviations: dol = dolomite, XPL= cross-polarized light, TL = transmitted light.. 48
Figure 4.1. a) Outcrop photograph of carbonate hosted irregular zones of secondary ore minerals in the NE part of study area b) The close-up photograph of malachite-limonite-goethite mineralization (from 698344E, 4225954N, UTM Zone 36S), c) smithsonite float, d) Goethite, hematite, limonite and zincite development at the NE part of the study area. 50
Figure 4.2. Geological map of the Çubuklu prospect showing rock sampling locations and associated Cu grades (in ppm). 51
Figure 4.3. Geological map of the Çubuklu prospect showing rock sampling locations and associated Zn grades (in ppm). 52
Figure 4.4. Geological map of the Çubuklu prospect showing rock sampling locations and associated Pb grades (in ppm). 53
Figure 4.5. Soil geochemistry map of the Çubuklu prospect showing the distribution of a) Cu (in ppm), b) Mo (in ppm), c) Zn (in ppm), d) Pb (in ppm). ... 54
Figure 4.6. The map of Çubuklu license showing Cu-Fe skarn and Cu-Mo porphyry, and Pb-Zn carbonate replacement prospects on ground magnetic map

(reduced to pole magnetic anomaly map) and locations of drill holes and Potallı underground mines..... 56
Figure 4.7. a) Outcrop photograph of skarn zone near the intrusion-limestone contact (from 698177E, 4225954N, UTM Zone 36S), b) The macrophotograph of secondary Fe-(hydr)oxides with relict euhedral garnet largely retrograded into euhedral carbonates, c) Microphotograph (XPL, TL image) of coarse-grained calcite (up to 4 mm long) cut by a vein with dolomite (rhombohedral crystals) infill. Abbreviations: ca = calcite, XPL= cross-polarized light, TL = transmitted light. 58
Figure 4.8. a) Drill core photograph of gray tonalite porphyry cut by beige garnet-calcite vein (drill hole: PSD-20, 60.10 m) b) Microphotograph (XPL, TL image) of oscillatory-zoned garnet and radial prehnite (drill hole: PSD-20, 60.10 m), c) Microphotograph (XPL, TL image) of completely sericitized hornblende within a quartz-dominant groundmass alongside coarse-grained plagioclase and pyrite (opaque crystals) (drill hole: PSD-20, 60.10 m), d) Microphotograph (XPL, TL image) of fine- to coarse-grained, sericitized K-feldspar phenocrysts cut by a calcite veinlet, probable mafic minerals altered into epidote, cubic opaque minerals possible pyrite (drill hole: PSD-6, 125.80 m) Abbreviations: grt = garnet, prh = prehnite, hb = hornblende, plg = plagioclase, ep = epidote, ksp = K-feldspar, ser = sericite, ca = calcite, XPL= cross-polarized light, TL = transmitted light..... 60
Figure 4.9. a) Drill core photo of the endoskarn-exoskarn contact (PSD-6, from 57.70 m), b) Microphotograph (XPL, TL image) of coarse amphibole replaced by clinopyroxene, c) Microphotograph (XPL, TL image) of isotropic garnet I cut by anisotropic garnet II veinlet d) Microphotograph (PPL, TL image) of the contact between endoskarn and exoskarn zone), e) Microphotograph (XPL, TL image) of endoskarn-exoskarn transition. Abbreviations: amp = amphibole, grt = garnet, cpx = clinopyroxene, qtz = quartz, srp = serpentine, ca = calcite, XPL= cross-polarized light, TL = transmitted light, PPL = plane-polarized light. 61
Figure 4.10. a) Drill core photograph of black limestone cut by garnet-chlorite vein (drill hole: PSD-20, from 94.30 m), b) Microphotograph (XPL, TL image) of fine-

grained isotropic garnet, chlorite, and carbonate (drill hole: PSD-20, from 94.30 m), c) Drill core photograph of whitish cream marble with stockwork magnetite-pyrite veinlets (drill hole: PSD-6, from 370.50 m), d) Photomicrograph (XPL, TL) of interlocking, equigranular, fine-grained calcite cut by with opaques, and fine grained tremolite (drill hole: PSD-6, from 370.50 m) Abbreviations: grt = garnet, chl = chlorite, ca = calcite, tr = tremolite, PPL = plane-polarized light. 63
Figure 4.11. a) Drill core photograph of exoskarn rock (drill hole: PSD-6, from 60.60 m), b) Microphotograph (XPL, TL image) of serpentine exhibiting mesh texture, surrounded by fine grained calcite, and opaques composing of magnetite and sulfide (drill hole: PSD-6, from 60.60 m), c) Drill core photograph of banded exoskarn rock but by late calcite veinlets (drill hole: PSD-6, from 125.80 m), d) Microphotograph (XPL, TL image) of serpentine, surrounded by opaques composing of magnetite-sulfide cut by late calcite veinlets (drill hole: PSD-6, from 125.80 m). Abbreviations: ca = calcite, srp = serpentine, XPL= cross-polarized light, TL = transmitted light. 65
Figure 4.12. Core box photograph of exoskarn, marble, black limestone transition (drill hole: PSD-6, from 415.60 m to 422.50 m). 66
Figure 4.13. a) Drill core photograph of magnesian exoskarn rock (drill hole: PSD-6, from 56.60 m) b) Drill core photograph of calcic exoskarn rock (drill hole: PSD-6, from 105.10 m), c) Microphotograph (PPL, TL image) of serpentine and opaque minerals in magnesian skarn (drill hole: PSD-6, from 56.60 m) d) Microphotograph (XPL, TL image) of calcite veinlets in marble (drill hole: PSD-6, from 105.10 m), e) Microphotograph (XPL, RL image) of fine to medium grains of subhedral pyrite, cut by magnetite replacing serpentine, trace amount of chalcopyrite inclusion (drill hole: PSD-6, from 56.60 m), f) Microphotograph (XPL, RL image) of fine to medium subhedral to euhedral pyrite with tiny inclusion of chalcopyrite (drill hole: PSD-6, from 105.10 m). Abbreviations: ca = calcite, srp = serpentine, mt = magnetite, py = pyrite, cpy = chalcopyrite, XPL= cross-polarized light, PPL = plane-polarized light, TL = transmitted light, RL= reflected light. 67

Figure 4.14. a) Microphotographs (XPL, RL image) of (drill hole: PSD-6, from 370.50 m) a) Anhedral to subhedral pyrite, magnetite, and disseminated chalcopyrite, b) Chalcopyrite inclusions in pyrite Abbreviations: mt = magnetite, py = pyrite, cpy = chalcopyrite, XPL= cross-polarized light, RL= reflected light. 68
Figure 4.15. Microphotographs (XPL, RL image) of (drill hole: PSD-20, from 94.30 m), a) Fine disseminations of framboidal pyrite I crystal, b) Fine grained anhedral clusters pyrite II, and pyrite III exhibiting perfectly fine grains of euhedral crystals c) Fine grained anhedral clusters with trace amount of chalcopyrite as inclusions Abbreviations: cpy = chalcopyrite, py = pyrite, XPL= cross-polarized light, RL= reflected light..... 69
Figure 4.16. The paragenetic sequence of skarn-type alteration and mineralization at the Çubuklu prospect. 70
Figure 4.17. The downhole plot of PSD-6 representing Cu (ppm) and Fe (%) grades versus depth and rock type (GRD: granodiorite porphyry; MDI: monzodiorite; FZ: fault zone; Skarn: Exoskarn; MRBL: marble; BLST: black limestone)..... 72
Figure 4.18. Drill box photograph of polymictic breccia (drill hole: PSD-16, 167.00 to 171.00 m)..... 73
Figure 4.19. a) Drill core photograph of dolomitized, sulfidic breccia (drill hole PSD-16, from 168.50 m), b) Microphotograph (XPL, TL image) of angular dolomite clast surrounded by dolomite matrix with opaque minerals that are primarily pyrite (drill hole: PSD-16, from 168.50 m). Abbreviations: dol = dolomite, XPL= cross-polarized light, TL = transmitted light. 74
Figure 4.20. The downhole plot of drill hole PSD-16 representing Ca (%) and Mg (%) versus rock type and depth (DBx: Dolomite matrix breccia; FBx: Fault breccia; BLST: Black limestone; DA: dacite porphyry). 75
Figure 4.21. Microphotographs (XPL, RL image) of a) Fine grained pyrite dissemination in matrix , b) Sphalerite displaying chalcopyrite disease and pyrite inclusion, c) Coarse grains of euhedral to subhedral pyrite, sphalerite with chalcopyrite blebs, d) Tetrahedrite- chalcopyrite-pyrite replacement relation, e) Fine grained, deformed, pyrite clast with tetrahedrite and covellite replacement

after chalcopyrite, f) Dissemination of fine grained galena, and sphalerite with chalcopyrite blebs, coarser pyrite (drill hole: PSD-16, from 168.50 m). Abbreviations: py = pyrite, cpy = chalcopyrite, sph = sphalerite, ttr = tetrahedrite, ga = galena, cv = covellite, XPL= cross-polarized light, RL= reflected light.....77
Figure 4.22. The downhole plot of drill hole PSD-16 representing Ag (ppm), Pb (ppm), Zn (ppm) versus rock type and depth (DBx: Dolomite matrix breccia; FBx: Fault breccia; BLST: Black limestone; DA: dacite porphyry). 79
Figure 4.23. Drill core photograph showing a typical silica replacement zone in carbonate-replacement domain with secondary ore mineral assemblage of zincite, cerrusite, limonite and goethite (drill hole: PSD-14). 80
Figure 4.24. The downhole plot of drill hole PSD-14 representing Ca (%) and Mg (%) versus rock type and depth (SC: Silicified carbonate zone; DBx: Dolomite breccia; BLST: Black limestone). 81
Figure 4.25. The downhole plot representing Ag (ppm), Pb (ppm), Zn (ppm) versus rock type and depth (SC: Silicified carbonate zone; DBx: Dolomite breccia; BLST: Black limestone). 82
Figure 4.26. The paragenetic sequence of the Çubuklu carbonate replacement-type alteration and mineralization. 83
Figure 4.27. Location map showing drill hole: PSD-8 and its trace through the Sultansazlığı basin. 84
Figure 4.28. Hand specimen image (a) and photomicrographs (b–f) of porphyry-related alteration (drill hole PSD-8, 161.20 m). a) Fractured drill core sample of granodiorite porphyry with molybdenite coating, b) Sericite alteration on plagioclase phenocryst, surrounded by fine-grained hydrothermal quartz (XPL, TL image), c–d) Fine-grained aggregates of hydrothermal biotite, which was later altered into chlorite and actinolite (PPL and XPL images, respectively), e) Hydrothermal biotite, quartz, epidote, and relict plagioclase (XPL, TL image), f) Weakly sericitized plagioclase, along with possible K-feldspar domain (XPL, TL image). Abbreviations: act = actinolite, chl = chlorite, ep=epidote, qtz = quartz, ser

= sericite, bio = biotite, plg =plagioclase, Ksp = K-feldspar, TL = transmitted light, XPL= cross-polarized light, PPL = plane-polarized light..... 86
Figure 4.29. a) Core box showing 3.8 m-long section (drill hole: PSD-8, between 192.60 and 196.40 meters) of approximately 20 m-long faulted contact separating porphyry-altered granodiorite porphyry from Cu-Fe mineralized exoskarn, b) Drill core photograph showing representative Fe-Cu exoskarn zone..... 87
Figure 4.30. Drill core photographs of granodiorite porphyry with a) B-type quartz-molybdenite vein (drill hole: PSD-8, from147.60 m), b) B-type quartz vein with sulfide-bearing centerline (drill hole: PSD-8, from 138.00 m)..... 88
Figure 4.31. Drill core photographs showing fracture-coating of molybdenite ± pyrite ± chalcopyrite, at various depths in drill hole: PSD-8..... 88
Figure 4.32. Representative microphotographs (XPL, RL image) of porphyry-mineralized samples. a) Cluster of fine-grained, acicular molybdenite in granodiorite porphyry, b) Disseminated chalcopyrite and molybdenite, c) Disseminated pyrite partially replaced by chalcopyrite along fractures, d) Fine-grained magnetite partially oxidized into hematite. All images from sample 161.20m (drill hole: PSD-8). Abbreviations: cpy = chalcopyrite, mo = molybdenite, py = pyrite, mt = magnetite, XPL = cross-polarized light, RL= reflected light. 89
Figure 4.33. The paragenetic sequence of porphyry-style alteration and mineralization at Çubuklu prospect. 90
Figure 4.34. The downhole plot of drill hole PSD-08 showing the variation of Cu and Mo grades as well as Fe contents. Porphyry-mineralized granodiorite porphyry (GRD) interval ends at 174.80 meters, followed by a fault zone (FZ) and then Fe-Cu-mineralized skarn starting at 195 meters. 92

CHAPTER 1

INTRODUCTION

1.1 Purpose and Scope

Subduction-related magmatic systems, occurring intermittently in convergent, collisional, and post-collisional tectonic settings, may comprise significant volumes of calc-alkaline to alkaline magmas. Such magmas are generally regarded to be highly productive for forming various types of metallic ore deposits such as skarn, porphyry, epithermal, and iron oxide copper-gold systems (e.g., Mitchell, 1992; Camus and Dilles, 2001; Richards, 2005 and 2011; Blundell et al., 2005; Shafiei et al., 2009).

The subduction and closure of the southern branches of Neotethys ocean led to widespread Late Cretaceous to Eocene arc-related magmatic activity along eastern and central Anatolia (Yazgan and Chessex, 1991; Beyarslan and Bingöl, 2000; Agard et al., 2005; Robertson et al., 2007; Kuşcu et al., 2010 and 2013; Rolland et al., 2012). In regions where such magmas are particularly emplaced in the carbonate-dominated sequences of the Taurides, they produce magmatic-hydrothermal mineralization in and around intrusions, some of which may turn into economic deposits of base (e.g., Fe, Cu, Pb, Zn, and Mo) and precious (Au and Ag) metals. Several important mining districts such as Divriği/Hekimhan, Çöpler, Keban, and Yahyalı contain economic ores that have been developed around Late Cretaceous to Eocene intrusions emplaced in Tauride carbonates (Kuşcu et al., 2001, 2007, 2010, 2011, 2013, and 2019; İmer et al., 2013 and 2016; Yıldırım et al., 2019).

Within the Tauride belt, the significant deposits associated with Eocene magmatism are found in Çöpler and Bizmişen (Erzincan), Doğanşehir (Malatya), Yahyalı (Kayseri), and Horoz (Niğde) (Figure 1.1).

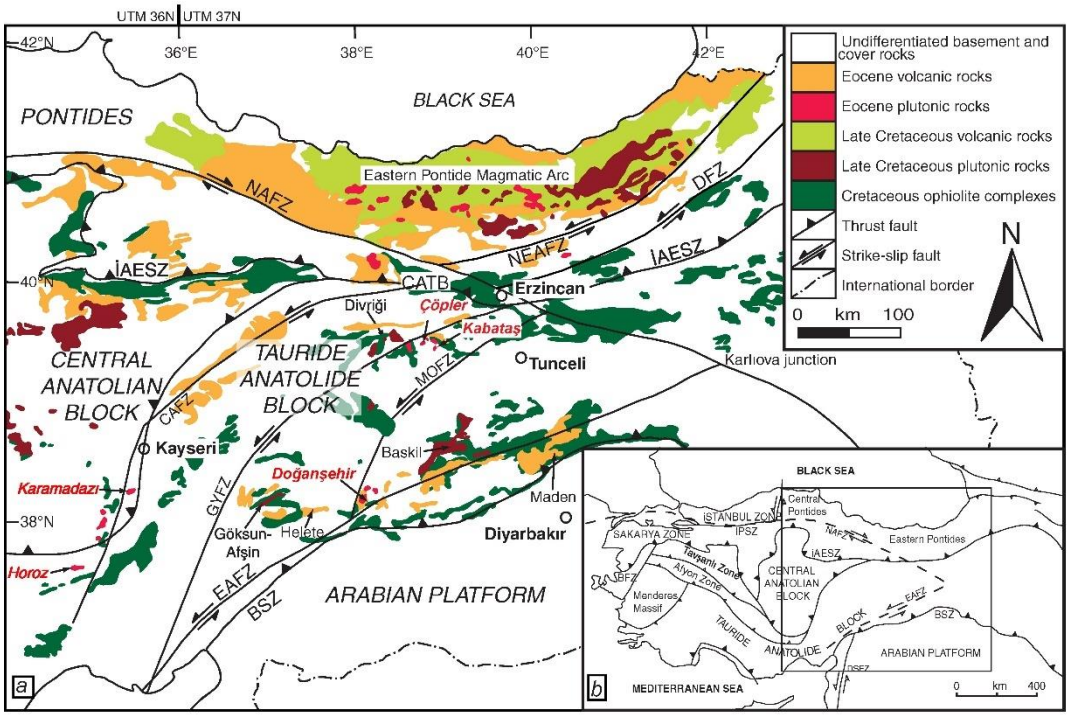


Figure 1.1. a) Eastern Anatolia geological map showing Cretaceous ophiolite, Cretaceous to Eocene plutonic and volcanic complexes, Paleozoic to Mesozoic basement and Tertiary sedimentary and/or volcanic cover represented by white areas (modified after MTA, 1989; Bozkurt, 2001; İmer et al., 2013), b) The major tectonic units of Turkey (modified after Okan and Tüysüz, 1999; İmer et al., 2013). Abbreviations: Bornova Flysch Zone, BSZ=Bitlis Suture Zone, CAFZ=Central Anatolian Fault Zone, CATB=Central Anatolian Thrust Belt, DFZ=Dumlu Fault Zone, DSFZ=Dead Sea Fault Zone, EAFZ=East Anatolian Fault Zone, GYFZ=Göksu–Yazyurdu Fault Zone; İAESZ=İzmir–Ankara–Erzincan Suture Zone, IPSZ=Intra-Pontide Suture Zone, MOFZ=Malatya–Ovacık Fault Zone, NAFZ=North Anatolian Fault Zone, NEAFZ=North East Anatolian Fault Zone.

The Karamadazı district in Yahyalı is a regionally important Fe-skarn deposit with reserves of 6.4 Mt at 54% Fe, formed between the contacts of Permian Akbaş Formation of Yahyalı Sequence and Eocene Karamadazı Granitoids (Oygür, 1986;

Kuşcu et al., 2001; Gençalioğlu-Kuşcu et al., 2001; Kuşcu et al., 2013). Furthermore, Aladağ region hosts numerous carbonate-hosted Zn-Pb deposits such as Aladağ with reserves of 0.437 Mt at 12.57% Zn and 6.67% Pb, and Ağcaşar with reserves of 0.265 Mt at 5.63% Zn, 3.71% Pb, plus minor Fe-skarn mineralization (Yiğit, 2009; Hanilçi and Öztürk, 2011).

The Çubuklu prospect (or the Postallı license) of Centerra Gold is a new target for potential Fe-Cu skarn and Pb-Zn carbonate-replacement mineralization located in the east of the Karamadazı Fe mine of Özkoyuncu Madencilik near Yahyalı. The Postallı license was originally acquired by a local mining company, Postallı Madencilik, in 2007. The company has five currently running underground operations from which Zn and Pb are being exploited, mainly from oxide ores. In 2021, Centerra Gold established an agreement with Postallı Madencilik to carry out further exploration activities in the Postallı license, especially targeting potential sulfide mineralization beneath the oxide zones.

This thesis study was carried out in the Çubuklu prospect and aims to answer the following research questions that have emerged during the framework of exploration studies at Çubuklu:

- What are the main mineralization types developed in and around felsic to intermediate composition intrusions at Çubuklu?
- What are the main alteration and mineralization characteristics in terms of distributions of ore zones, alteration styles, ore textures and minerals?
- What is the spatial distribution of distinct alteration and mineralization styles?

1.2 Methodology

Fieldwork was conducted at the Çubuklu prospect between 2021 and 2023 by Centerra Gold. This included outcrop mapping at a scale of 1:10.000 scale.

Additional fieldwork was carried out in May 2023 in order to collect outcrop and drill core samples for petrographic work. Quick-logging of four drill holes intersecting porphyry, skarn, and carbonate-replacement type alteration and mineralization was also completed.

Petrographic studies were carried out in order to identify rock types, alteration/mineralization types, and also to establish a simple ore paragenesis using thin sections and polished blocks. Samples were prepared at the laboratories of the Minerals Research and Exploration Institute of Turkey (MTA). A total of 48 thin sections were prepared from samples representing different lithologies and showing varying degrees of alteration. A further 15 polish blocks were prepared from samples showing various mineralization types as observed at the Çubuklu prospect. All samples were examined by a Nikon brand polarizing microscope in the Geological Engineering Department of the Middle East Technical University.

Molybdenite Re-Os dating was carried out on a sample from B-type quartz–sulfide vein within potassic altered granodiorite porphyry to determine the timing of porphyry-style mineralization at the Çubuklu prospect. Re-Os analyses were performed at the Activation Laboratories Ltd. (Ontario, Canada). The method involves isotope dilution mass spectrometry using Carius-tube, solvent extraction, anion chromatography and negative thermal ionization mass spectrometry techniques in order to determine ^{187}Re and ^{187}Os concentrations in molybdenite (Selby and Creaser, 2007). To conduct thic analysis, a mixed double spike containing known amounts of isotopically enriched ^{185}Re, ^{190}Os, and ^{188}Os analysis was used (Markey et al., 2007), where a Thermo Scientific Triton mass spectrometer by Faraday collector used for isotopic analysis.

1.3 Location of the Study Area

The study area, Çubuklu prospect (38°09′04.85″ N 35°14′59.85″ E), is located in the eastern part of the Çubuklu, which is a small neighborhood in the Yahyalı district of

Kayseri province in Central Türkiye. It is situated approximately 300 km southeast of the capital Ankara and about 65 km south of the city of Kayseri (Figure 1.2).



Figure 1.2. Location map of the Çubuklu prospect in Yahyalı District, Central Anatolia (retrieved from Google Earth).

1.4 Overview of Intrusion-Related Base Metal Deposits

Intrusion-related base and precious metal deposits form in and around intrusions emplaced within upper crustal levels. Such magmatic bodies may produce large volumes of saline fluids with significant amounts of base metals, and may subsequently form porphyry and skarn deposits as well as zones of carbonate-replacement ores within calcareous wall-rocks (Sinclair, 2007; Pirajno, 2009; Sillitoe, 2010).

As the most important resource of Cu and Mo, porphyry deposits usually occur on convergent margins above subduction zones and are associated with synchronous

calc-alkaline magmas (Sillitoe, 2000; Richards, 2003; Cooke et al., 2005; Seedorff et al., 2005). In many porphyry districts, a close spatial relationship exists between porphyry-style mineralization and other hydrothermal mineralization types including epithermal deposits, base and precious metal veins, skarn, and carbonate-replacement ores (Sillitoe, 1973; Meinert et al., 2005; Sillitoe, 2010).

Cu-Au-Mo porphyry systems are typically centered in and around intrusions, whereas proximal Cu-Au skarns form within carbonate rocks and associated occur proximal or distal base metal vein and replacement Zn, Pb, Cu, Ag, and Au mineralization (Figure 1.3) (Lang and Eastoe, 1988; Sillitoe, 1995, 1999, 2010; Catchpole et al., 2015). Therefore district-scale metal zonation from Cu-Mo through Zn-Pb to Ag-Au is generally included in the geochemical footprints of the porphyry systems (Emmons, 1927; Jones, 1992; Dilles and Einaudi, 1992; Babcock et al., 1995; Seedorff et al., 2005; Sillitoe, 2010).

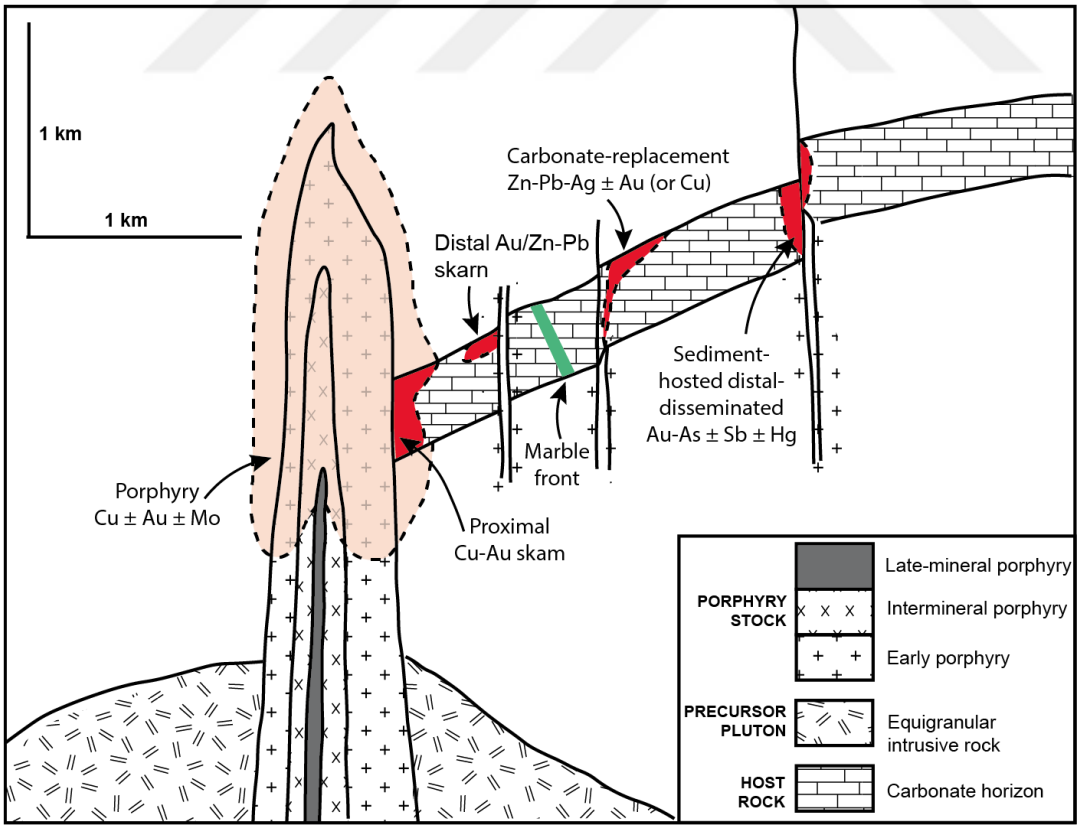


Figure 1.3. The model of porphyry Cu system that illustrates spatial association of central porphyry Cu (± Au ± Mo) deposit in a multiphase intrusion stock and proximal and distal skarn, carbonate-replacement, and sediment-hosted deposits (modified from Sillitoe, 1995, 1999, 2000, 2010).

1.4.1 Porphyry Deposits

Porphyry systems commonly have three main characteristics; 1) hydrothermal alteration and mineralization affecting large volumes of rocks, 2) the spatial and genetic association between mineralization and intrusive bodies exhibiting porphyritic texture, and 3) stockwork veins and veinlets containing disseminated sulfides of iron (Fe), copper (Cu), molybdenum (Mo), lead (Pb), and zinc (Zn), along with native gold (Au), as well as tungsten (W), bismuth (Bi), and tin (Sn) minerals (Pirajno, 2009).

Porphyry systems are divided into five classes on the basis of their metal contents: (1) porphyry Cu±Mo±Au; (2) porphyry Mo; (3) porphyry W; (4) porphyry Sn; and (5) porphyry Au systems. Additionally, further classification comprises the combination of igneous rock composition, and the principle and by-product metal content, such as syenitic porphyry Cu-(Au) (Seedorff et al., 2005).

The grade of ore formation occurrence in porphyry systems may associate with type of host rock consisting of igneous, sedimentary, and metamorphic lithologies (e.g Titley, 1993) since permeability may affect the grade development on the basis of magmatic fluid penetration and dispersion, where impermeable, poorly fractured wall rock like marble resulting in high-grade formation (Sillitoe, 2005).

In porphyry Cu deposits, the intrusions may involve multiple phases categorized based on their temporal emplacement in relation to alteration and mineralization events; before (early porphyries, which may exhibit either the highest grade or weak mineralization), during (intermineral porphyries, characterized by relatively lower mineralization), near the end (typically barren, late mineral porphyries), and after

(typically barren post-mineral porphyries) (Kirkham, 1971; Gustafson, 1978; Sillitoe, 2005, 2010) (Figure 1.3).

1.4.2 Skarn Deposits

Skarn is defined as rock type primarily calc-silicate mineralogy, such as garnet and pyroxene, which may not necessarily suggest a unique geologic setting or a certain protolith composition, but rather a specific combination of temperature, pressure, fluid, and composition of the host rock, therefore found on all continents and in almost all rock ages (Robb, 2005; Meinert et al., 2005; Pirajno, 2009). As a one of the prevalet source of Fe, Cu, W, Pb, Zn, Mo, Sn Au, and Ag deposits, skarn can derive from a various metasomatic activity associated with magmatic, metamorphic, meteoric, and/or marine fluids (Meinert et al., 2005; Robb, 2005).

Skarns can be categorized based on the rock type and associated mineralization (Robb, 2005; Meinert et al., 2005; Pirajno, 2009). Exoskarn and endoskarn are commonly used terms to describe the positioning of skarn relative to the causative pluton where endoskarn refers to skarn mineralization occurring internally within the causative intrusion and exoskarn refers to skarn mineralization occurring externally to the pluton, in the surrounding sedimentary rocks (Einaudi and Burt, 1982; Meinert et al., 2005). Furthermore, skarns are classified in the basis of the dominant composition of the protolith and the generated skarn minerals such as magnesian, calcic, and mangan (Meinert et al., 2005; Robb, 2005).

Intrusion related skarn deposits commonly form as a consequence of three processes, which are prograde stage isochemical contact metamorphism due to the pluton emplacement and crystallization, followed by prograde stage metasomatism and replacement due to the Si, Al, and Fe introduction, and final retrograde stage meteoric fluid influx and metal precipitation (Figure 1.4) (Einaudi et al., 1981; Meinert, 1992; Corbett and Leach, 1998; Robb, 2005; Pirajno, 2009).

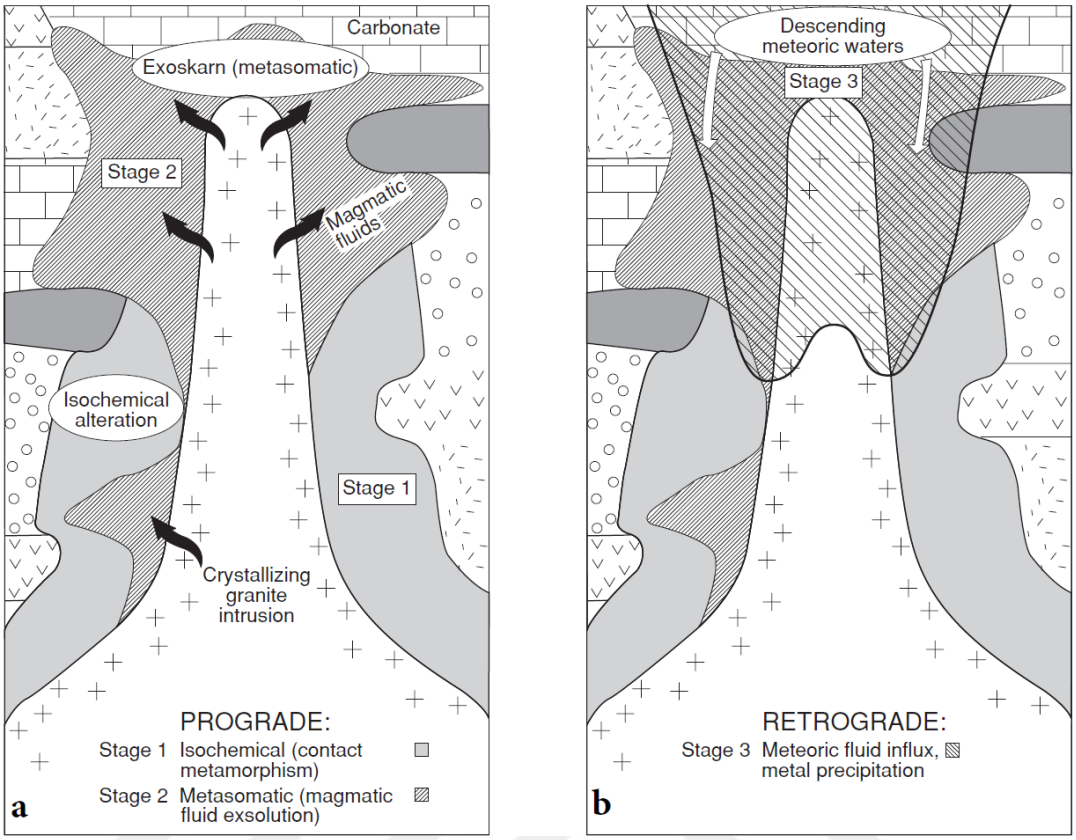


Figure 1.4. The formation of intrusion-related skarn deposits as result of prograde stage (a) and retrograde stage (b) (Corbett and Leach, 1998; Robb, 2005).

The subsequent prograde and retrograde stages result in replacement of limestone, which typically forms calcic skarn mineral assemblages consisting of garnet, clinopyroxene, wollastonite, epidote, and magnetite. On the other hand, dolomitic wall rock replacement results in the formation of magnesian skarns characterized by minerals such as diopside, forsterite, serpentine, magnetite, and talc in silica-poor environments (Einaudi et al., 1981; Meinert et al., 2005; Robb, 2005).

1.4.3 Carbonate Replacement Deposits

Formation of porphyry-related skarn, carbonate replacement and sedimentary hosted deposits clearly depends on the surrounding carbonate rock presence (Sillitoe, 2005). Zn- Pb ± Ag carbonate replacement deposits are formed by replacements of receptive carbonate beds, as a result of fluid neutralization, strata-bound in nature (Seward and Barnes, 1997; Rush and Seegers, 1990; Love et al., 2004). Au mineralization may occur on the periphery of porphyry related carbonate hosted systems, where the permeability of the rock is enhanced due to decalcification, whereas local jasperoid formations may also be present (Sillitoe, 2005).

CHAPTER 2

LITERATURE REVIEW

2.1 Regional Setting

The vast Tethyan Ocean, consisting of numerous branches, existed between two mega-continents, Gondwana in the south and Laurussia in the north, since the Carboniferous (Şengör, 1987; Ricou, 1994; Stampfli, 1996). The successive evolution of Paleo-Tethyan and Neo-Tethyan oceanic basins, which are commonly regarded as the main branches of the Tethyan ocean, is reflected in the current terrane distribution of Anatolia (Figure 2.1). However, there are different interpretations of the definitions and positions of these oceans (Şengör, 1984 and 1987; Stampfli, 2000; Robertson et al., 2005; Okay, 2008).

Based on the early classification of Ketin (1966), the main tectonic fragments that form the continental mass of modern-day Anatolia include the Pontides exhibiting Laurussian affinities, and the Anatolides-Taurides and the Arabian Platform exhibiting Gondwanan affinities. Following Ketin's work, these large tectonic entities have been further subdivided into many smaller domains by various researchers (e.g., Göncüoğlu et al., 1997; Okay and Tüysüz, 1999; Moix et al., 2008).

The Anatolide-Tauride tectonic fragment was separated from the northerly Pontides and the southerly Arabian Platform by the Tethys Ocean and its subsidiary seaways during the Phanerozoic (e.g., Ketin, 1966; Şengör and Yılmaz, 1981; Okay, 2008). Today, the nearly E–W-extending İzmir-Ankara-Erzincan Suture Zone, characterized by ophiolitic rocks and ophiolitic mélange, marks the transition between the Pontides and the Anatolide-Tauride, whereas the Assyrian (or Bitlis Zagros) Suture Zone bonds the Anatolides with the Arabian platform (Figure 2.1).

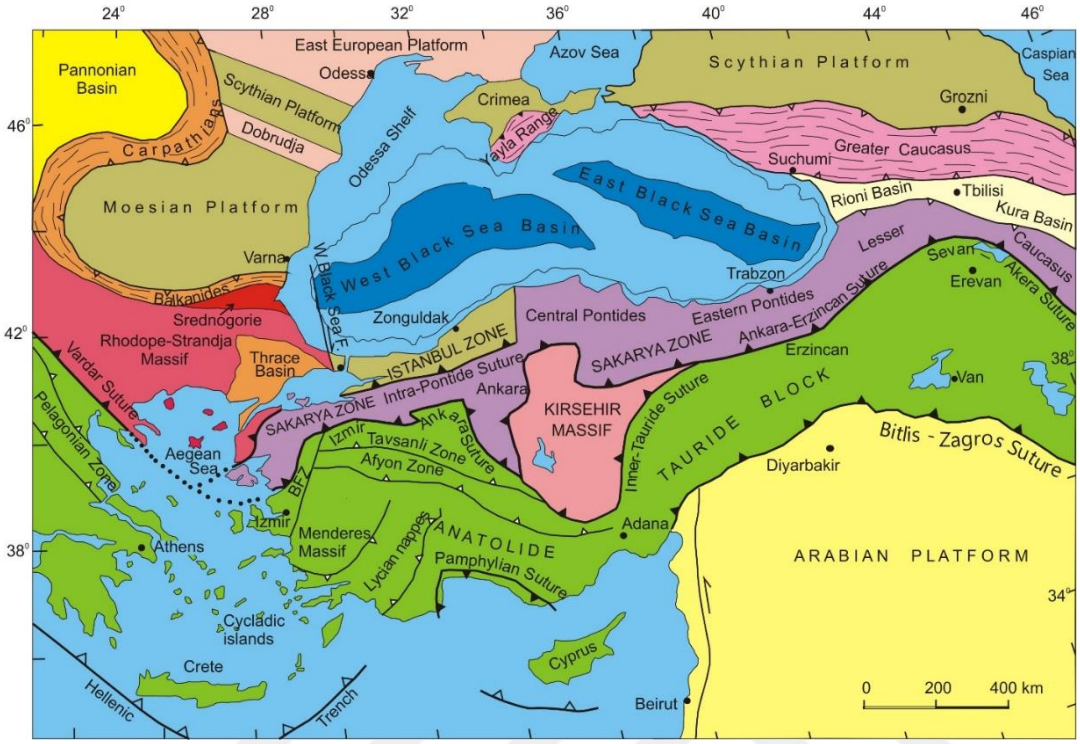


Figure 2.1. The tectonic map illustrating continental blocks and major sutures of Anatolia and the surrounding regions (Okay and Tüysüz, 1999).

2.1.1 Geodynamic/Tectonic Evolution of Anatolide-Taurides

The Anatolide-Tauride fragment represents one of a few of the Cimmerian continental tectonic blocks that were rifted off from the northern margin of Gondwana due to subduction initiation of the Paleotethys and subsequent opening of the Neotethys as a back-arc basin (Şengör, 1979 and 1987; Şengör and Yılmaz, 1981; Stampfli et al., 1991; Okay and Tüysüz, 1999). Consequently, the tectonic fragment experienced the major Cimmerian and Alpine deformation periods, the latter associated with the closure of the Neotethys during the Mesozoic–Cenozoic (Şengör, 1979; Robertson et al., 2009).

The Anatolide-Tauride terrane is a composite tectonic entity that is made up of an extensive Paleozoic–Mesozoic carbonate sequence (Taurides) and several metamorphic massifs (Anatolides) including the prominent Menderes and Kırşehir Massifs (also known as the Central Anatolian Crystalline Complex). As a Cimmerian terrane, the Taurides recorded the Devonian opening of the Paleotethys ocean to their north and the Permian opening of the Neotethys ocean to their south (Moix et al., 2008). From Permian until the Late Cretaceous the Tauride units do not show any major evidence of deformation and metamorphism except for occasional stratigraphic breaks (Okay, 1986; Mackintosh and Robertson, 2012). The Anatolides occupy a northerly position relative to the Taurides and show much stronger evidence of deformation and metamorphism due to the closure of the Paleotethys and Neotethys oceanic basins through collision with the Pontides (Okay, 2008). This is particularly evident in the metamorphic domains that remain in the footwall of the subduction interface with the Pontides including the Tavşanlı and Afyon Zones as well as the Menderes Massif (Okay, 1984). On the other hand, the relative positioning of the Central Anatolian Crystalline Complex (CACC) with respect to the Taurides during the Late Paleozoic–Early Mesozoic has been a topic of major debate. According to some researchers, the CACC is a micro-block separated from the Taurides by a small oceanic basin named as the Inner Tauride Ocean (Şengör and Yılmaz, 1981; Şengör, 1982; Okay, 1984; Gökten and Floyd, 1987; Gökten, 1993; Görür et al., 1998; Görür and Tüysüz, 2001; Pourteau et al., 2010; Robertson et al., 2013). This hypothesis is in part based on the presence of ophiolitic rocks and ophiolitic melange between the Taurides and the southern margin of the CACC. These ophiolitic rocks were interpreted to be the remnants of the Inner Tauride Ocean. In contrary, some researchers argued against the presence of an Inner-Tauride oceanic basin, and suggested that the CACC represents the metamorphosed northern margin of the Anatolide-Tauride fragment (Poisson et al., 1996; Yaliniz et al. 2000; Köksal et al., 2013). According to this model, the unroofing of the CACC in the Mesozoic led to southward movement of the overlying ophiolite complexes, so that

these ophiolites are not remnants of an oceanic lithosphere positioned between the CACC and the Taurides.

The convergence between the Pontides and the southerly Anatolide-Tauride and Arabian Blocks resulted in closure of various branches of Neotethys, and amalgamation of the Anatolide-Tauride fragment to the Pontides in the Late Cretaceous and to the Arabian Platform in the Late Cenozoic (Dewey et al., 1986; Robertson et al., 2007; Allen and Armstrong, 2008; Hüsing et al., 2009; Okay et al., 2010; Ballato et al., 2011; McQuarrie and van Hinsbergen, 2013). The successive closure of these ocean basins led to strong internal deformation within the Anatolide-Tauride Block as part of the regional Alpine orogeny (Okay, 2008). In particular, the suturing between the Pontides along the Izmir-Ankara-Erzincan belt exposed the Anatolide-Tauride Block to obduction, subduction, and continental collision (Yılmaz et al., 1997; Okay and Tüysüz, 1999; Kaymakcı et al., 2009; Meijers et al., 2010; Parlak et al., 2013).

During the Middle Cretaceous, Anatolide-Tauride platform was emplaced by tectonic slices of ophiolitic mélange and massive ophiolitic bodies resulting in high pressure-low temperature metamorphism mainly of the Anatolides including the CACC (Göncüoğlu et al., 1997; Robertson et al., 2009, Pourteau et al., 2010; Parlak, 2016). The Taurides on the other hand have experienced internal slicing and thrusting of distinct tectonostratigraphic units due to subduction and closure of the Neotethys basins on its margins. Consequently, the Tauride range presents a typical napped structure, where a relatively autochthonous block (the Geyikdağı Unit; Özgül, 1976 and 1984) forming a central axis has been overthrusted from both north and south by large nappe blocks of carbonates (Özgül, 1984).

The collision of Pontides with the Anatolide-Tauride blocks and CACC during the Late Cretaceous to Early Paleocene, resulted in the İzmir-Ankara-Erzincan suture zone formation and the northern Neotethys closure (e.g., Yılmaz et al., 1997; Okay and Tüysüz, 1999; Kaymakcı et al., 2009; Meijers et al., 2010; Parlak et al., 2013).

All of these oceanic basins subducted northwards, producing localized arc magmatism along the northern margins of these basins through Central Anatolia, Eastern Taurides, and Eastern Pontides (Yazgan and Chessex, 1991; Yılmaz et al., 1993; Kadıoğlu et al., 2006; Parlak et al., 2006; Rızaoğlu et al., 2009; Robertson et al., 2012; Figure 2.2).

During Eocene or Oligocene, interpretations propose a "soft" collision between the Arabia outer passive margin and Anatolide-Tauride, based on the deformation observed throughout much of Anatolia (e.g., Hempton, 1987; Yılmaz et al., 1993; Jolivet and Faccenna, 2000; Rolland et al., 2012; McQuarrie and van Hinsbergen, 2013; Ballato et al., 2018; Darin et al., 2018).

The final closure of the southern Neotethys Ocean along the Bitlis Suture occurred during the Miocene, due to the collision of the Arabian Platform with the Anatolide-Tauride (Şengör and Yılmaz, 1981; Dewey et al., 1986; Yiğitbaş and Yılmaz, 1996; Okay et al., 2010). During the Plio-Quaternary the westward migration of Anatolia towards the Aegean subduction zone (Şengör et al. 1985; Tatar et al. 2002; Reilinger et al. 2006), resulted in left-lateral displacement along the transform fault zones of East Anatolia such as Ecemiş Fault zone and Göksu Fault zone (Koçyiğit and Beyhan 1998; Jaffey and Robertson, 2001; 2004; Umhoefer et al., 2007), the Göksu Fault Zone, and upliftment of Taurides (Robertson et al., 2012).

Since the Miocene, extensive volcanism occuring Eastern Anatolia, may have been caused by either the delamination of the subcontinental lithospheric mantle (Pearce et al., 1990; Göğüş and Pysklywec, 2008) or by the steepening and break-off of the slab following collision (Keskin, 2003; Şengör et al., 2003; Faccenna et al., 2006; Lei and Zhao, 2007).

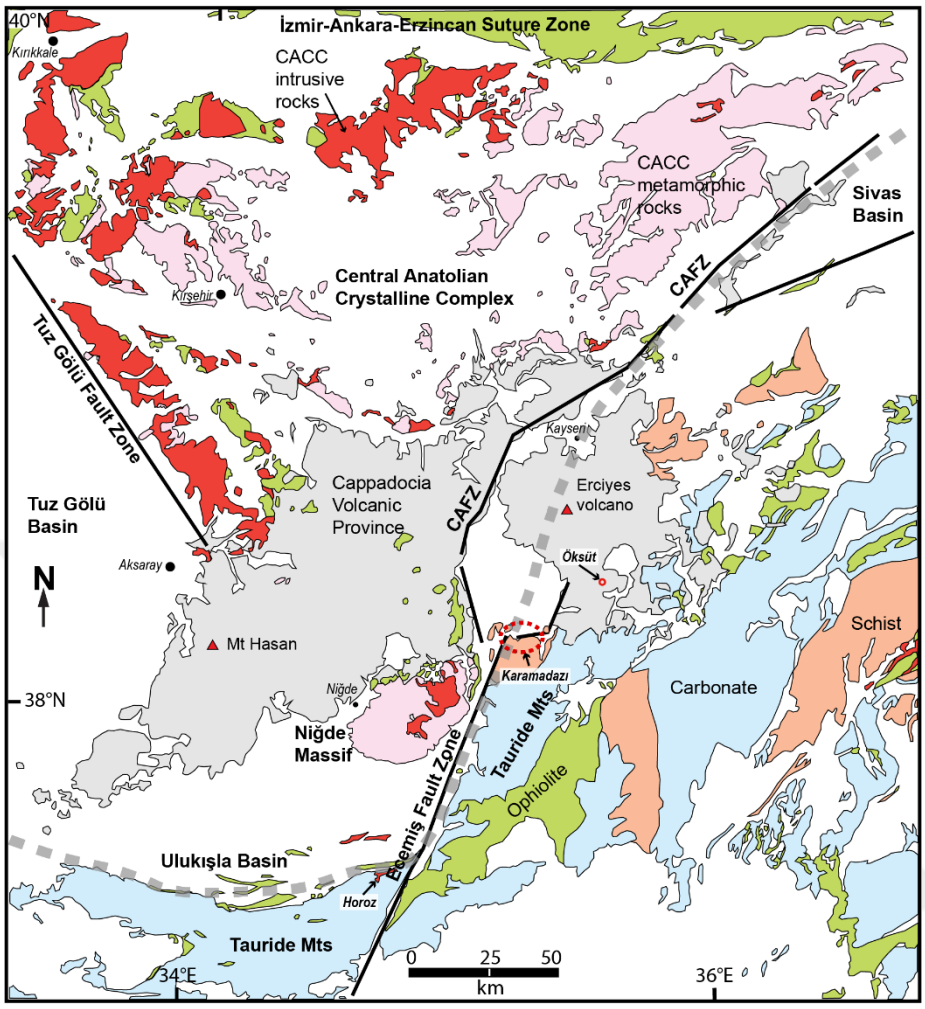


Figure 2.2. The major geological features of Central Anatolia including Karamadazı region, situated within the Yahyalı metamorphics and bounded by the Ecemiş Fault (modified after Radwany et al., 2017)

2.1.1.1 Geology of the Aladağ Region

The Taurides are composed of Neorprotozoic basement rocks and Palaeozoic to Early Tertiary sedimentary units (e.g Gürsu et al., 2004, Göncüoğlu, 2010). The presence of numerous tectonostratigraphic units as bivergent nappes are closely linked by the Neotethys branches closure during the Late Cretaceous (Göncüoğlu, 2010). During the Middle Cretaceous obduction of ophiolites through the Anatolide-

Tauride block resulted in high-pressure, low-temperature metamorphism of the northern side such as the formation of Tavşanlı zone while the emplacement of Cretaceous sedimentary deposition occurred along distal margin of obduction (Okay, 2008). During the Late Paleocene–early Eocene, the contraction process due to continental collision between Anatolide-Tauride and Pontides resulted in the metamorphism of Menderes Massif associated with southward-thrusting of the Lycian Nappes. According to Okay (2008), the majority of present nappe structures has developed during the Eocene. During the Early Miocene, a south-eastward thrusting of the Lycian nappes over the Beydağları autochthonous was occured (Okay, 2008).

According to Özgül (1976 and 1984), Bozkır, Bolkar Dağı, Aladağ, Geyik Dağı, Antalya and Alanya units are the 6 main tectono-stratigraphic units of Taurides. The Geyikdağ Unit, forming the central autochthonous belt displaying Paleozoic succesions, was overthrusted by the northerly Bozkır, Bolkar and Aladağ units and the southerly Alanya and Antalya Units (Göncüoğlu, 2012).

The Aladağ region in the Taurus Mountains was previously investigated by different researchers. This region was named differently according to researcher and their research area such as Karadağ Series by Graciansky (1968), Hadim Nappe (Blumenthal, 1944), around Şeydişehir-Bozkır-Hadim, north of Alanya–Anamur in the Middle Taurus; Middle Taurus Unit (Özgül 1971), around Bozkır - Hadim; Belemedik Palaeozoic (Blumenthal, 1947), around Belemedik in the Eastern Taurus; Black Aladağ Series (Blumenthal, 1941) and in the Aladağ-Yahyalı region (Özgül, 1976).

Tekeli (1980) suggested that the structural evolution of Aladağ occurred in three different stages. These periods include the disruption of the passive continental margin covering the Late Triassic–Early Cretaceous interval by faulting in the Cenozoic and the first ophiolite emplacement of the continental margin and the emplacement of the peridotite nappe in the Maastrichtian.

The Aladağ unit consists of the Early Paleozoic Tufanbeyli Autochthon, the Upper Paleozoic-Lower Mesozoic Yahyalı Nappe, the Upper Paleozoic-Jurassic Siyah Aladağ Nappe, the Upper Triassic Minaretepeler Nappe, the Late Carboniferous-Upper Permian Çataloturan Nappe, the Middle Triassic–Jurassic Beyaz Aladağ Nappe, and the Senonian Ophiolitic melange (Figure 2.3) (Tekeli et al., 1984).

2.1.1.1.1 Tufanbeyli Autochthon

The Early Paleozoic Tufanbeyli Autochthon consists of quartzite sandstone, shale, recrystallize limestone and gray shales, which is situated under ophiolitic mélange (Figure 2.3) (Ocakoğlu, 2002).

2.1.1.1.2 Yahyalı Nappe

The lowest nappe of the Aladağ unit is the Yahyalı Nappe, which is located northernmost part, and is observed under the Siyah Aladağ Nappe (Figure 2.3) (Tekeli et. al., 1984). The Yahyalı Nappe is composed of intensely deformed and metamorphosed Upper Paleozoic-Lower Mesozoic sequence. The oldest unit is Upper Devonian recrystallized limestone including fossils and Carboniferous recrystallized limestone with quartzite, dolomite, and schist interbeds overly this oldest unit. Lower Triassic conglomeratic limestone contains recrystallized micritic matrix and underlies dolomite abundant conglomeratic limestone with marl, mudstone, and schist interbeds (Tekeli et. al., 1984).

2.1.1.1.3 Siyah Aladağ Nappe

The Siyah Aladağ Nappe is observed in the south of the Yahyalı Nappe (Figure 2.3). Locally overturned and folded nappe is composed of Upper Devonian limestones with coral colonies alternating with marl and mudstone as the oldest unit (Tekeli et al., 1984). Late Devonian unit is overlain by Carboniferous limestones alternating

with quartzite and marl, and Jurassic thick limestones with bituminous and dolomite (Tekeli et al., 1984 and Ayhan, 1983).

2.1.1.1.4 Minaretepeler Nappe

The Upper Triassic Minaretepeler Nappe is tectonically underlain by the Siyah Aladağ Nappe (Figure 2.3). It comprises limestone, massive - thick layered limestone, maroon colored alternation of marl, limestone, dolomite, and dolomitic limestone from bottom to top (Tekeli et. al., 1984).

2.1.1.1.5 Çataloturan Nappe

The Çataloturan Nappe is tectonically underlain by the Minaretepeler Nappe (Figure 2.3). This nappe is composed of the Lower Carboniferous bituminous, black colored, mid-bedded limestones alternated with green colored limestones with volcanic components (Aksay, 1980). This Lower Carboniferous unit reflects a regressive transition to the deep water (shelf edge) facies whereas Upper Permian sediments belong to an open platform facies. Former unit is overlain by very thick-bedded gray chert with Upper Permian limestones interbeds (Ayhan, 1983).

2.1.1.1.6 Beyaz Aladağ Nappe

The widespread nappe of the Aladağ unit, which is overlain by the ophiolitic nappe (Figure 2.3). The Middle Triassic-Jurassic Beyaz Aladağ Nappe is composed entirely of thick-bedded gray, white colored dolomite, and dolomitic limestones, deposited in shelf lagoon environment of a platform/bank facies in Upper Triassic-Lower Jurassic (Tekeli et al., 1981).

2.1.1.1.7 Ophiolitic Mélange

In the Aladağ region, Senonian Ophiolitic Mélange occurs on Upper Triassic-Lower Cretaceous platform carbonate sequences with an unconformity (Tekeli et al., 1984). The mélange is composed of regular basal sequence, olistostromal par and chaotic part, from bottom to top, respectively (Tekeli et al., 1984).

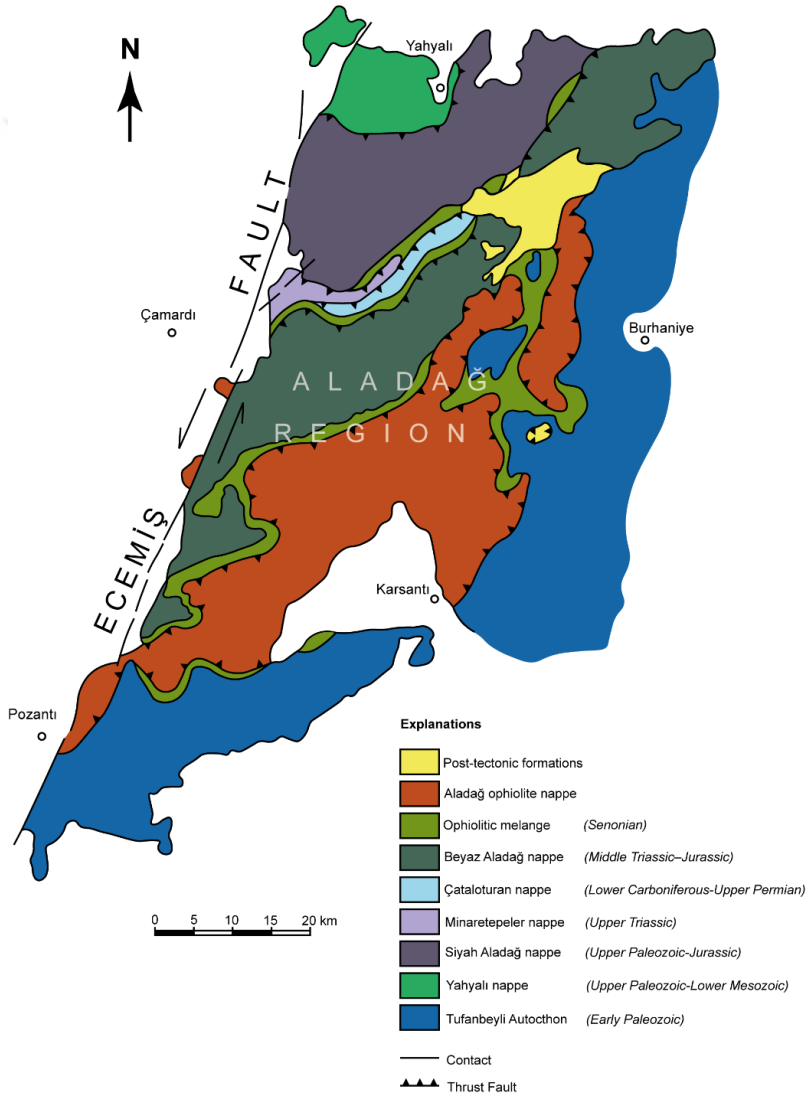


Figure 2.3. Map showing the main units of the Aladağ region to the east of the Ecemiş Fault (after Tekeli et al., 1984).

2.1.2 Geology of the Karamadazı District

The Karamadazı region is located in the Yahyalı district of Kayseri Province. The Karamadazı iron deposit has been previously investigated by several researchers due to its geographical position within the Eastern Taurus Mountains and its substantial economic prospects (Kuşcu et al., 2001). Oygür et al. (1978) provided preliminary findings indicating that the ore deposits in the region are of skarn-type mineralization (Kuşcu et al., 2001). The reserve of the Karamadazı Fe skarn is 6.4 Mt at 54% Fe (Oygür, 1986). Blumenthal referred to this area as Siyah Aladağ Permo-carboniferous limestone (1941, 1944). According to Tekeli et al. (1981), the area was referred to as the Yahyalı Sequence, while Ulakoğlu (1983) named as Paleozoic Rocks. Furthermore, tectono-stratigraphic features of Aladağ region investigated by Ayhan and Lengeranlı (1986). The region recognized as the lower-grade metamorphic equivalent of the Niğde Massif located next to the southern boundary of the Central Anatolian Crystalline Complex, referred to as the Yahyalı Metamorphics by Göncüoğlu (1991, 1992).

2.1.2.1 The Yahyalı Sequence

The Yahyalı Sequence is an Upper Palaeozoic–Lower Mesozoic para-autochthonous nappe, which is underlain by an allochthonous peridotite nappe (Tekeli, 1980; Göncüoğlu et al., 1991). On the other hand, between the Precambrian and Permian, unconformities are observed by Ulakoğlu (1983). From the older to the younger, five main formations are observed in The Yahyalı Sequence: The Yahyalı Metamorphic Complex (Precambrian), Karacatepe Formation (Cambrian), Çalmardı Formation (Devonian), Ağcaşar Formation (Carboniferous), and Akbaş Formation (Permian) (Figure 2.4). The stratigraphy of the Yahyalı sequence provided in Figure 2.5.

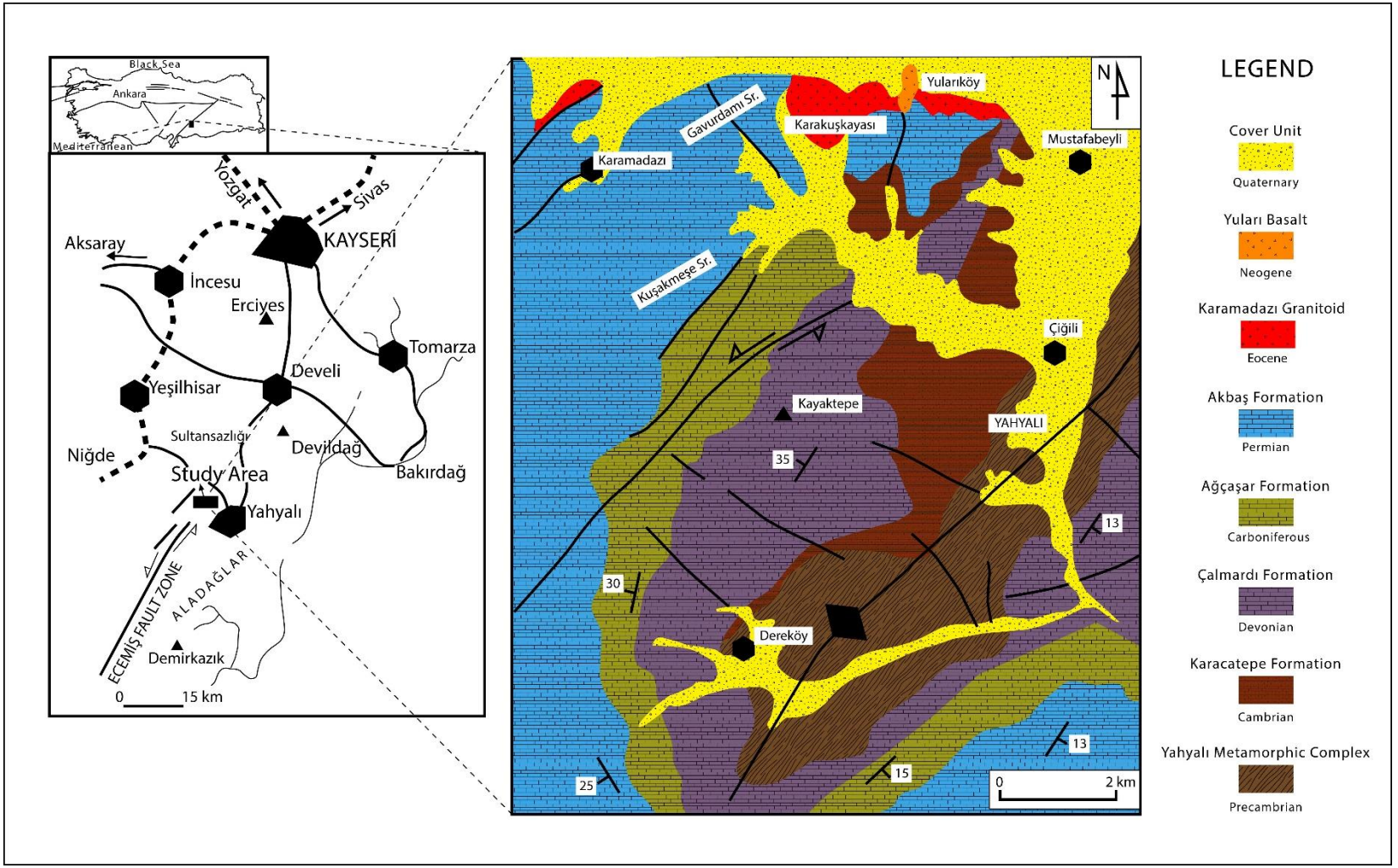


Figure 2.4. The location and regional geologic map of Karamadazı Area modified from Ulakoğlu (1983) after Kuşcu et al. (2001).

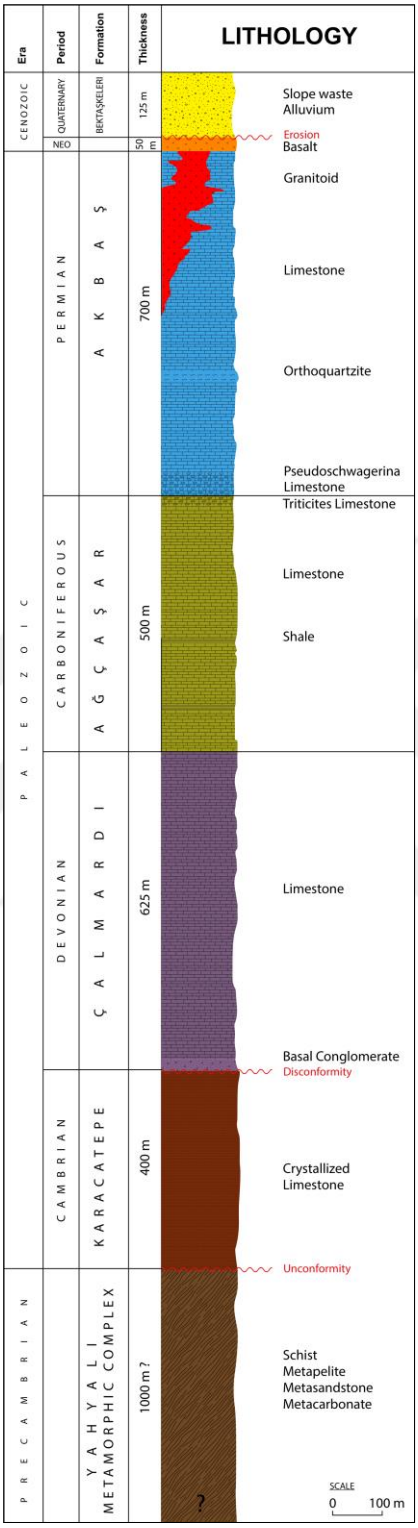


Figure 2.5. The generalized stratigraphic columnar section of Karamadazı area simplified after Ulakoğlu (1983).

2.1.2.1.1 Yahyalı Metamorphic Complex

The Yahyalı Metamorphic complex is composed of gray-black, green to beige coloured metamorphic: metapelite containing minerals such as quartz, muscovite, chlorite, albite, garnet, epidote, tourmaline, magnetite; metasandstone containing needle-shaped quartz, plagioclase, mica minerals; calc-schist, and metacarbonates. The Yahyalı metamoprhic complex is unconformably overlain by Karacatepe Formaiton (Ulakoğlu, 1983; Figure 2.5).The thickness of the formation varies between 600 m and 1000 m. (Ulakoğlu, 1983). Yahyalı Metamorphic Complex was subsequently renamed by Ayhan and Lengeranlı (1986), as the Devonian-Silurian Kirazlı Formation which is composed of schist, quartzite, and recrystallized limestone.

2.1.2.1.2 Karacatepe Formation

The Cambrian Karacatepe formation is represented by 400 meters thick recrystallized limestones, which is unconformably overlain by the Çalmardı formation (Ulakoğlu, 1983; Figure 2.5). There is a significant stratigraphic hiatus between this formation and the Devonian Çalmardı formation (Ulakoğlu, 1983). Whereas, the Karacatepe Formation, named as the Denonian Karsavuran Formation by Ayhan and Lengeranlı (1986), which consists of similar lithological characteristics.

2.1.2.1.3 Çalmardı Formation

The Çalmardı formation consists of a basal conglomerate at the bottom and continues with recrystallized limestones towards the top. This formation is conformably overlain by the Carboniferous Ağcaşar Formation. It reaches a total thickness of about 625 m in thick layers (Ulakoğlu, 1983; Figure 2.5). Basal conglomerate unit includes eroded fragments from the metamorphic basement pebbles, which are

angular or less rounded poorly sorted and cement is limonite limestone without fossils in the formation (Ulakoğlu, 1983). Limestone unit has a total thickness of 825 m, displaying the Mylonitic textured, where the fossils content shows that the age of this unit is Lower, Middle and Upper Devonian (Ulakoğlu, 1983). However, Çalmardı formaiton has been divided into as the Ayraklıtepe Formation of the Yahyalı Nappe and the Köşkdere Formation of the Siyah Aladağlar Nappe by Ayhan and Lengeranlı (1986). Where Ayraklı formation exhibit similarities since characterized by Devonian recrystallized limestone with a thickness up to 750 meters (Ayhan and Lengeranlı, 1986).

2.1.2.1.4 Ağcaşar Formation

The Ağcaşar formation is conformably overlain by the Permian Akbaş Formation (Figure 2.5). The total thickness of the formation with medium type bedding is thought to be approximately 500 meters. The Ağcaşar formation consists of three members (Ulakoğlu, 1983). Lower Carboniferous shale unit consists of lenses, very thinly laminated, and in different colors (Ulakoğlu, 1983). As a most common unit, Carboniferous limestone exhibits micro-sparitic texture, where thickness is about 500 meters (Ulakoğlu, 1983). Triticites limestone unit is the uppermost level of the formation, it is a guide layer at the Permian-Carboniferous boundary. The unit appears in a mixture of gray-yellow-beige colors, forming thin bedding of 10-50 cm. The skeletal-sparitic rock is composed of fossil skeletons and sparitic cement. (Ulakoğlu, 1983).

2.1.2.1.5 Akbaş Formation

The Akbaş Formation is dominantly composed of gray limestones with thick layers and is about 700 m thick (Figure 2.5). This formation consists of 4 members: Pisolithic limestone, Pseudoschwagerina limestone, limestone, orthoquartzite (Ulakoğlu, 1983). Pisolithic limestone member can be considered as a key level on

the Carboniferous-Permian boundary, in the form of long lenses and has a thickness varying between 10 cm to 1 m. This member varies in burgundy, beige, gray, green, brown, and pink in color and consists of 2 mm to 2 cm sized pisolites and spray cement. It is considered to be a typical level in the Taurus Mountains and should be interpreted as Lower Permian basement (Ulakoğlu, 1983). Whereas, as a key Lower Permian level is Pseudoschwagerina limestone member, which forming thin lenses, ranging from 10 cm to 50 cm with skeletal-sparitic texture (Ulakoğlu, 1983).The prevailing unit in the formation is the limestone member and it is observed as the most widespread unit in the study area with 700 meters thickness, displaying dolomitic limestone characteristics and sparitic texture in gray and light gray colors (Ulakoğlu, 1983). Orthoquartzite member is observed in the form of lenses exposed by erosion without fossils fossil record (Ulakoğlu, 1983). On the other hand, the Akbaş Formation is divided into the Karlığıntepe Formation of the Yahyalı Nappe and the Zindandere Formation of the Siyah Aladağlar Nappe by Ayhan and Lengeranlı (1986). Where the Karlığıntepe Formation comprises recrystallized limestone with quartzite, schist, and phyllite interlayers, and dolomite-rich micritic limestone layers at the top (Ayhan and Lengeranlı, 1986). According to Ayhan and Lengeranlı (1986), the topmost formation of the Yahyalı Nappe is the Triassic Kocatepe Formation, which comprises marl, mudstone, siltstone, and dolomites. This formation is divided into two members: the Karamadazı member characterized by the bottom oolitic conglomerate limestone, followed by layers of marl, siltstone, sparitic limestone, with levels of sericite and chlorite schists and the Üçkardeştepe member characterized by dolomite and limestone, mudstones (Ayhan and Lengeranlı, 1986).

2.1.2.1.6 The Karamadazı Granitoid

The Karamadazı Granitoid is a large, compositionally heterogeneous intrusive complex mainly outcropping between the Yuları Village in the east and the Karamadazı Village in the west (Figure 2.4). This granitoid forms the causative

intrusion of the Karamadazı Fe skarn deposit. It is made up of a number of distinct intrusions of granite, granodiorite, quartz monzonite, and quartz diorite composition (Oygür et al., 1978; Oygür, 1986; Kuşcu et al., 2001; Koçak, 2008). Aplitic dikes and mafic enclaves are also reported as common features of the Karamadazı granitoid (Kuşcu et., 2001; Kocak, 2008). All intrusions are typical I-type, calc-alkaline intrusions that are metaluminous to weakly peraluminous, and they show arc-affinities (Gençalioğlu-Kuscu et al., 2001).

Geochronological data from the granitoid rocks is scarce. Koçak (2008) reported a whole-rock Rb-Sr age of 65 ± 13 Ma from a leucogranitic unit. Due to the large error, this age failed to constrain the timing of intrusive activity accurately. Later, Kuşcu et al. (2013) reported two $^{40}Ar/^{39}Ar$ ages (from hornblende and biotite), one from a granodiorite and another one from a monzodiorite unit hosting the skarn mineralization. These two ages (48.74 ± 0.67 Ma and 46.58 ± 0.82 Ma) correlate with each other and indicated that the intrusions were emplaced during the middle Eocene.

2.1.2.1.7 Yuları Basalt

The localized basalt dike outcrops through the south of Yuları village (Figure 2.4). Yuları Basalt is underlain by the Karamadazı granitoid, and is interpreted to be the remnant of the Erciyes eruption (Ulakoğlu, 1983).

2.1.2.1.8 Bektaşkeleri Formation (Cover Units)

Bektaşkeleri formation covers a wide area, which is unconformably underlain by the Akbaş Formation (Figure 2.5). This formation is composed of alluvium and slope wastes with a thickness ranging from 25 cm to 125 m (Ulakoğlu, 1983).

CHAPTER 3

GEOLOGY OF ÇUBUKLU DISTRICT

The Çubuklu prospect is situated about 11 km northwest of the town of Yahyalı in the Kayseri Province, and immediately east of the Karamadazı Village (also known as the Çubuklu district; Figure 3.1). The Karamadazı Fe mine of Özkoyuncu Madencilik is located about 3–4 km to the northeast of the tenement (Figure 3.1). The tenement covers an area that is approximately 4 km in length and 2.5 km in width (Figure 3.2).

Mineralized units are exposed on the northern foothills of the Tauride carbonate nappe named as the Yahyalı Nappe, and the ridges extending to the south of the Çubuklu district reach up to elevations of approximately 1550 meters above sea level at the Keybet Hill. The flat-lying Sultansazlığı basin borders this mountain range in the north, towards which a significant drop elevation can be observed (Figure 3.1). Part of the license includes a portion of this basin at elevations of approximately 1100 m above sea level. Quaternary alluvial cover of the Sultansazlığı basin also extends into the study area along the northeast-oriented creeks that incised the Tauride range carbonates (Figure 3.1). The northeast-southwest oriented dextral strike-slip faults exhibiting nearly 60 meters of offsets in some localities, probably associated with the strike-slip faults of the Ecemiş Fault Zone, which borders the area from the west and east (Kuşcu et al, 2001).



Figure 3.1. Map showing the study area (Postallı Madencilik license), located nearly 11 km northwest of Yahyalı Town. The boundaries of the Postallı license are highlighted in red.

At Çubuklu, four main lithological units are identified, and from oldest to youngest these are: the Carboniferous metamorphic rocks, the Paleozoic-Mesozoic carbonate rocks, the Eocene Karamadazı Granitoid, and the Quaternary cover unit (Figure 3.2). Among these, the Paleozoic-Mesozoic carbonate sequence has the most widespread surface exposure in the study area, whereas narrow outcrops of the Carboniferous schist unit mainly occur along a NE-trending structure about 2 km SW of the Çubuklu district. Distinct lithologies belonging to the Karamadazı Granitoid, on the other hand, are mainly encountered in the drill hole. Skarn- and carbonate-replacement-style mineralization are generally observed along the contact zones of

carbonate rocks located in the Yahyalı Sequence, and adjacent to the Karamadazı Granitoid. The geological map of the study area is provided in Figure 3.2.

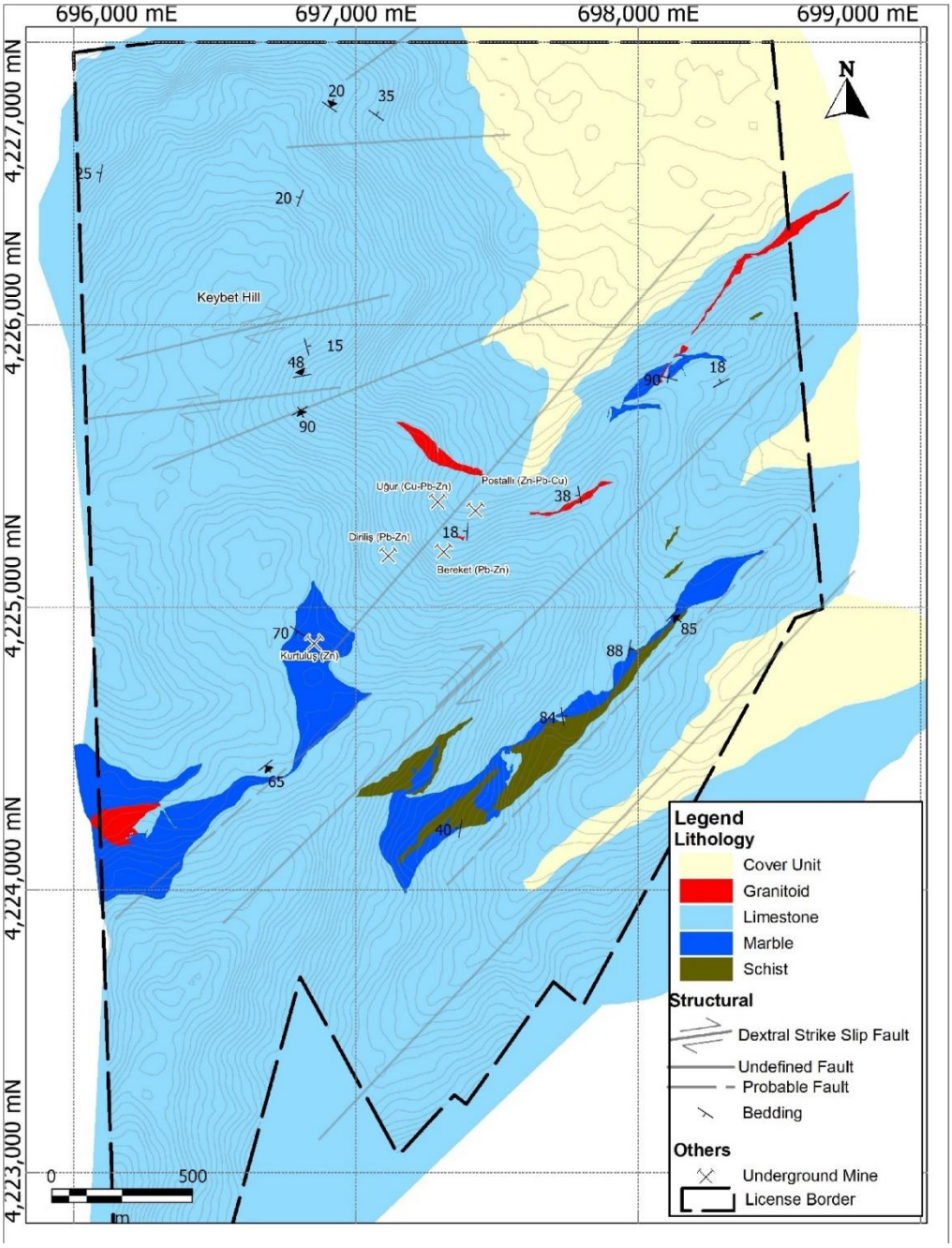


Figure 3.2. Geological map of the Çubuklu prospect showing distribution of main lithological units, structures, and the locations of the Postallı underground galleries.

3.1 Carboniferous Metamorphic Rocks

A narrow sequence of metamorphic rocks crops out within the Çubuklu license area. (Figure 3.2). According to the Kayseri L34 Section geological map of the General Directorate of Mineral Research and Exploration of Turkey (MTA), these represent the oldest unit of the license area, and their ages are inferred to be Carboniferous. Whereas the metamorphic unit comprising chlorite-sericite schists are included within the Triassic Kocatepe Formation of Ayhan and Lengeranlı (1986).

The metamorphic sequence is represented by intensely foliated and deformed schist units. Schists are exposed along a NE-SW-oriented ridge to the southwest of the Çubuklu district, but they were not intersected in any of the drill holes. Along this trend they can be traced for about 1340 meters, with apparent thickness ranging from 5 to 200 m (Figure 3.2). The schist unit is positioned subjacent to a limestone sequence, from which it is likely separated by a continuous NE-SW-trending, steeply dipping fault. This structure complicates the true nature of the contact between the schists and the carbonates.

In the outcrop, schists are generally light to dark gray and green in color due to presence of chlorite, sericite, and carbonate. Pyrite oxidation imparted a yellowish color to the outcrops locally. Complex schistosity observed both in the outcrop and in thin section is primarily defined by phyllosilicates including chlorite and sericite, whereas carbonate-rich layers are more competent in the surface exposures (Figure 3.3a). Petrographic study of collected outcrop samples from this unit indicated that schists mainly comprise chlorite and carbonate with lesser sericite, quartz, and pyrite with mineral abundances varying across different layers. Based on the dominant minerals these can be broadly grouped into chlorite-sericite-carbonate schist and calc-schist, the latter containing at least 60 modal% carbonate minerals (Figure 3.3b-c). Although the protoliths are not known, these likely derived from an intercalating sequence of siliciclastic and calcareous sedimentary rocks.

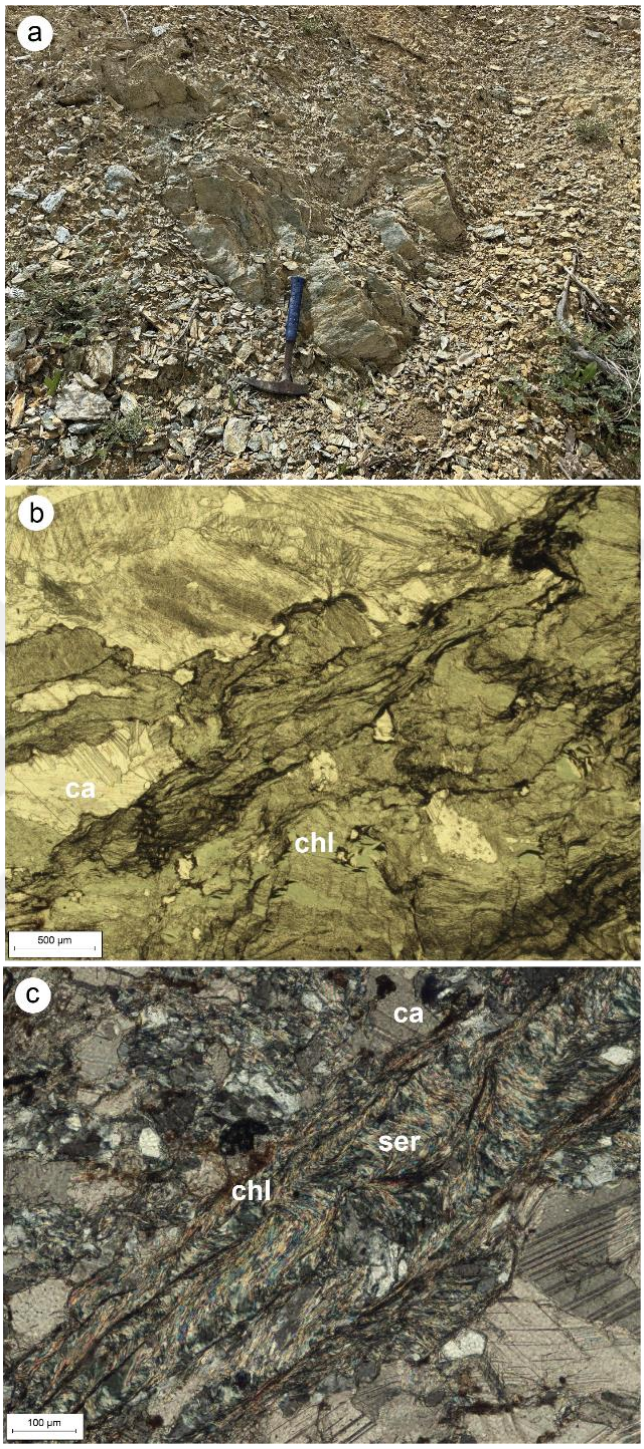


Figure 3.3. a) Outcrop photograph of chlorite-calcite schist, b) Microphotograph (PPL, TL image) of deformed chlorite layers, c) Microphotograph of (XPL, TL image) sericite-chlorite layer and fine to coarse grains of calcite. Abbreviations: chl = chlorite, ser = sericite, ca = calcite, XPL = cross-polarized light, PPL = plane-polarized light, TL = transmitted light.

3.2 Paleozoic Mesozoic Carbonate Rocks

The Permian Akbaş Formation (Ulakoğlu, 1983), primarily consisting of limestone and minor orthoquartzite lenses, hosts Karamadazı skarn mineralization and has been significantly recrystallized along the contacts of the Karamadazı granitoid (Kuşcu et al., 2001). The Permian Akbaş Formation is unconformably overlain by the Lower Triassic Dişdöken Formation, and the Middle–Late Triassic Kocatepe Formations classified by Ayhan and Lengeranlı (1986) where Kocatepe Formation, as the uppermost part of the Yahyalı Nappe, characterized by marl, mudstone, siltstones, and dolomites covering the Çubuklu prospect.

Based on field observations and drill logging mainly in the vicinity of Keybet Hill, the Paleozoic–Mesozoic sedimentary rocks have been classified into two alternating successions of (1) gray limestones and (2) a sequence of dark gray/black calcareous and siliciclastic sedimentary rocks (Figure 3.4).

Gray limestones are generally massive looking in the outcrop and are medium- to thick-bedded. They are mineralogically homogeneous and comprise variably sized grains of calcite and dolomite (Figure 3.5). These are often micritic rather than being originated as chemical precipitates.

Dark colored (dark gray to black) sedimentary succession is texturally and compositionally distinct and have a heterogeneous character compared to gray limestone. These exhibit layers dominated by varying amounts of calcite and dolomite interbedded with siliciclastic-rich layers comprising phyllosilicates (clays and chlorite) and graphite, the latter indicating organic-rich nature of this succession. Diagenetic pyrite is also a common constituent of these lithologies occurring as fine disseminations of framboidal to more recrystallized cubic crystals. Clayey-silty, siliciclastic layers have thicknesses ranging generally from a few millimeters to up to two meters (Figure 3.4 a).

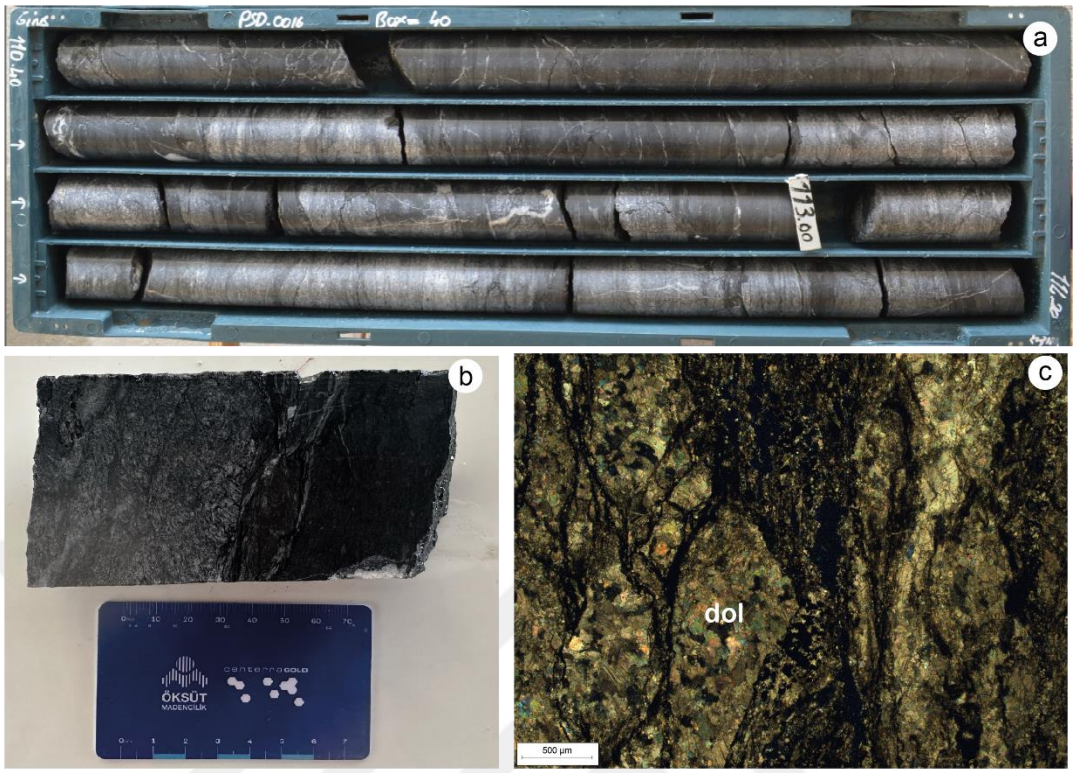


Figure 3.4. Drill core photograph of black limestone with clay and silt interlayers (drill hole: PSD-16, from 110.40 m to 114.20 m), b) Macrophotograph of black limestone (drill hole: PSD-16, from 111.50 m), c) Microphotograph (XPL, TL image) of elongated interlayers of dolomite and organic matter (drill hole: PSD-16, from 111.50 m). Abbreviations: dol=dolomite, XPL= cross-polarized light, TL = transmitted light.

In the study area, the transition between gray limestone and dark-colored calcareous-siliciclastic sequence can be rather easily identified as gray limestone is often resistant to erosion, whereas the latter forms recessive topography due its clay-silt and graphite content. This relationship can be particularly well-observed in the northwestern sector of the study area around the Keybet Hill (Figure 3.5).



Figure 3.5. Outcrop photograph showing an alternating sequence of gray and black limestone in the Keybet Hill. Organic- and clay-rich layers display a recessive topography compared to gray limestones. Minor strike-slip fault offsets of a few meters can be traced through this sequence.

The calcareous lithologies often show locally very intense brecciation especially in the drill core. Some of these breccias are karstic in character, whereas the remaining are either tectonic or hydrothermal in origin. Karstic breccias are distinguished from the other two varieties by the presence of irregular, cuspate and wispy clasts in the gray limestone. Rims of these clasts are dissolved and enclosed by white, sparry calcite and/or dolomite. These breccias are also well developed in the dark gray/black, organic-rich layers by large, angular to sub-angular clasts cemented again by carbonate (Figure 3.6). Additionally, in places brecciation develops along the existing bedding resulting in formation of bedding-parallel tabular clasts and surrounding white carbonate cement.



Figure 3.6. Drill core photograph of clast-supported breccia composed of angular to subangular black limestone clasts with calcite matrix (drill hole: PSD-16, from 152.00 to 155.70 m).

Apart from these two main successions, a very thin, discontinuous, laterally extending conglomerate layer was observed at the base of the Kocatepe Formation of the Karamadazı Member (Ayhan and Lengeranlı, 1986). Yellowish-brown to cream colored conglomerates are clast-supported and monomictic, comprising fine- to coarse-grained limestone clasts with a calcite-smithsonite matrix (Figure 3.7). These were only encountered along up to a maximum 0.5 m-long intervals.

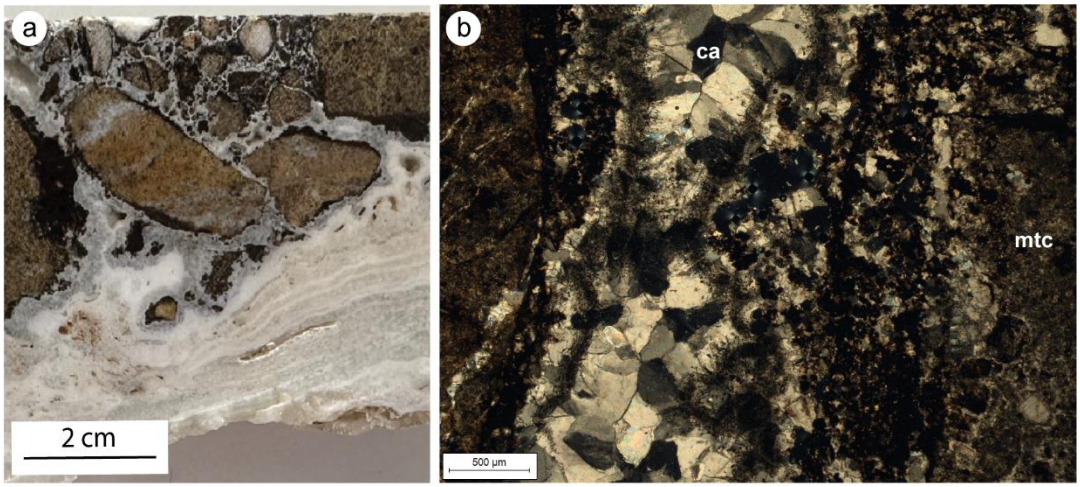


Figure 3.7. a) Macrophotograph of fine- to coarse-grained, clast-supported, monomictic conglomerate with calcite-smithsonite matrix (drill hole: PSD-16, from 228.30 m), b) Microphotograph (XPL, TL image) of calcite matrix and micritic limestone clasts (drill hole: PSD-16, from 228.30 m). Abbreviations: ca = calcite, mtc = micritic limestone, XPL= cross-polarized light, TL = transmitted light.

3.3 Eocene Karamadazı Granitoid

The Karamadazı Granitoid is an intrusive body of felsic to intermediate composition that is located about 3 km to the ENE of the Çubuklu prospect (Figure 3.2). This granitoid, emplaced into the Paleozoic–Mesozoic carbonate rocks and caused the formation of main Karamadazı Fe skarn orebody, was not identified as a major unit in the Çubuklu license. The only magmatic rock exposures in the study area occur as narrow, NE- or NW-trending dikes that exploited major fault planes. Nevertheless, a ground magnetic survey across the Çubuklu license indicated domains of strong magnetic highs (Figure 3.8), suggesting presence of a large intrusive body underneath the carbonate succession.

Subsequent drilling at Çubuklu by Centerra Gold confirmed the presence of a composite intrusive body consisting of coarse-grained felsic to intermediate composition plutonic rocks and finer-grained dikes in the property. Based on the aeromagnetic map in Figure 3.8, the core of the intrusive complex lies in the northeast border of the license, in close proximity of the Karamadazı mine, and several dikes emanate from this core extending farther southwest, into the study area. Additionally, a second prominent magnetic high lies underneath the southeastern end of the license (Figure 3.8), possibly representing either the southern extent of the main intrusion or alternatively a separate intrusion. Nevertheless, this area has not been drill-tested, so the origin of this magnetic positive is currently unknown.

The main outcropping igneous unit at Çubuklu is a NE-trending dike that is continuous for nearly 1.5 km along strike (Figure 3.2). Its width varies from 5 to 50 meters on the north-east side. Additionally, a smaller stock covering an area of 150 x 230 meters is exposed on the southwestern sector. The main dike has been emplaced within a fault plane extending through limestone and is thus strongly weathered (Figure 3.9 a). The small stock to the west has also possibly exploited a minor structure (Figure 3.9 b).

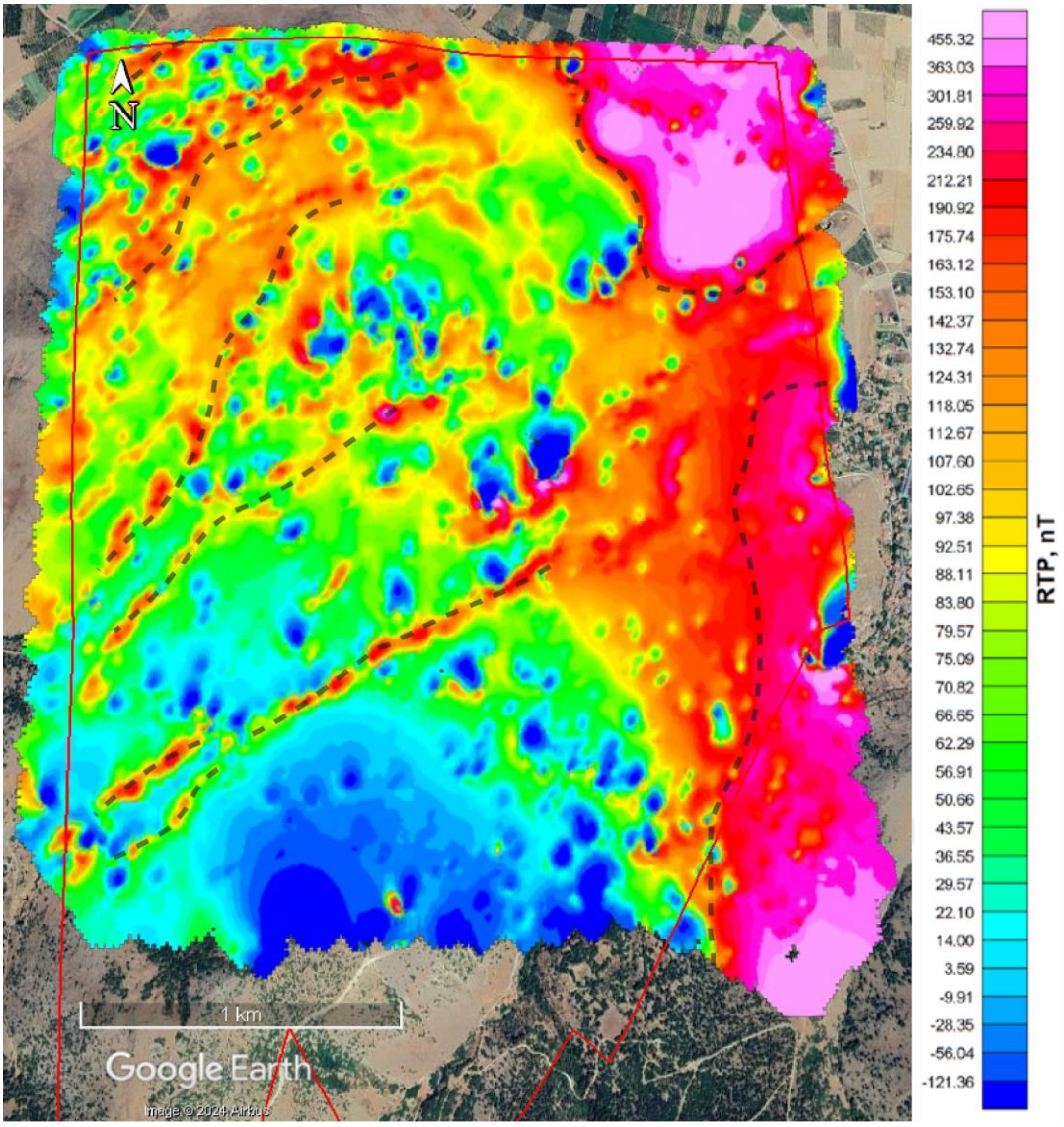


Figure 3.8. Ground magnetic map of the Çubuklu license (reduced to pole magnetic anomaly map), red lines and black dashed lines represent tenement boundaries and magnetic-high zones, respectively.

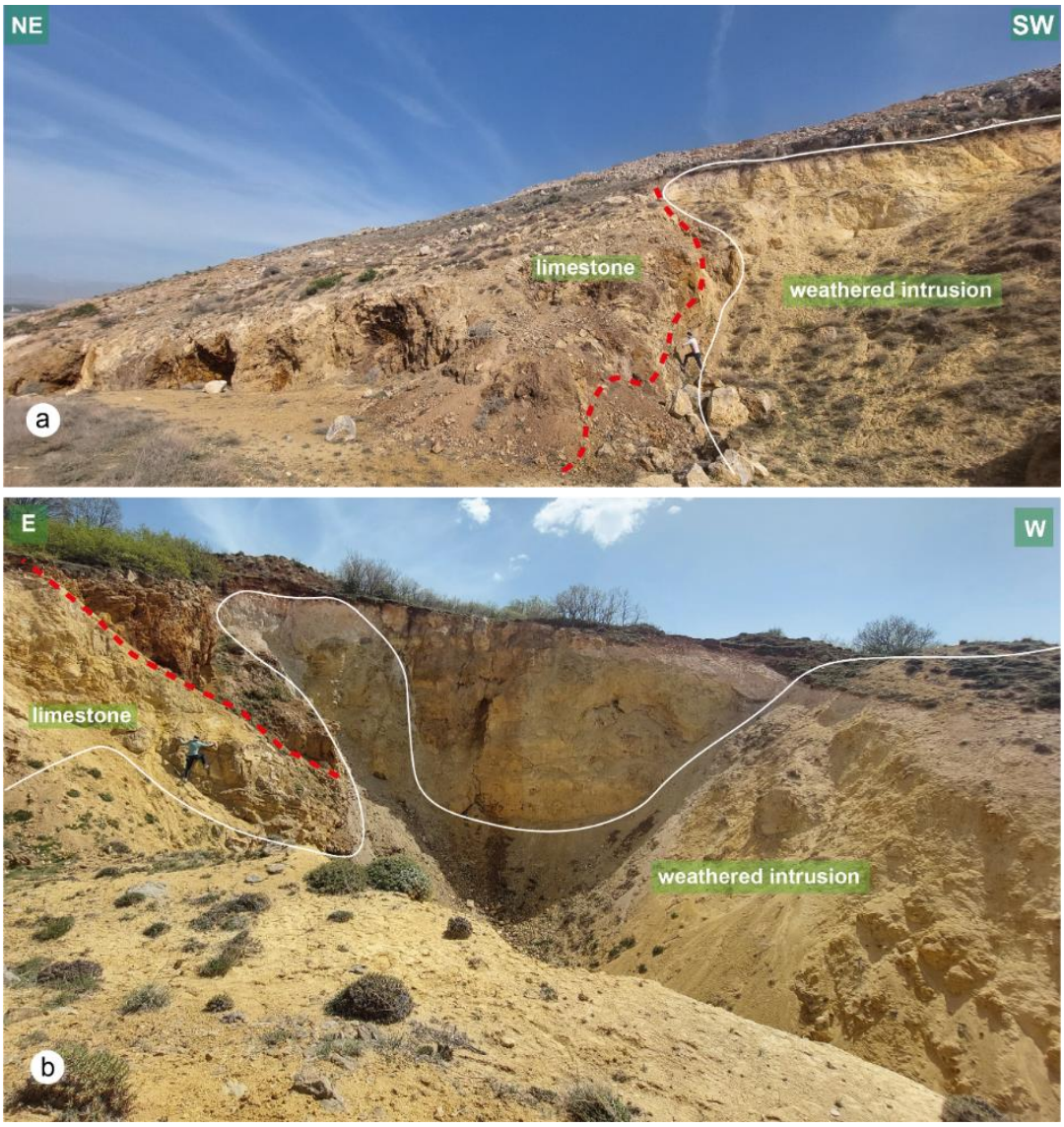


Figure 3.9. Outcrop photograph of the faulted contact between limestone and weathered intrusion from a) dike exposed at northeast part of the tenement b) stock covering southwestern part of the study area.

Drill core, outcrop, and petrographic analyses of igneous rocks revealed the presence of several compositionally/mineralogically distinct intermediate to felsic igneous units. Dacitic to tonalitic porphyries were observed in drill cores from the Keybet Hill, whereas granodiorite to diorite as well as monzodiorite, quartz diorite and andesitic dike units were identified in the northwestern sector. Although clear

textural and mineralogical differences exist between many of the identified lithologies, moderate- to strong-intensity alteration make distinction of compositionally close or similar units difficult.

Granodiorite porphyry: Granodiorite porphyry is closely associated with the main skarn zones, which is characterized by a porphyritic texture displaying abundant plagioclase phenocrysts (about 40 modal%; Figure 3.10 a-b). These coarse-grained plagioclase phenocrysts (up to 4 mm-long) display polysynthetic twinning and show glomeroporphyritic texture, which is characteristic for this unit K-felspar is also likely present (about 10 modal%), but weak- to moderate-intensity clay/sericite alteration precludes accurate identification of this mineral phase. The groundmass of weakly-altered granodiorite porphyry is composed of fine-grained quartz (about 20 modal%) and tabular prismatic biotite (about 30 modal%) crystals, the latter mostly altered into chlorite and epidote. Another distinguishing feature of this unit is the presence of accessory titanite. Zircon and apatite are the other accessory phases identified in the granodiorite porphyry.

Quartz diorite: Quartz diorite was identified between the sharp contact of skarn zones. It displays equigranular, phaneritic texture (Figure 3.10 c-d). Medium-to coarse-grained plagioclase (about 80 modal%) is the main mineral and shows partial alteration to sericite. It often exhibits oscillatory zoning. Tabular prismatic crystals of biotite (about 10 modal%) have been mostly replaced by chlorite (Figure 3.10 c-d). Other identified minerals are minor quartz (about 5 modal%) and K-feldspar (about 5 modal%), whereas zircon and apatite are accessory phases.

Dacite porphyry: Dacite porphyry, outcropping as a NE-trending dike, was intersected beneath the Keybet Hill. It displays fine-grained porphyritic texture, where groundmass component is quite abundant. Therefore, this unit was interpreted to represent a shallowly-emplaced sub-volcanic rock. Dacite porphyry is distinguished by the presence of coarse-grained quartz with typical embayed texture (Figure 3.10 e-f). Other phenocrysts include plagioclase, hornblende, and biotite, all set in a groundmass dominated by microcrystalline quartz. Plagioclase shows sericite

(likely illite) alteration. Coarse (up to 1 mm-long), tabular prismatic crystals of hornblende and biotite have also been altered into sericite. Biotite is also opacitized along the rims due to development of Fe-Ti-oxides. Zircon is present as an accessory phase. Dacite porphyry is commonly cut by barren calcite veinlets.

Andesite porphyry dikes: Andesitic dikes with variable thicknesses between 0.2 and 1.5 m were observed as crosscutting the granodiorite porphyry in drill core (Figure 3.10g). These are predominantly composed of a fine-grained, highly chloritized groundmass making up about 60–70% of the sample (Figure3.10h). Ferromagnesian minerals (possibly hornblende) are partially to completely altered into chlorite and pyrite, whereas relict crystals of plagioclase often show chlorite replacement. Quartz phenocrysts are quite low in abundance, which distinguishes this unit from dacite porphyry.

Tonalite porphyry: Tonalite porphyry is observed in drill cores from the Keybet Hill is characterized by porphyritic texture displaying abundant glomeroporphyritic textured plagioclase phenocrysts (about 50 modal%;). Fine to medium grains of tabular hornblende crystals and plagioclase show sericite alteration. The ground mass is composed of fine-grained quartz (about 30 modal%) and hornblende (about 20 modal%), the distinguish feature of the tonalite porphyry is the absence of K-feldspar.

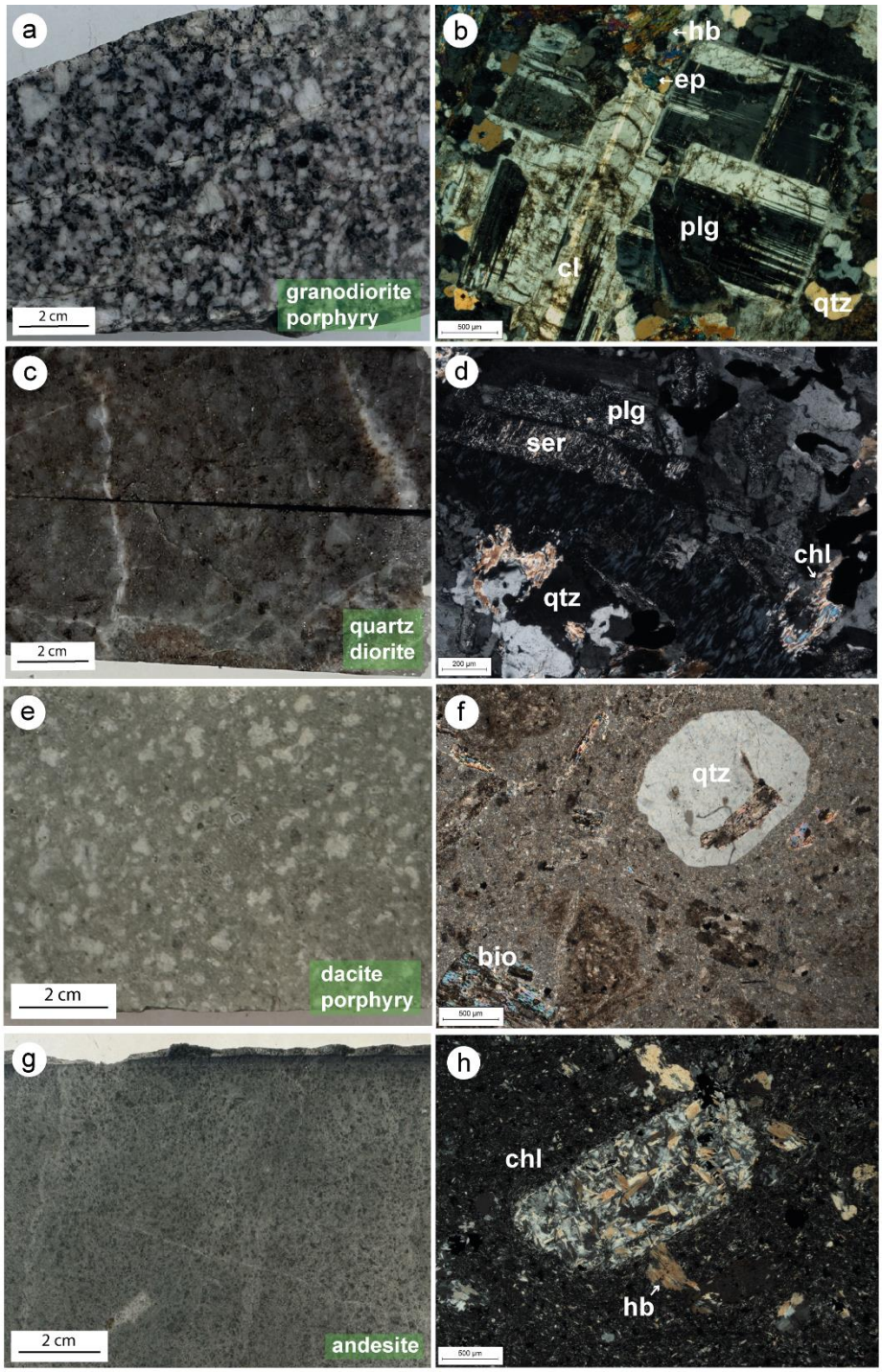


Figure 3.10. a) Drill core photograph of granodiorite porphyry (drill hole: PSD-6, from 78.50 m), b) Microphotograph (XPL, TL image) of clay-altered plagioclase, chloritized hornblende, quartz and epidote (drill hole: PSD-6, from 78.50 m), c) Drill core photograph of quartz diorite (drill hole: PSD-6, from 154.70 m), d) Microphotograph of (XPL, TL image) fine to coarse grained sericite altered

plagioclase, chloritized biotite, and quartz (drill hole: PSD-6, from 154.70 m), e) Drill core photograph of dacite porphyry (drill hole: PSD-16, from 535.80 m), f) Microphotograph (XPL, TL image) of coarse quartz and biotite phenocrystals in fine grained groundmass (drill hole: PSD-16, from 535.80 m), g) Drill core photograph of andesitic dike (drill hole: PSD-6, from 85.50 m), h) Microphotograph (XPL, TL image) of plagioclase phenocryst replaced by chlorite in chloritized groundmass (drill hole: PSD-6, from 85.50 m). Abbreviations: qtz = quartz, bio = biotite, ep =e pidote, plg = plagioclase, hb = hornblende, ser = sericite, chl = chlorite, cl = clay, XPL= cross-polarized light, TL = transmitted light.

3.4 Quaternary Cover Unit

Quaternary alluvial units cover the northeast sector of license. This area is where a magnetic high is delineated, in the southern edge of the Sultansazlığı basin. According to Ulakoğlu (1983), the Quaternary cover unit, namely the Bektaşkeleri Formation, consists of alluvium and local scree deposits with a thickness of up to 125 m. Drill holes completed in the northeastern sector targeting the possible porphyry mineralization around the magnetic high intersected this young sequence. In the drill cores from this sector, the thickness of the alluvium varies between 10 to 125 m. Yellowish-brown alluvium is mainly composed of clay with occasional intervals of gray limestone and weathered granodiorite fragments. The cover unit is underlain by strongly fractured granodiorite, with a transitional zone of alluvium with granodiorite fragments (Figure 3.11).



Figure 3.11. Transition between the Quaternary alluvium and the underlying granodiorite porphyry (drill hole: PSD-8; 105.70 to 111.20 m).

3.5 Structure

A number of faults and fold structures were identified in the Çubuklu district. Bedding is particularly well-developed in the Paleozoic–Mesozoic calcareous sedimentary rocks. Strike directions and dip angles are highly-variable (Figure 3.2), likely due to disruption by nappe emplacement during the Late Mesozoic and early Cenozoic as well as due to repeated fault activity in this seismically-active region. Nevertheless, preferred strike orientations throughout the study area seem to be predominantly in the northeast direction. In northwest of the Keybet Hill, the gently NE- and SW-dipping beds define an anticline. Another antiform structure is similarly recognized in the central area of the southern sector, where beddings exhibit a nearly east to southwest dipping orientation.

Major faults within the study area are NE-SW- and ENE-WSW-trending dextral strike-slip faults with offsets up to 50 meters as identified in the northwest of Keybet Hill (Figure 3.5). In the northeast, an altered andesite porphyry dike exploited a NE-trending fault (040N/69), which juxtaposed it against a highly-deformed limestone unit. Also, steeply-dipping, NE-trending foliation is well-developed within limestone/marble outcrops adjacent to an old Zn-oxide working (Figure 3.12 and 3.13). Along the southwestern extent of this structure, the Carboniferous schists also display a similar foliation.

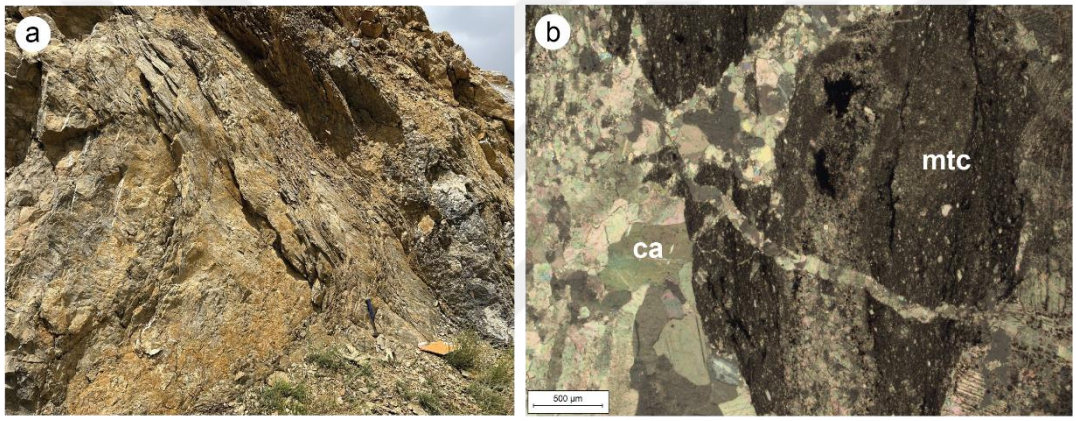


Figure 3.12. a) Outcrop photograph of strongly-deformed limestone with fracture-fill limonite and calcite, b) Microphotograph (XPL, TL image) of micritic limestone including fine-grained quartz cut by late, fine-grained calcite veinlets. Opaque minerals are possibly pyrite or Fe-oxides formed after pyrite. Abbreviations: ca = calcite, mtc = micritic limestone, XPL= cross-polarized light, TL = transmitted light.

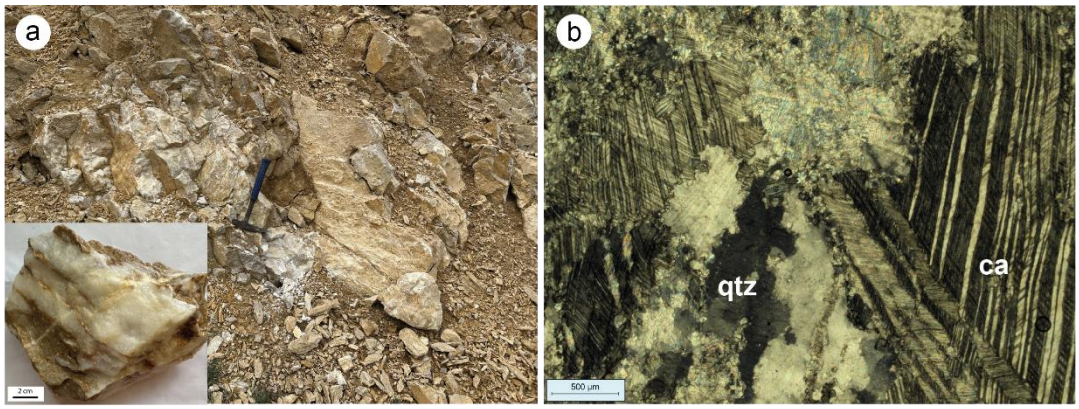


Figure 3.13. a) Outcrop photograph of cream, pale white marble with whitish sugary-textured, coarse-grained calcite bands, b) Microphotograph (XPL, TL image) of fine- to medium-grained, foliated calcite cut by late, narrow calcite veinlets and quartz. Abbreviations: ca = calcite, qtz = quartz, XPL= cross-polarized light, TL = transmitted light.

Deformation related to faulting was also commonly observed in drill core, especially underneath Keybet Hill. Here, a number of faulted contacts were intersected. Such intercepts are characterized by tectonic breccias that are particularly well-developed in the highly competent gray limestone unit. Tectonic breccias have angular to sub-rounded clasts that locally show significant clast rotation and displacement, and therefore they are classified as mosaic breccias (Figure 3.14).

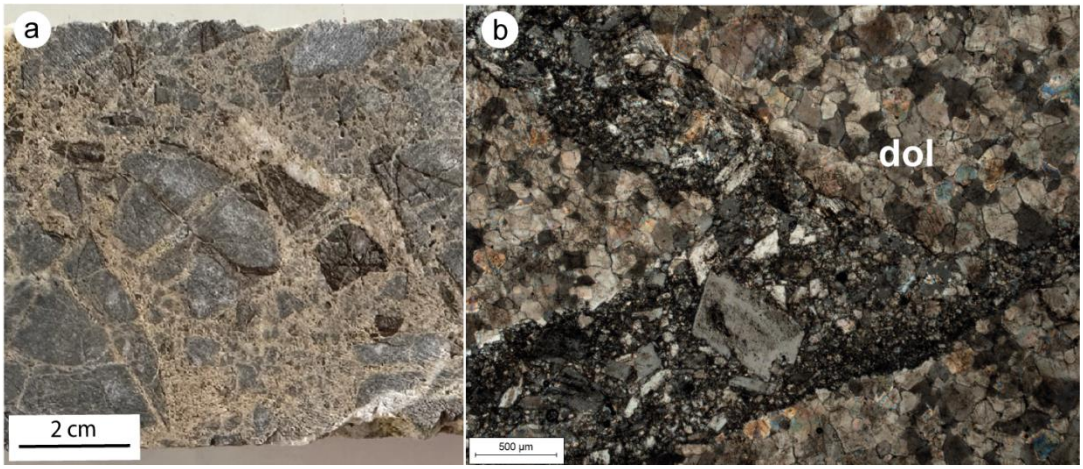


Figure 3.14. a) Drill core photograph of gray, yellowish brown, fine to coarse grained, polymictic, clast supported, fault breccia with carbonate matrix, strongly silicified gray limestone, calcite clasts, and limonite veinlets (drill hole: PSD-16 from 460.80 m) b) Microphotograph of (XPL, TL image) angular to subangular dolomitic clast surrounded by deformed dolomite matrix (drill hole: PSD-16 from 460.80 m). Abbreviations: dol = dolomite, XPL= cross-polarized light, TL = transmitted light..

Apart from these major structures, a prominent faulted contact was noted in several of the drill holes completed in the northeastern sector, underneath the young alluvial deposits of the Sultansazlığı basin. Although well-developed in drill core as evidenced by several meters-long intercepts of clayey fault gouge, the nature of this fault could not be determined due to limited data.

CHAPTER 4

ALTERATION AND MINERALIZATION STYLES AT ÇUBUKLU

The Çubuklu prospect contains three distinct mineralization types, all related to magmatic-hydrothermal processes developed within and around intrusive rocks of the Karamadazı district. The main mineralization types at Çubuklu include the Fe-Cu skarn and Zn-Pb±Cu carbonate-replacement. The third mineralization type is represented by a porphyry Cu-Mo zone, which is a newly recognized mineralization style formerly unknown in the Yahyalı district.

The skarn and carbonate-replacement ores of the Çubuklu show many similarities to other known deposits/prospects of the Yahyalı area. Postallı Madencilik is located between the Özkoyuncu Fe mine, and the Çadırkaya Fe mine with Pb-Zn mineralization. Postallı Madencilik has been operating five underground mines that mainly contain structurally controlled, vein-type Pb-Zn ores that are generally in oxide form. These are: Kurtuluş, with a grade of 6-46% Zn and 1-3% Pb; Diriliş, with a grade of 10-15% Zn and 5-10% Zn; Bereket, with a grade of 10-35% Zn and Postallı underground mine with a grade of 2-12% Zn and 2-12% Pb is connected through Uğur underground mine, grading 5% Zn and Cu 2-14%, where the presence vein type base metal sulfides such as sphalerite+ bornite + chalcopyrite + native Cu mentioned.

Outcrops of the Çubuklu prospect comprise the secondary ore mineral assemblages of malachite, azurite, smithsonite, zincite, cerussite, and hematite, limonite and goethite forming irregular bodies within limestone (Figure 4.1).

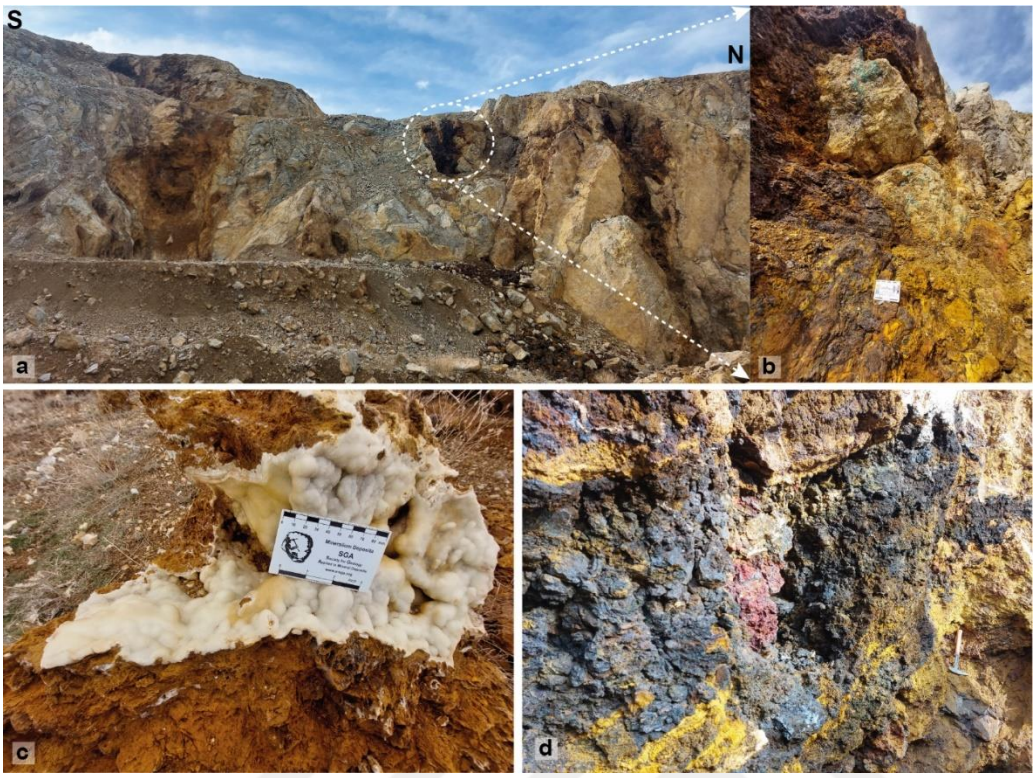


Figure 4.1. a) Outcrop photograph of carbonate hosted irregular zones of secondary ore minerals in the NE part of study area b) The close-up photograph of malachite-limonite-goethite mineralization (from 698344E, 4225954N, UTM Zone 36S), c) smithsonite float, d) Goethite, hematite, limonite and zincite development at the NE part of the study area.

According to the rock sampling results, secondary Cu, Zn, and Pb mineralization occurs in three major domains. These are the northeastern part with high Cu grades; the central part with high Zn, Pb grades in and/or near Postallı Madencilik underground mines; and the southwestern part of area near intrusion stock with high Zn, Pb, and Cu grades (Figures 4.2–4.4).

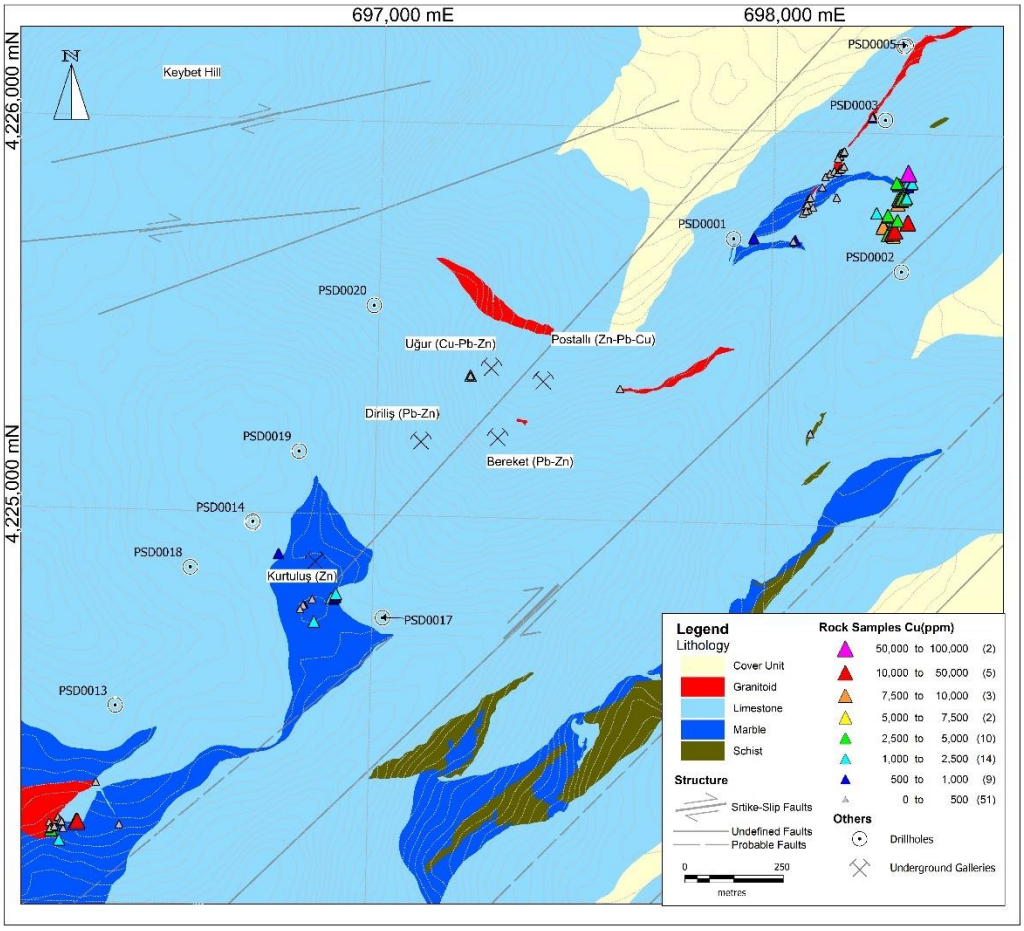


Figure 4.2. Geological map of the Çubuklu prospect showing rock sampling locations and associated Cu grades (in ppm).

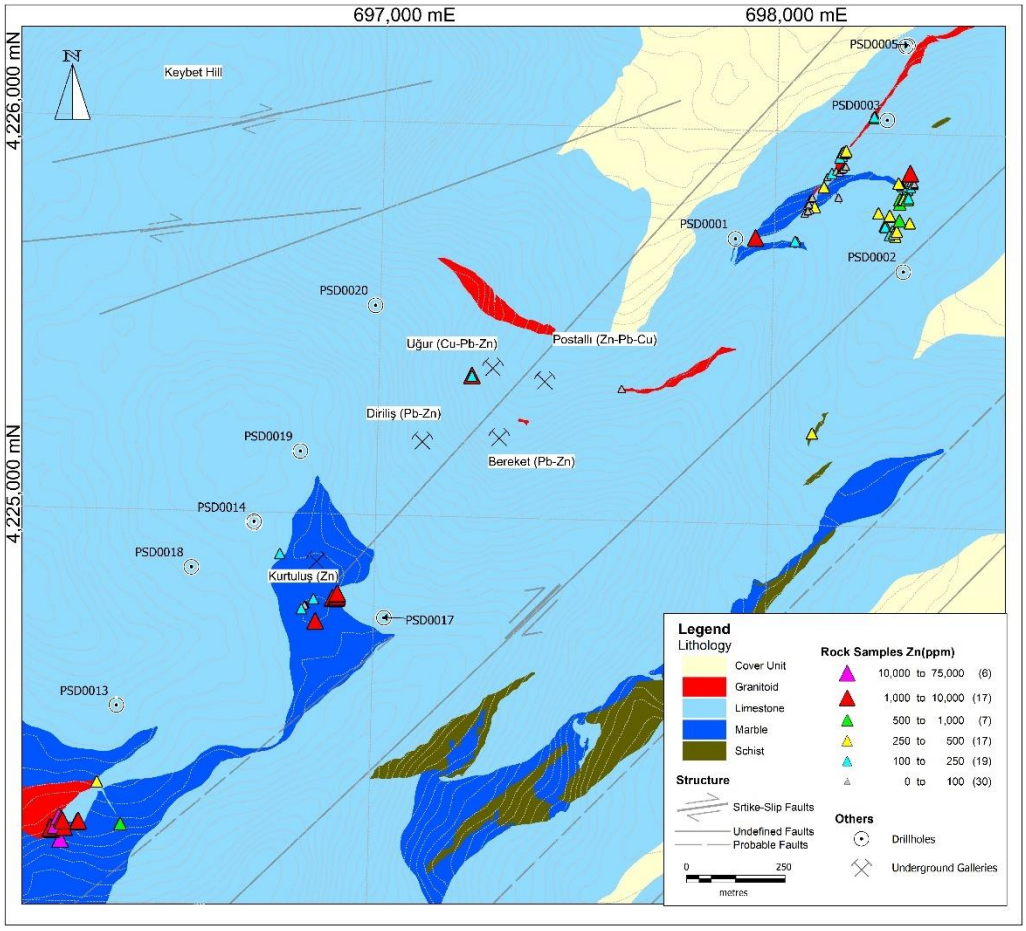


Figure 4.3. Geological map of the Çubuklu prospect showing rock sampling locations and associated Zn grades (in ppm).

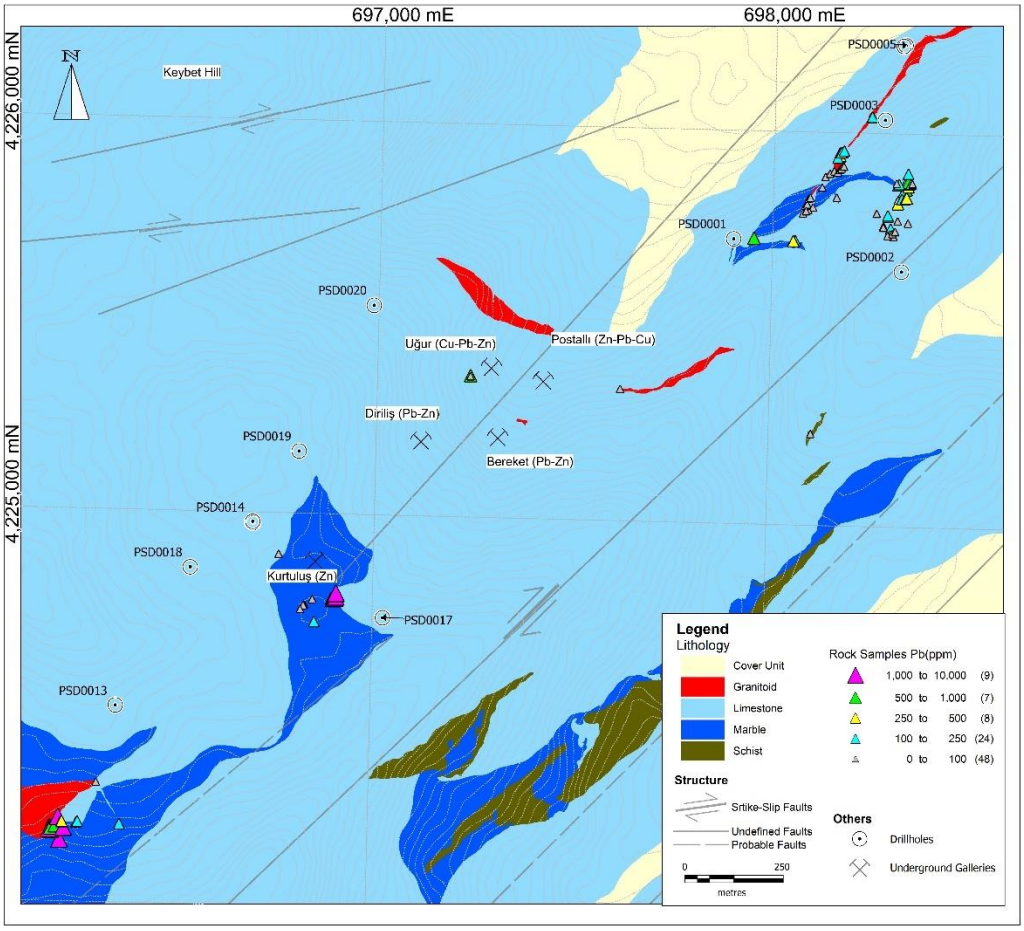


Figure 4.4. Geological map of the Çubuklu prospect showing rock sampling locations and associated Pb grades (in ppm).

Based on surface geochemistry, the northeastern part of the study area and the southwestern intrusion stock stand out with Mo and slightly Cu anomalies. Furthermore, Cu anomalies exhibit a NE-SW trend through the central-western part of the area, while Mo anomalies show more dispersed patterns, possibly related to dike (Figure 4.5 a-b). On the other hand, Zn and Pb anomalies are not found on the NE side; instead, they are mostly concentrated in the southwest part of the study area around the Postallı underground mines, extending through the Çadırkaya Pb-Zn deposit (Figure 4.5 c-d).

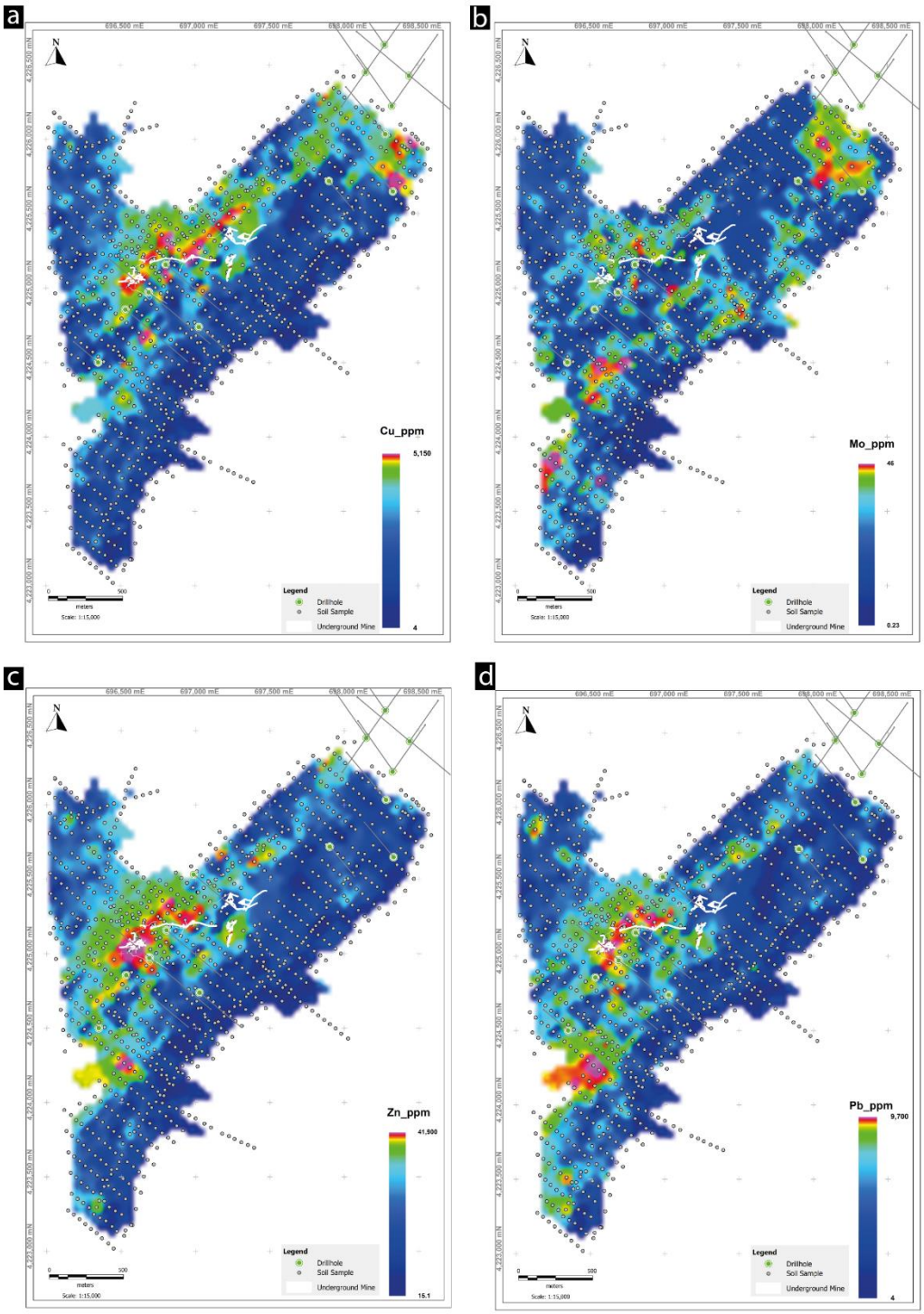


Figure 4.5. Soil geochemistry map of the Çubuklu prospect showing the distribution of a) Cu (in ppm), b) Mo (in ppm), c) Zn (in ppm), d) Pb (in ppm).

Considering surface geochemistry and geophysical surveys, the drilling plan carried out at Çubuklu prospect aims to assess Pb-Zn±Cu ores of Postallı Madencilik, and the high magnetic anomaly in the northeastern region. Consequently, the Çubuklu prospects revealed as porphyry and skarn-style in the NE part, carbonate replacement style in central southwestern part of the study area (Figure 4.6).

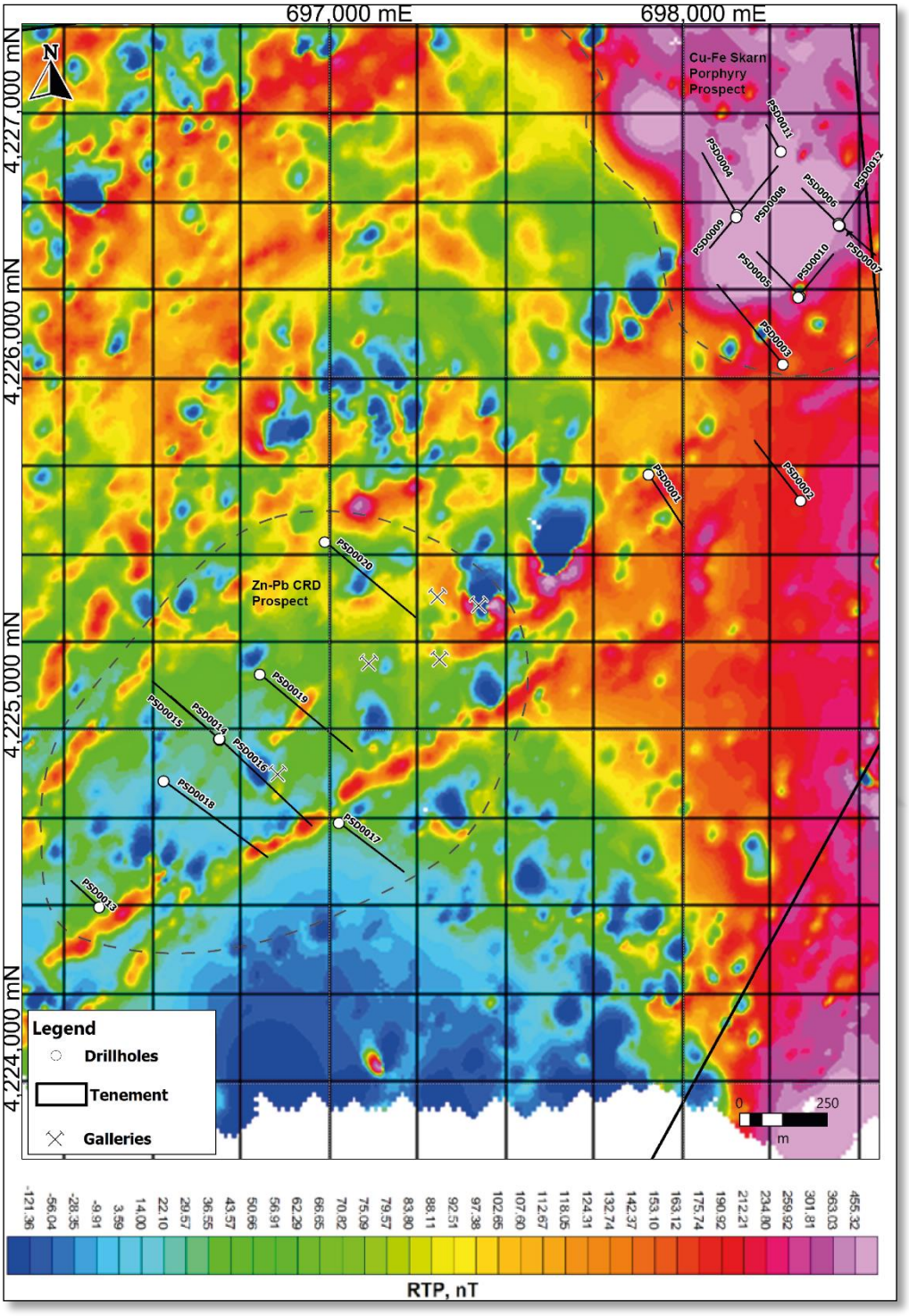


Figure 4.6. The map of Çubuklu license showing Cu-Fe skarn and Cu-Mo porphyry, and Pb-Zn carbonate replacement prospects on ground magnetic map (reduced to pole magnetic anomaly map) and locations of drill holes and Potallı underground mines.

4.1 Skarn-Type Alteration and Mineralization

Skarn-type alteration and mineralization occurs as irregular replacement zones between the Paleozoic–Mesozoic carbonate lithologies and the intrusive rocks of the Karamadazı Granitoid mainly including granodiorite porphyry, quartz-diorite porphyry, and diorite. Skarn mineralization was mainly identified in drill cores from the northeastern part of the tenement. The only visible exposure with a definite skarn alteration was identified at the faulted and highly sheared intrusive limestone contacts again in the northeastern sector (Figure 4.7 a). At this location, the faulted contact contains abundant secondary Fe-(hydr) oxides with relict euhedral garnet largely retrograded into euhedral carbonates (Figure 4.7 b-c). Most skarn alteration and mineralization are localized in this part of the tenement.

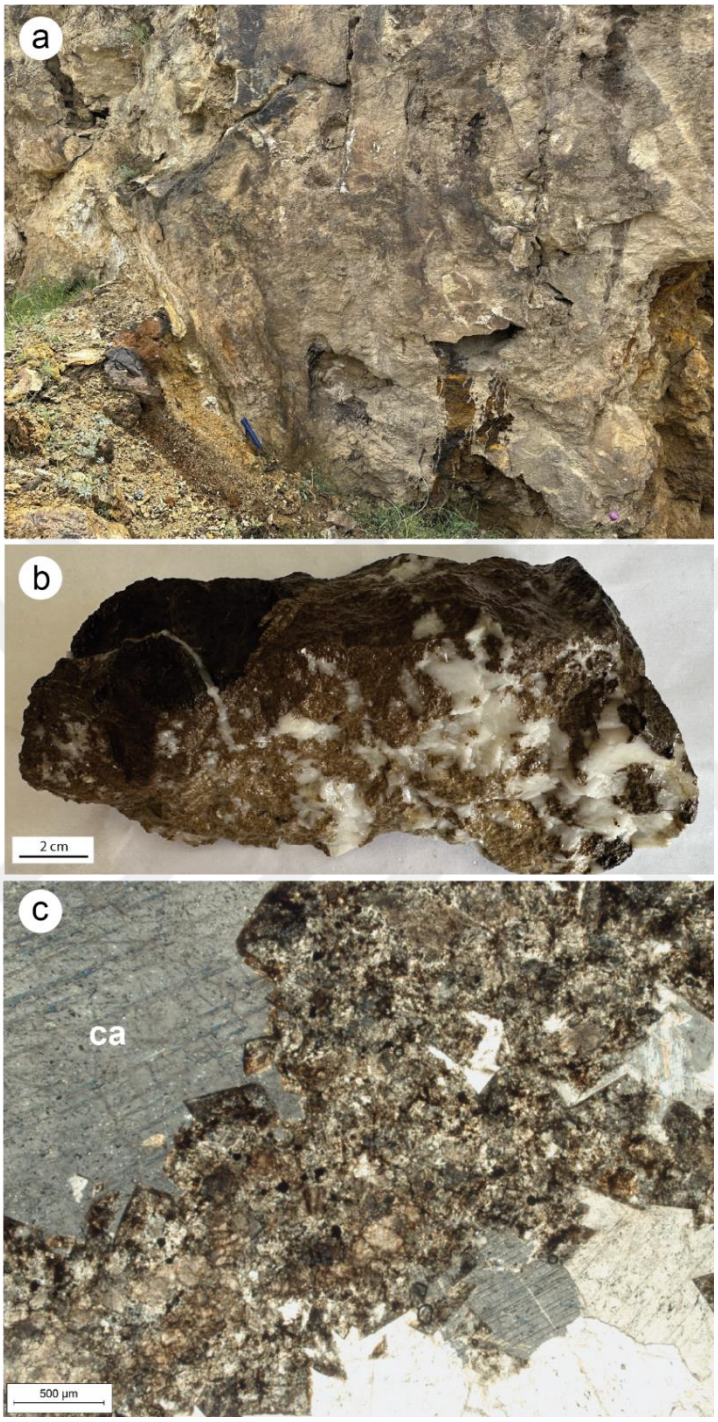


Figure 4.7. a) Outcrop photograph of skarn zone near the intrusion-limestone contact (from 698177E, 4225954N, UTM Zone 36S), b) The macrophotograph of secondary Fe-(hydr)oxides with relict euhedral garnet largely retrograded into euhedral carbonates, c) Microphotograph (XPL, TL image) of coarse-grained calcite (up to 4 mm long) cut by a vein with dolomite (rhombohedral crystals) infill. Abbreviations: ca = calcite, XPL= cross-polarized light, TL = transmitted light.

4.1.1 Endoskarn

Endoskarn is locally well-developed in the intrusive lithologies along narrow intervals in drill core. It is distinguished by altered igneous rocks that still partly retain their igneous textures but are largely modified mineralogically due to intense metasomatic alteration, which occurs as vein and pervasive replacement (Figures 4.8a and 4.9 a).

Endoskarn is characterized by the presence of medium- to coarse-grained, euhedral garnet and fine to medium-grained clinopyroxene (Figures 4.8 b and 4.9 b-c). Aggregates of fine- to medium-grained garnet exhibit oscillatory or sector zoning (Figure 4.8 b). These are possibly grandite in composition. However, most garnets have been replaced by retrograde minerals such as fine-grained aggregates of sericite and prehnite, and locally by chlorite (Figure 4.8 b-c). Therefore, garnet was only identified as rare relict crystals in the endoskarn zone. The selective replacement of feldspar by minor sericite, ferromagnesian minerals by epidote and chlorite occurs along with pyrite mineralization as well as frequent calcite veinlets (Figure 4.8 d).

Two distinct types of garnets were noted in the skarn assemblages. Early garnets (grt-I) are generally medium-grained (Figure 4.9 b-c). Later, coarser, anisotropic garnets with oscillatory or sector zoning (grt-II) were observed as cross-cutting the early isotropic garnets in the sharp contact between pervasively altered endoskarn and exoskarn represented by serpentine, and calcite veinlet with opaque minerals (Figure 4.9 a-e). In the endoskarn, clinopyroxene, alongside minor epidote and quartz, mainly replace tabular prismatic amphibole (Figure 4.9 b-c) in the igneous protoliths.

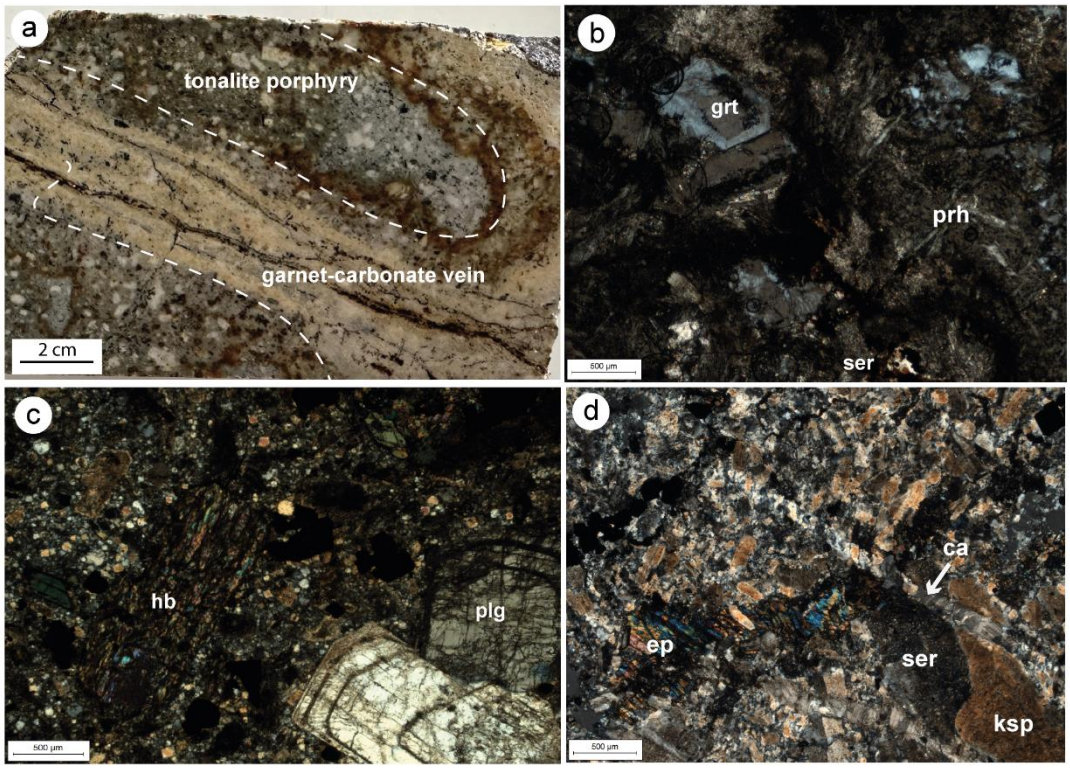


Figure 4.8. a) Drill core photograph of gray tonalite porphyry cut by beige garnet-calcite vein (drill hole: PSD-20, 60.10 m) b) Microphotograph (XPL, TL image) of oscillatory-zoned garnet and radial prehnite (drill hole: PSD-20, 60.10 m), c) Microphotograph (XPL, TL image) of completely sericitized hornblende within a quartz-dominant groundmass alongside coarse-grained plagioclase and pyrite (opaque crystals) (drill hole: PSD-20, 60.10 m), d) Microphotograph (XPL, TL image) of fine- to coarse-grained, sericitized K-feldspar phenocrysts cut by a calcite veinlet, probable mafic minerals altered into epidote, cubic opaque minerals possible pyrite (drill hole: PSD-6, 125.80 m) Abbreviations: grt = garnet, prh = prehnite, hb = hornblende, plg = plagioclase, ep = epidote, ksp = K-feldspar, ser = sericite, ca = calcite, XPL= cross-polarized light, TL = transmitted light.

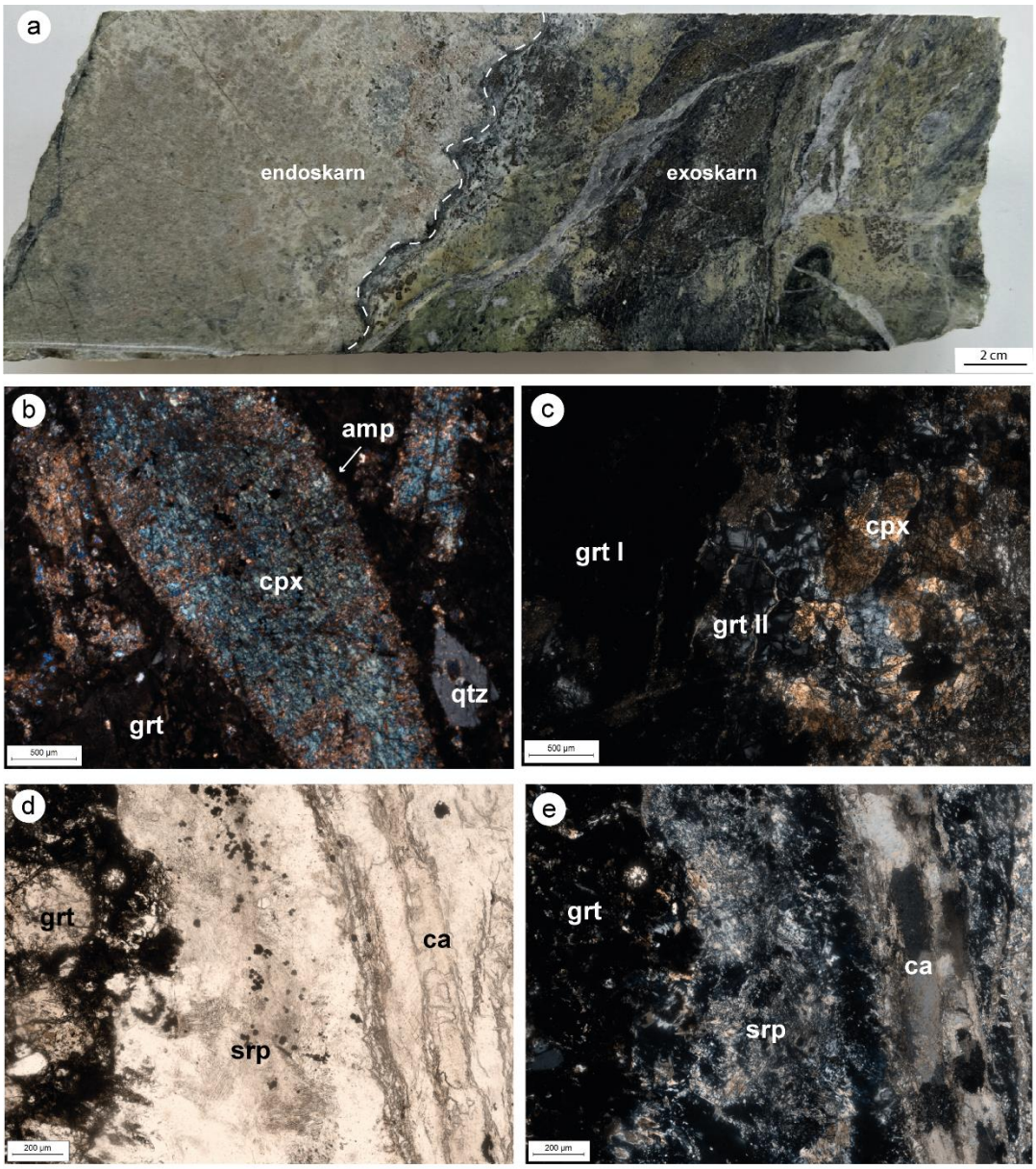


Figure 4.9. a) Drill core photo of the endoskarn-exoskarn contact (PSD-6, from 57.70 m), b) Microphotograph (XPL, TL image) of coarse amphibole replaced by clinopyroxene, c) Microphotograph (XPL, TL image) of isotropic garnet I cut by anisotropic garnet II veinlet d) Microphotograph (PPL, TL image) of the contact between endoskarn and exoskarn zone), e) Microphotograph (XPL, TL image) of endoskarn-exoskarn transition. Abbreviations: amp = amphibole, grt = garnet, cpx = clinopyroxene, qtz = quartz, srp = serpentine, ca = calcite, XPL= cross-polarized light, TL = transmitted light, PPL = plane-polarized light.

4.1.2 Exoskarn

In the Çubuklu prospect, exoskarn is better developed compared to endoskarn, but these also developed in mostly narrow intervals up to 50 meters thick. Two very distinct exoskarn types were identified. Magnesian exoskarn rocks are characterized by metasomatic alteration of dolomitic sedimentary rock. Calcic exoskarn, on the other hand, were primarily developed in sedimentary protoliths dominated by calcium carbonate, rather than dolomite.

Calcic exoskarn: Rare zones of calcic exoskarn were developed due to metasomatic alteration of the calcium carbonate-rich layers of mainly the organic-rich limestone lithologies, and rarely in marble (Figure 4.10 a-c). Finely-laminated lithologies have been altered into fine-grained, subhedral, isotropic garnet overprinted by an assemblage of chlorite, pyrite, and minor magnetite alongside rare tremolite (Figure 4.10 b-d). Wollastonite, a typical calc-silicate mineral that occurs in distal calcic exoskarn, near the marble front, was not observed in Çubuklu. This is likely due to the relatively low abundance of Ca-rich lithologies at the property area.

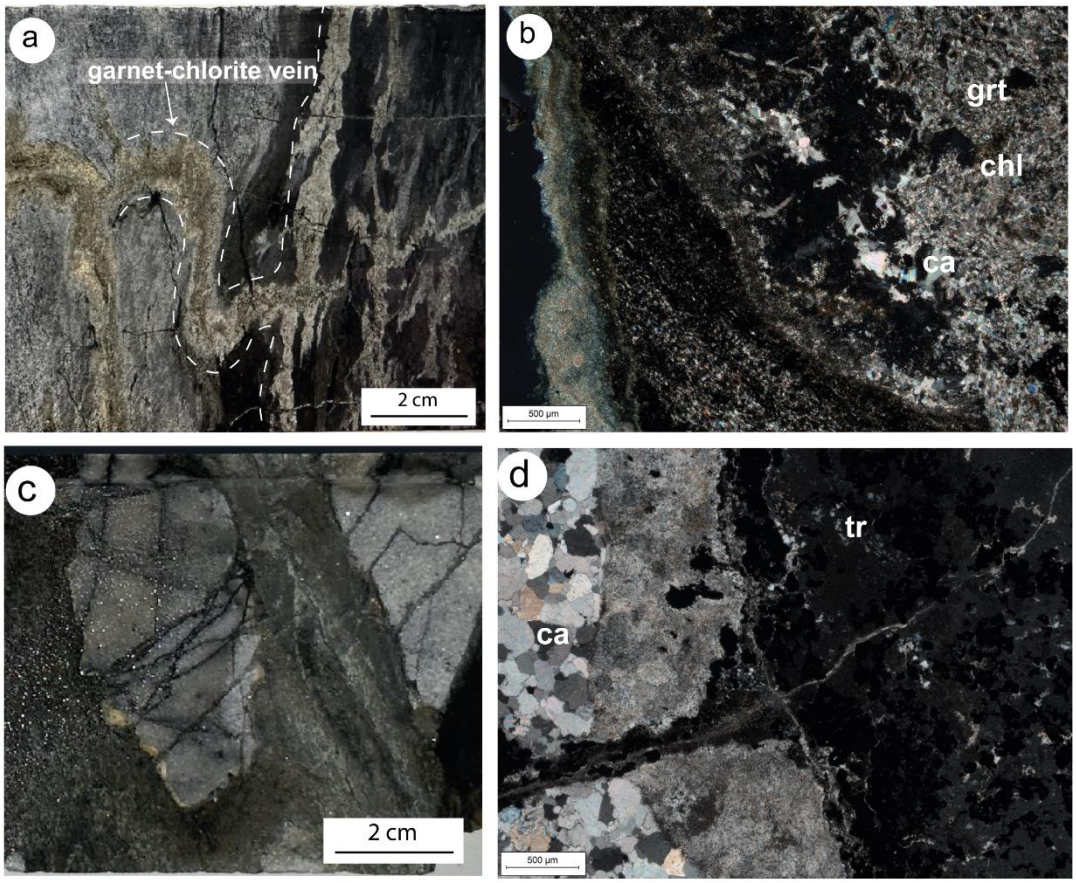


Figure 4.10. a) Drill core photograph of black limestone cut by garnet-chlorite vein (drill hole: PSD-20, from 94.30 m), b) Microphotograph (XPL, TL image) of fine-grained isotropic garnet, chlorite, and carbonate (drill hole: PSD-20, from 94.30 m), c) Drill core photograph of whitish cream marble with stockwork magnetite-pyrite veinlets (drill hole: PSD-6, from 370.50 m), d) Photomicrograph (XPL, TL) of interlocking, equigranular, fine-grained calcite cut by with opaques, and fine grained tremolite (drill hole: PSD-6, from 370.50 m) Abbreviations: grt = garnet, chl = chlorite, ca = calcite, tr = tremolite, PPL = plane-polarized light.

Magnesian exoskarn: Magnesian exoskarn is better and more widely developed at Çubuklu compared to calcic exoskarn owing to the dolomitic nature of the surrounding carbonate lithologies (Figure 4.11 a-c). Forsterite was probably the dominant skarn mineral at the prograde stage. However, in most samples it has been retrograded into lower temperature, hydrous minerals, and so was only observed as a relict phase. Retrograde alteration primarily produced lizardite as a magnesium silicate hydroxide member of serpentine group, after forsterite as fine to medium grains (up to 2.5 mm) (Figure 4.11 b-d). Apart from replacing forsterite crystals, significant serpentine was also identified as vein infill. Serpentine-rich veins are generally up to 1.5 mm thick and are wispy in nature. Talc was also identified locally and was possibly developed through further hydration of serpentine. Other retrograde minerals in this alteration type include chlorite, tremolite, and calcite. In magnesian exoskarn, chlorite is typically colorless and have gray to white interference colors, suggesting a Mg-rich composition in keeping with the magnesian nature of the skarn. Pyrite and magnetite are generally abundant in this domain. Samples of magnesian exoskarn in which original bedding is retained have well-developed bands of medium- to coarse-grained pyrite and magnetite. A sequence of exoskarn zone exhibits transition of thinly calcite-sulfide-magnetite fractured marble, marble, and black limestone (Figure 4.12).

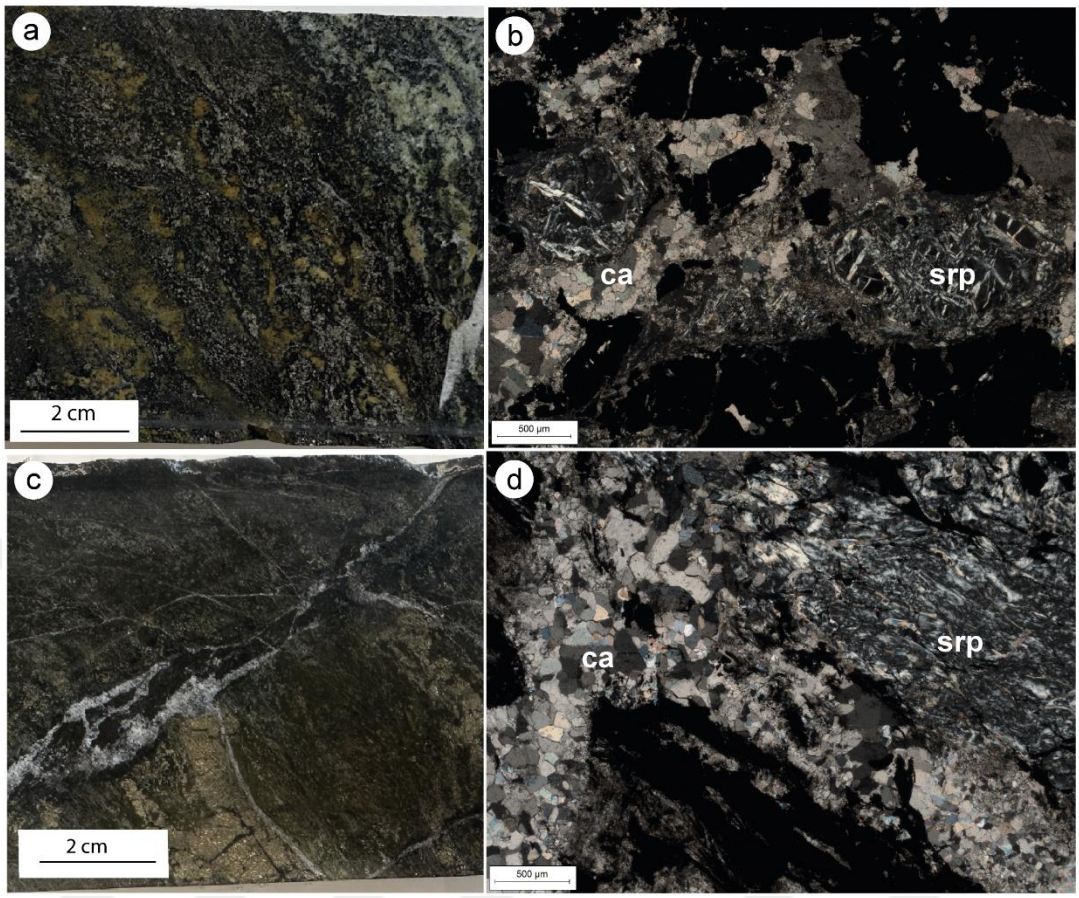


Figure 4.11. a) Drill core photograph of exoskarn rock (drill hole: PSD-6, from 60.60 m), b) Microphotograph (XPL, TL image) of serpentine exhibiting mesh texture, surrounded by fine grained calcite, and opaques composing of magnetite and sulfide (drill hole: PSD-6, from 60.60 m), c) Drill core photograph of banded exoskarn rock but by late calcite veinlets (drill hole: PSD-6, from 125.80 m), d) Microphotograph (XPL, TL image) of serpentine, surrounded by opaques composing of magnetite-sulfide cut by late calcite veinlets (drill hole: PSD-6, from 125.80 m). Abbreviations: ca = calcite, srp = serpentine, XPL= cross-polarized light, TL = transmitted light.



Figure 4.12. Core box photograph of exoskarn, marble, black limestone transition (drill hole: PSD-6, from 415.60 m to 422.50 m).

At Çubuklu, both magnesian and calcic skarn zones contain weak Fe-Cu skarn mineralization. Endoskarn, on the other hand, is largely barren, and thus have no economic significance. The main ore mineralization of Çubuklu skarn consists of pyrite, chalcopyrite, magnetite, all appear to develop during retrograde alteration. Minor oxidation resulted in formation of limonite and hematite. Typically, high intensity mineralization of magnesian-exoskarn rock exhibiting mostly abundance of pyrite (25%)-magnetite (20%)-chalcopyrite (%1), respectively, as pervasive, and banded form (Figure 4.13 a-c-e). Fine- to medium-grained pyrite seems to be early in the paragenesis, and is locally cut by fine-grained, granular magnetite. Minor chalcopyrite is present as enveloping earlier pyrite and magnetite (Figure 4.13 e). In calcium carbonate-rich marble, both magnetite and chalcopyrite occur in lesser amounts compared to magnesian exoskarn (Figure 4.13 b-d-f). Disseminated mineralization primarily comprises fine- to medium-grained pyrite, where small

inclusion of chalcopyrite is present along with rare fine-grained magnetite mineralization (Figure 4.13 f).

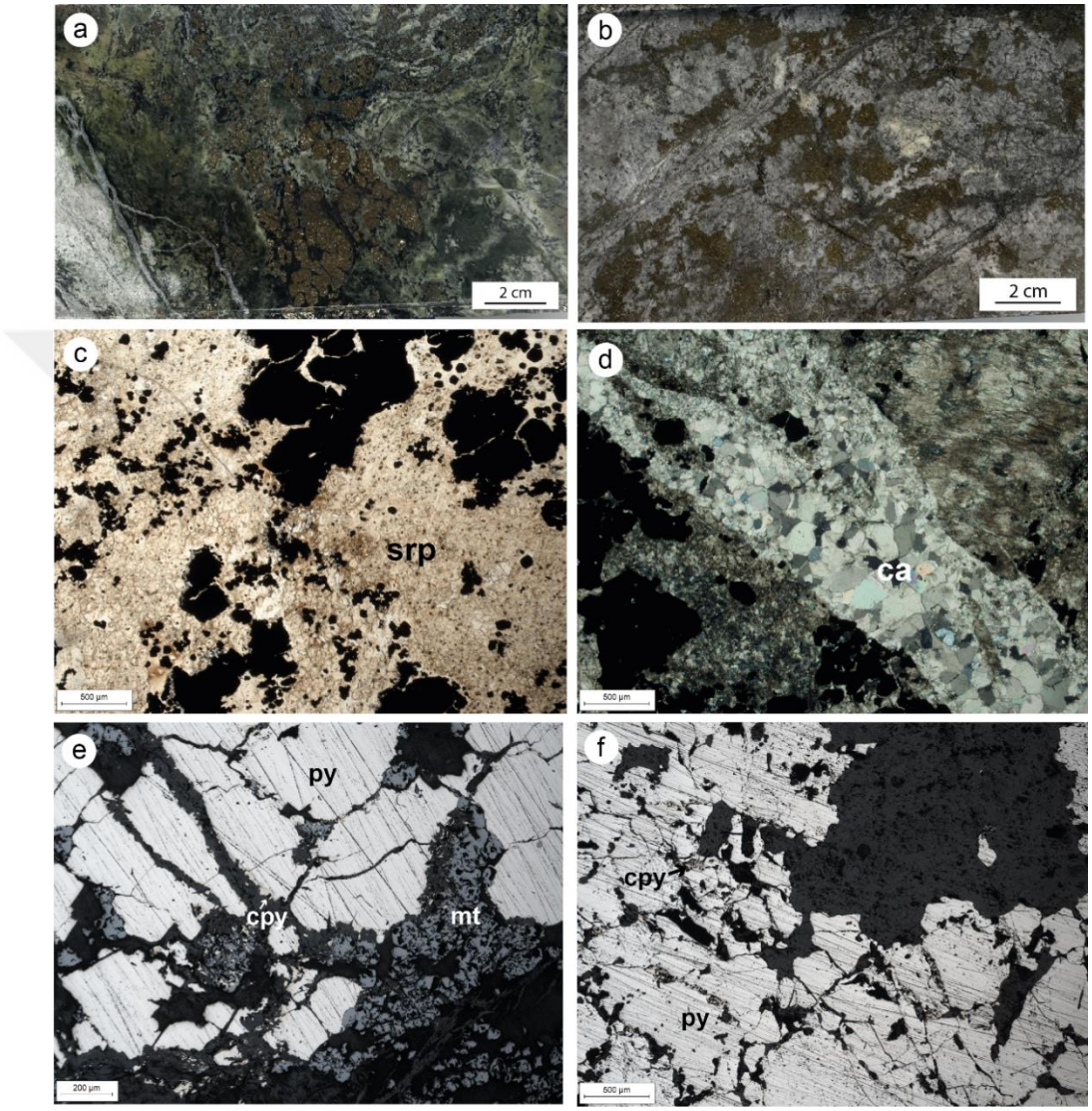


Figure 4.13. a) Drill core photograph of magnesian exoskarn rock (drill hole: PSD-6, from 56.60 m) b) Drill core photograph of calcic exoskarn rock (drill hole: PSD-6, from 105.10 m), c) Microphotograph (PPL, TL image) of serpentine and opaque minerals in magnesian skarn (drill hole: PSD-6, from 56.60 m) d) Microphotograph (XPL, TL image) of calcite veinlets in marble (drill hole: PSD-6, from 105.10 m), e) Microphotograph (XPL, RL image) of fine to medium grains of subhedral pyrite, cut by magnetite replacing serpentine, trace amount of chalcopyrite inclusion (drill hole: PSD-6, from 56.60 m), f) Microphotograph (XPL, RL image) of fine to

medium subhedral to euhedral pyrite with tiny inclusion of chalcopyrite (drill hole: PSD-6, from 105.10 m). Abbreviations: ca = calcite, srp = serpentine, mt = magnetite, py = pyrite, cpy = chalcopyrite, XPL= cross-polarized light, PPL = plane-polarized light, TL = transmitted light, RL= reflected light.

Vein-type mineralization of calcium carbonate-rich marble also mainly contains anhedral to subhedral, fine-grained pyrite, along with trace amount of chalcopyrite and magnetite, where chalcopyrite occurs as inclusions in pyrite (Figure 4.14).

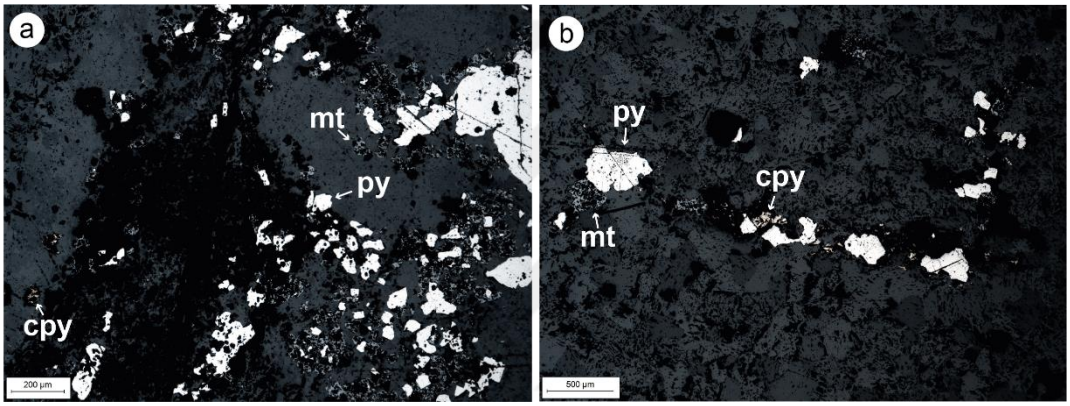


Figure 4.14. a) Microphotographs (XPL, RL image) of (drill hole: PSD-6, from 370.50 m) a) Anhedral to subhedral pyrite, magnetite, and disseminated chalcopyrite, b) Chalcopyrite inclusions in pyrite Abbreviations: mt = magnetite, py = pyrite, cpy = chalcopyrite, XPL= cross-polarized light, RL= reflected light.

Where mineralization occurs in organic-rich, dark colored calcareous lithologies, at least three distinct pyrite types were identified. Early pyrite (pyrite I) is represented by fine-grained diagenetic pyrite. These may occur as framboidal crystals or as euhedral, cubic crystals likely formed through recrystallization of framboidal pyrite (Figure 4.15 a). A later phase of pyrite (pyrite-II) is found as fine-grained, clusters of anhedral crystals with abundant gangue and lesser chalcopyrite inclusions. Late-stage pyrite (pyrite-III) on the other hand, is distinguished by medium-grained, cubic/pyritohedron crystals that are inclusion free. These pristine pyrite crystals

(pyrite-III) were most probably formed following a later recrystallization event at the study area (Figure 4.15 b-c). The paragenetic sequence of skarn type of mineralization of the Çubuklu prospect is provided in Figure 4.16.

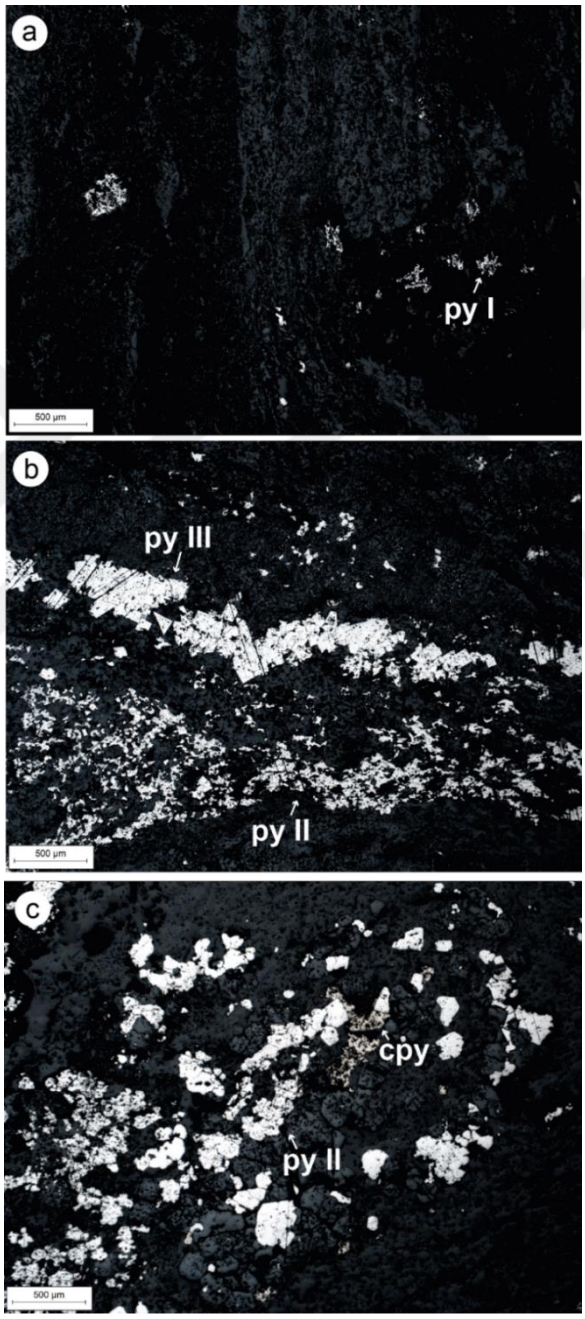


Figure 4.15. Microphotographs (XPL, RL image) of (drill hole: PSD-20, from 94.30 m), a) Fine disseminations of framboidal pyrite I crystal, b) Fine grained anhedral

clusters pyrite II, and pyrite III exhibiting perfectly fine grains of euhedral crystals c) Fine grained anhedral clusters with trace amount of chalcopyrite as inclusions Abbreviations: cpy = chalcopyrite, py = pyrite, XPL= cross-polarized light, RL= reflected light.

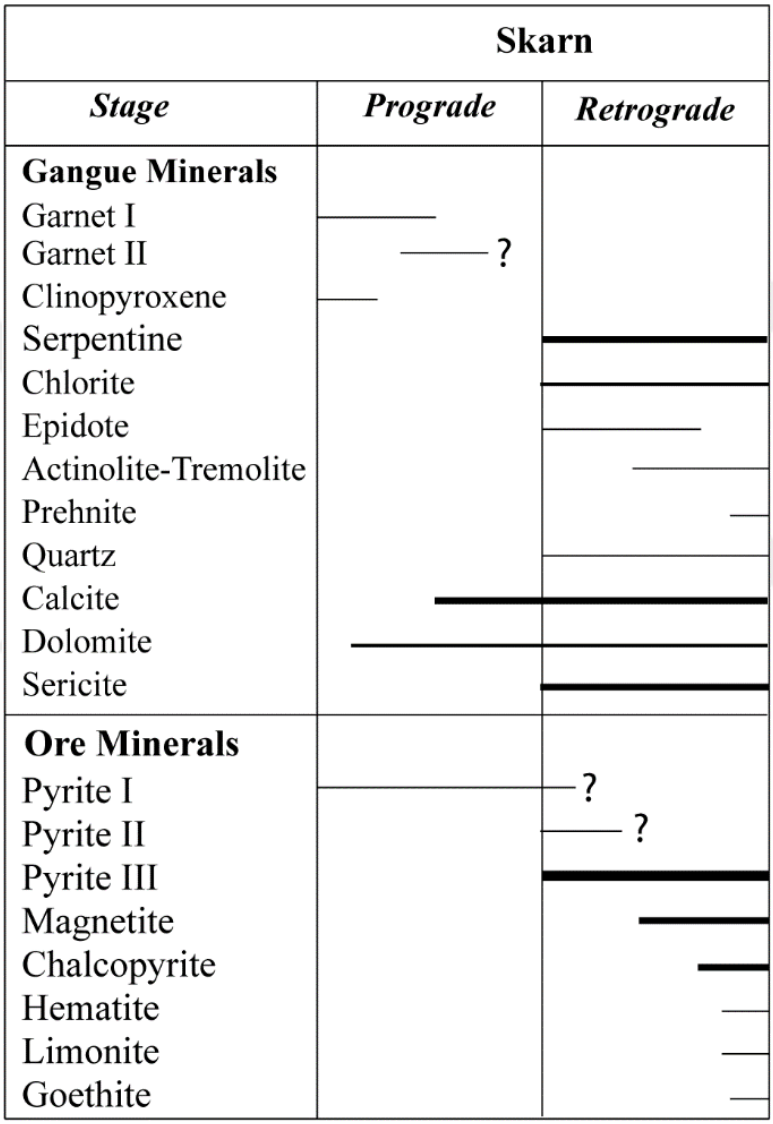


Figure 4.16. The paragenetic sequence of skarn-type alteration and mineralization at the Çubuklu prospect.

One of the best representative drill holes based on the rock type and alteration variability (PSD-6), mainly consists of a total of 110 meters-long magnesian exoskarn with a variable abundance of magnetite-chalcopyrite-pyrite mineralization. It exhibits an irregular contact with nearly a 120-meter-long sericite-chlorite altered primarily granodiorite, and rare monzodiorite. At a depth of 344 meters, there is a nearly 70-meter-long marble with low-intensity pyrite-chalcopyrite and magnetite mineralization in contact with metasedimentary rocks composed of dolomite-graphite, continues with barren marble.

The close association of copper and iron grade with magnesian exoskarn rocks is illustrated as a downhole plot of representing copper (ppm), and iron (pct) grades versus associated rock type and depth (Figure 4.17).

Short intercepts of Cu (ppm) are listed below (Table 1), including 9.3 meters grading 2733 ppm Cu, maximum of 5239 ppm Cu over a one-meter-long interval at 59.50 m; 9.8 meters-long interval with 3349 ppm copper grade, maximum of 5802 ppm Cu over a one-meter-long interval at depth of 183.40 m; 2.6meters grading 4739 ppm Cu, maximum of 5573 ppm Cu over a one-meter-long interval at 341.10 m depth.

Table 1. Significant intercepts of drill hole: PSD-6.

HOLE ID	**From (m)**	**To (m)**	**Length (m)**	**Intercept (ppm)**
PSD-6	54.8	64.1	9.3	2733ppm Cu
	182.7	192.5	9.8	3349ppm Cu
	341.4	344	2.6	4739ppm Cu

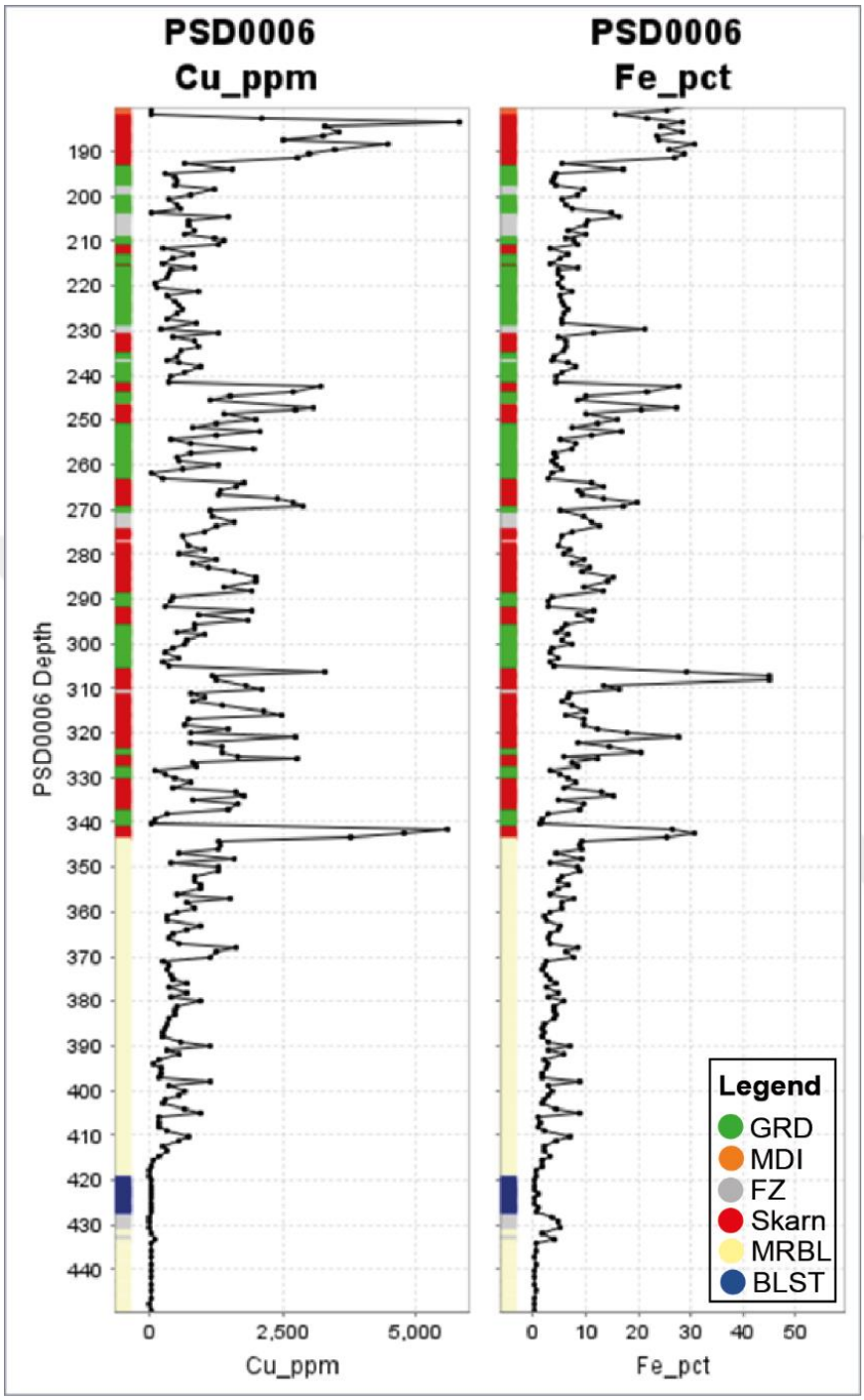


Figure 4.17. The downhole plot of PSD-6 representing Cu (ppm) and Fe (%) grades versus depth and rock type (GRD: granodiorite porphyry; MDI: monzodiorite; FZ: fault zone; Skarn: Exoskarn; MRBL: marble; BLST: black limestone).

4.2 Carbonate-Replacement-Style Alteration and Mineralization

Carbonate-replacement-style alteration and mineralization of the Çubuklu district is mainly hosted by a compositionally heterogeneous carbonate sequence. Unlike skarn ores, carbonate-replacement Pb-Zn±Cu ores are found away from the intrusive contacts and are strictly stratabound in nature. This mineralization style is associated with distinct alteration types readily including dolomitization and silica replacement of the host carbonate lithologies, where dissolution and hydrothermal breccias are commonly widespread.

Main carbonate-replacement mineralization occurs within the dolomitized, dark colored (black) limestone sequence. An approximately 4 meters-long intercepts of dark gray, fine- to coarse-grained, polymictic breccia composed of angular to sub-angular dolomite, sulfide (primarily pyrite), and other lithic clasts host the mineralization (Figure 4.18).

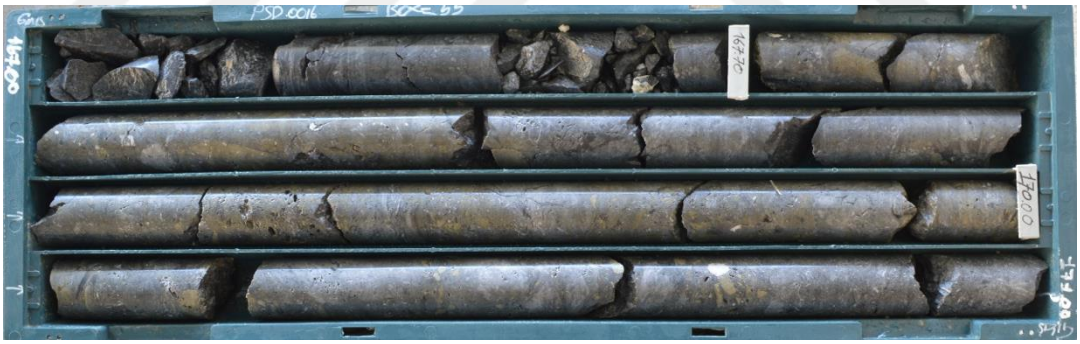


Figure 4.18. Drill box photograph of polymictic breccia (drill hole: PSD-16, 167.00 to 171.00 m).

Dolomitization is the most common alteration developed in close association with carbonate-replacement zones. This is most easily distinguished in dark gray-black limestone as this unit is originally composed of abundant calcite rather than dolomite (Figure 4.20). Consequently, dolomitization (and attendant brecciation) of this protolith directly signifies presence of hydrothermal activity in relation to carbonate-replacement-type mineralization. In the dolomitized breccias, the clasts originally made up of micritic calcite, have been completely transformed into hydrothermal dolomite, surrounded by a dolomite matrix and sulfides (Figure 4.19 a-b).

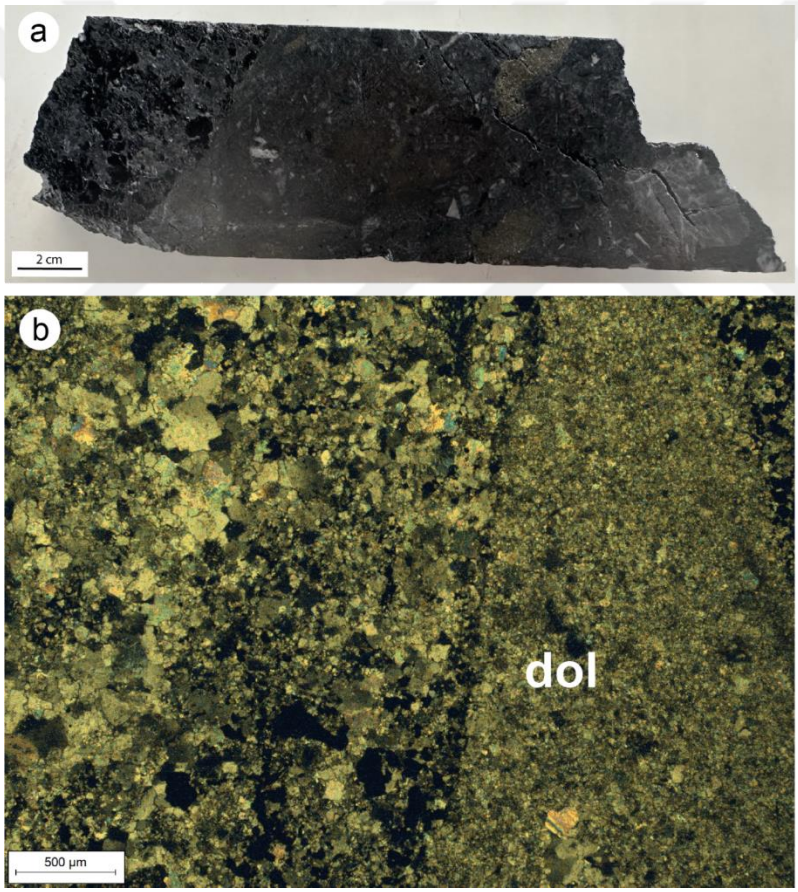


Figure 4.19. a) Drill core photograph of dolomitized, sulfidic breccia (drill hole PSD-16, from 168.50 m), b) Microphotograph (XPL, TL image) of angular dolomite clast surrounded by dolomite matrix with opaque minerals that are primarily pyrite (drill hole: PSD-16, from 168.50 m). Abbreviations: dol = dolomite, XPL= cross-polarized light, TL = transmitted light.

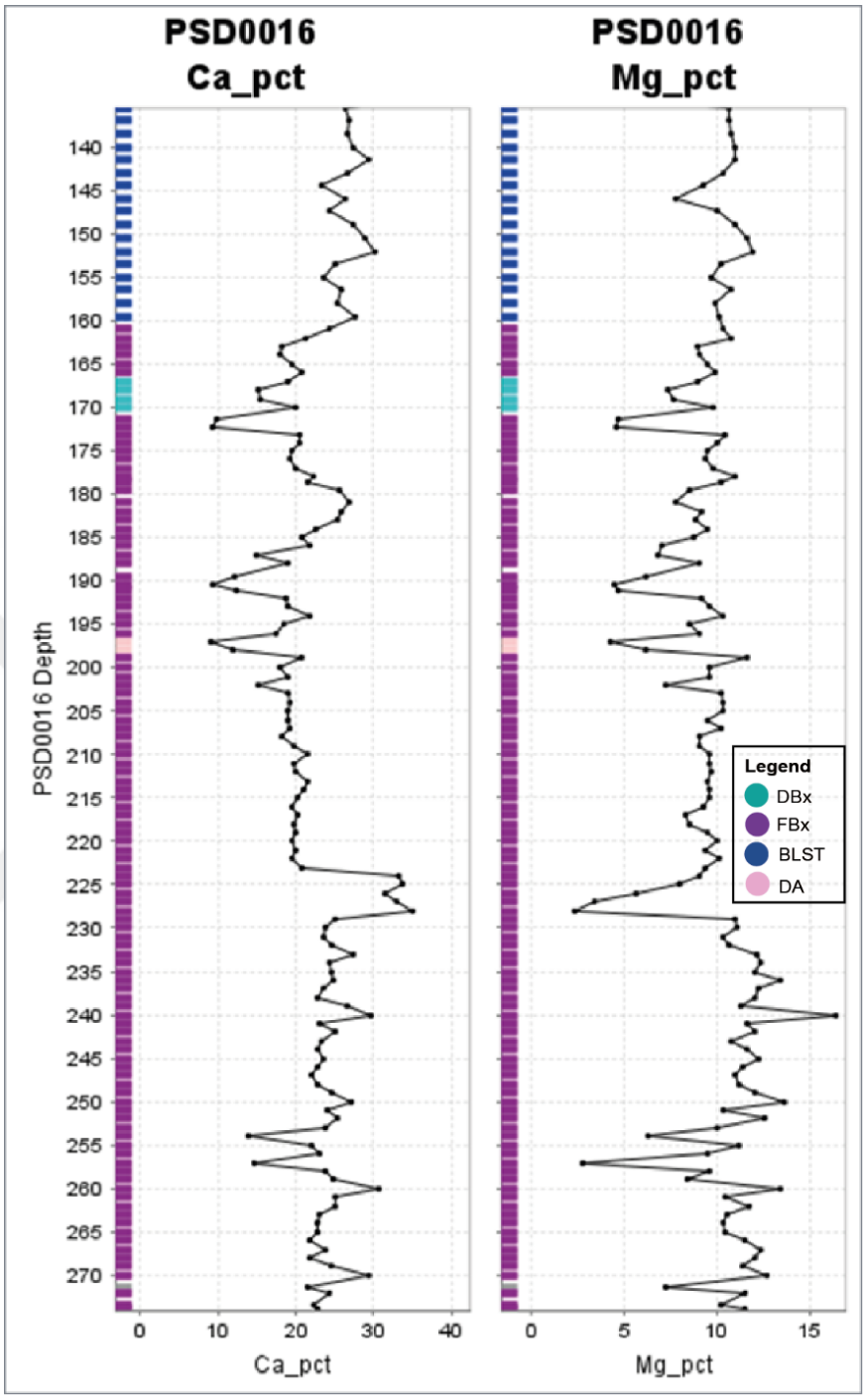


Figure 4.20. The downhole plot of drill hole PSD-16 representing Ca (%) and Mg (%) versus rock type and depth (DBx: Dolomite matrix breccia; FBx: Fault breccia; BLST: Black limestone; DA: dacite porphyry).

Altered and mineralized breccias have dolomite-rich matrices that also contain disseminated pyrite, sphalerite, galena, chalcopyrite, and rare tetrahedrite and covellite (Figure 4.21 a). The most abundant sulfide mineral is pyrite (up to about 30–40 vol.%) occurring both as pyritic clasts and also in the matrix. Pyrite in the clasts contains aggregates of pyrite that show textural evidence for cataclastic deformation (Figure 4.21 e). Pyrite in the breccia matrix, on the other hand, is coarser-grained and occurs as subhedral to euhedral disseminations (Figure 4.21 b-c-f). These euhedral pyrites are likely products of recrystallization from earlier fine-grained pyrite.

Disseminations of sphalerite are reddish to brownish in color under transmitted light, suggesting Fe-rich compositions. They occur in the breccia matrix as well with an average abundance in well-mineralized intervals of about 5%. Sphalerite commonly envelopes pyrite or fills the fractures within pyrite (Figure 4.21 b). Additionally, it typically contains tiny blebs of chalcopyrite (chalcopyrite disease texture), suggesting replacement by chalcopyrite (Figure 4.21 b-c). The abundance of chalcopyrite is about 1–2 vol.%.

Minor tetrahedrite is a late replacement product after chalcopyrite and occurs along microfractures within this mineral (Figure 4.21 d). Trace covellite was also detected as a replacement mineral after chalcopyrite and possibly tetrahedrite. The absence of secondary Fe-(hydr) oxide minerals such as hematite and goethite as well as of secondary Cu minerals in the mineralized breccia intervals indicates that covellite was likely formed through hypogene oxidation of the mineralizing fluids, and that it is not a supergene phase (Figure 4.21 e). Sparse galena was also detected in the breccias but its timing within the ore paragenesis is not clear as it does not exhibit any cross-cutting relationship to other sulfide minerals (Figure 4.21 f). Thus, a simple ore paragenesis was established as early pyrite, first followed by sphalerite (galena?), then by chalcopyrite, and late tetrahedrite and covellite.

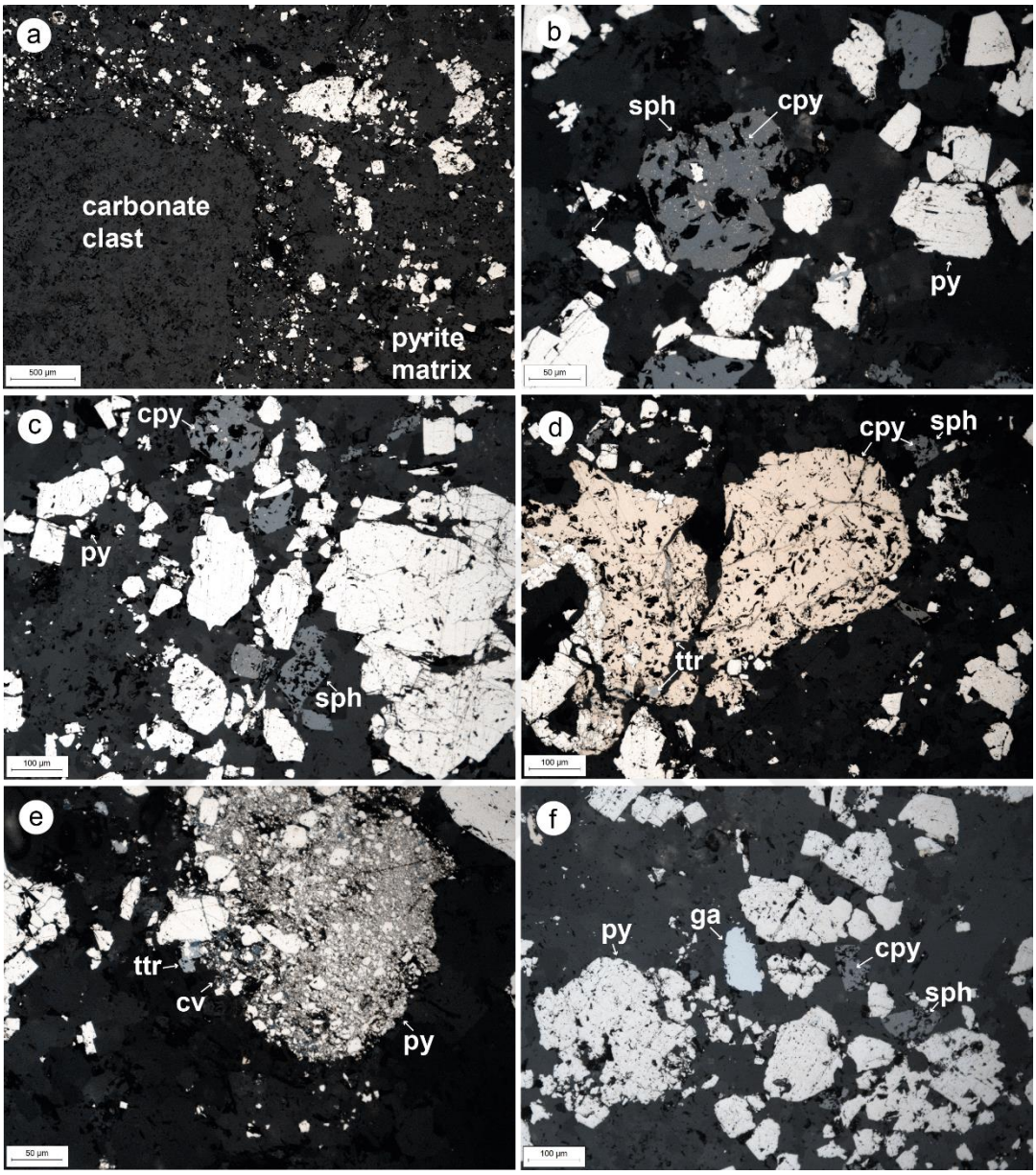


Figure 4.21. Microphotographs (XPL, RL image) of a) Fine grained pyrite dissemination in matrix , b) Sphalerite displaying chalcopyrite disease and pyrite inclusion, c) Coarse grains of euhedral to subhedral pyrite, sphalerite with chalcopyrite blebs, d) Tetrahedrite- chalcopyrite-pyrite replacement relation, e) Fine grained, deformed, pyrite clast with tetrahedrite and covellite replacement after chalcopyrite, f) Dissemination of fine grained galena, and sphalerite with chalcopyrite blebs, coarser pyrite (drill hole: PSD-16, from 168.50 m). Abbreviations: py = pyrite, cpy = chalcopyrite, sph = sphalerite, ttr = tetrahedrite, ga = galena, cv = covellite, XPL= cross-polarized light, RL= reflected light.

Short intercepts of sulfide ore zone including 3 meters grading 15333 ppm Pb, 5410 ppm Zn, 1280 ppm Cu, 22 ppm Ag, maximum of 4.9% Pb per meter (Table 2; Figure 4.22).

Table 2. Significant intercepts of drill hole: PSD-16.

From (m)	**To (m)**	**Intercept Length (m)**	**Ag (ppm)**	**Cu (ppm)**	**Pb (ppm)**	**Zn (ppm)**
168	171	3	22	1280	15333	5410

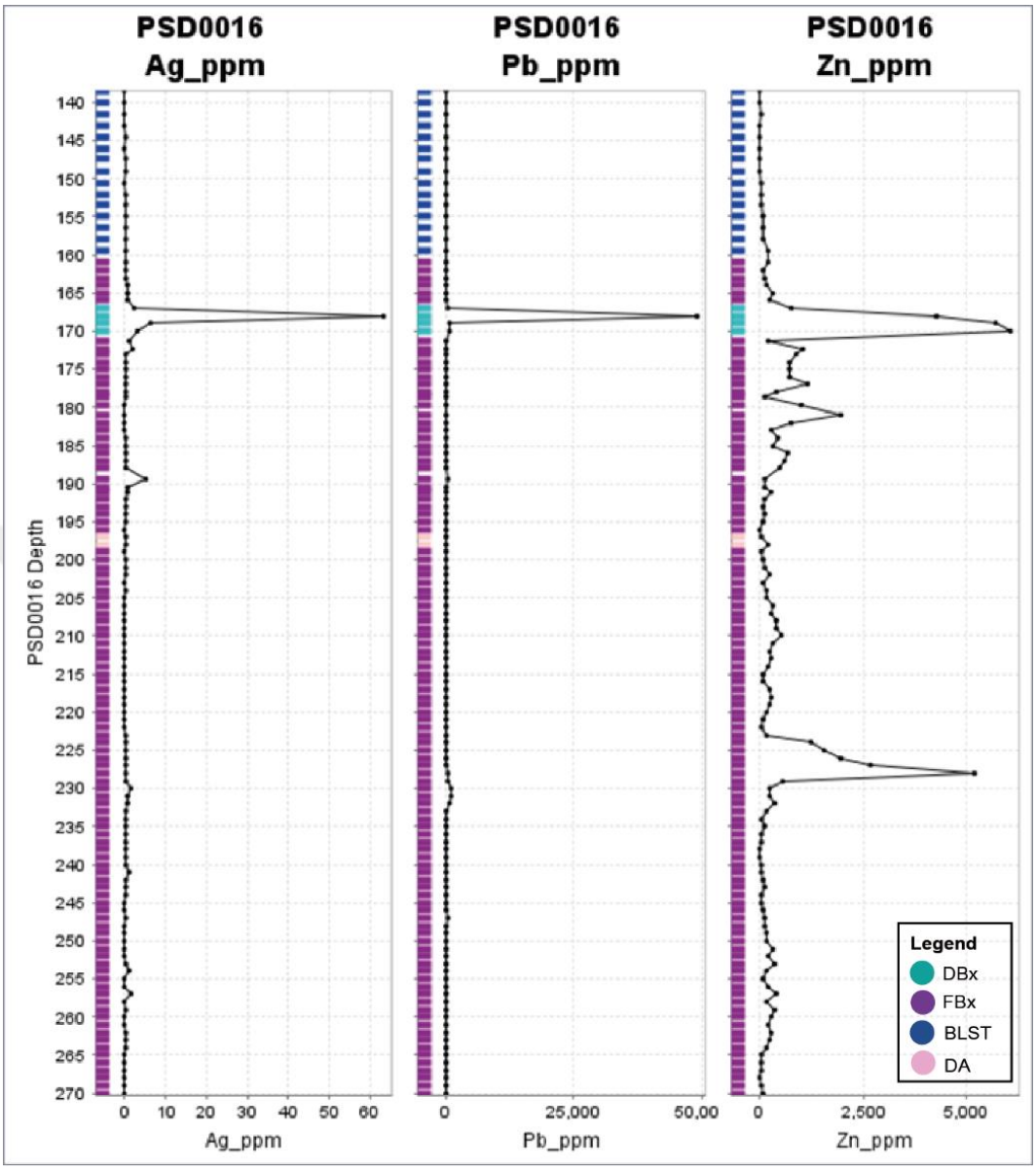


Figure 4.22. The downhole plot of drill hole PSD-16 representing Ag (ppm), Pb (ppm), Zn (ppm) versus rock type and depth (DBx: Dolomite matrix breccia; FBx: Fault breccia; BLST: Black limestone; DA: dacite porphyry).

At Çubuklu, primary, sulfidic carbonate-replacement ores are present in the underground galleries of Postallı Mining, but such zones were rarely encountered during exploration by Centerra Gold. In fact, majority of Zn-Pb mineralization

occurs as oxide ore, that contains secondary ore minerals including smithsonite, zincite, cerrusite, and goethite/limonite.

Based on the drill core logging and assay data, the most common stratabound-style, carbonate-replacement Pb-Zn oxide mineralization is characterized by decalcification, and partial to complete silica replacement of carbonate rocks, accompanied by depletion of calcium and a slight increase magnesium (Figure 4.24). Occasionally near the contacts with the host rock, clast-supported, polymictic breccias may be present, which are composed of fine- to coarse-grained, angular to rounded heterogeneous black limestone, smithsonite, zincite, and limonite clast in smithsonite, zincite, and limonite matrix (Figure 4.23).



Figure 4.23. Drill core photograph showing a typical silica replacement zone in carbonate-replacement domain with secondary ore mineral assemblage of zincite, cerrusite, limonite and goethite (drill hole: PSD-14).

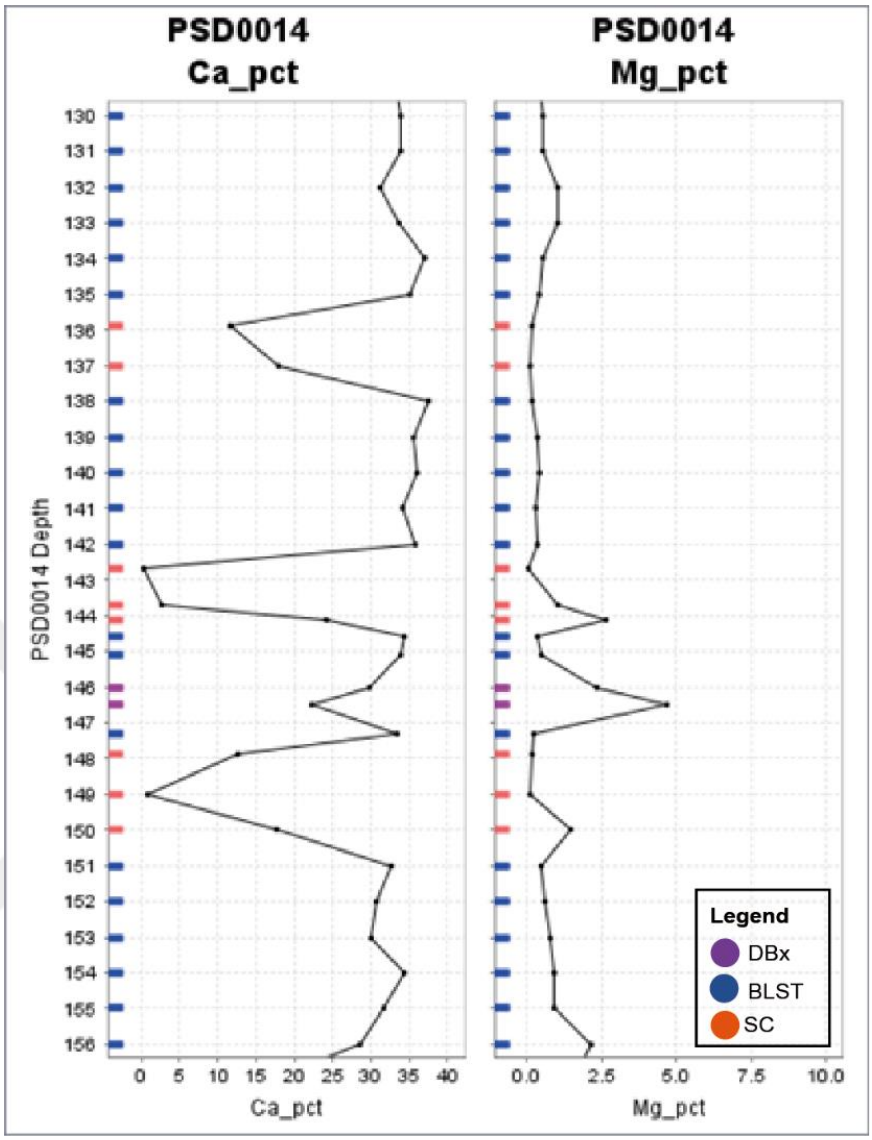


Figure 4.24. The downhole plot of drill hole PSD-14 representing Ca (%) and Mg (%) versus rock type and depth (SC: Silicified carbonate zone; DBx: Dolomite breccia; BLST: Black limestone).

The oxide ore mineralization of short intercepts comprises primarily zinc, lead, and silver, with additional copper and gold grade increase. Among these, the highest intercept of 3.1 meters grading 10.5 ppm Ag, 1070 ppm Cu, 494 ppm Pb, 27.5% Zn from 147.90 meters depth, including a higher-grade interval of 40.99% Zn per meter at the depth of 149 m (Figure 4.25; Table 3).

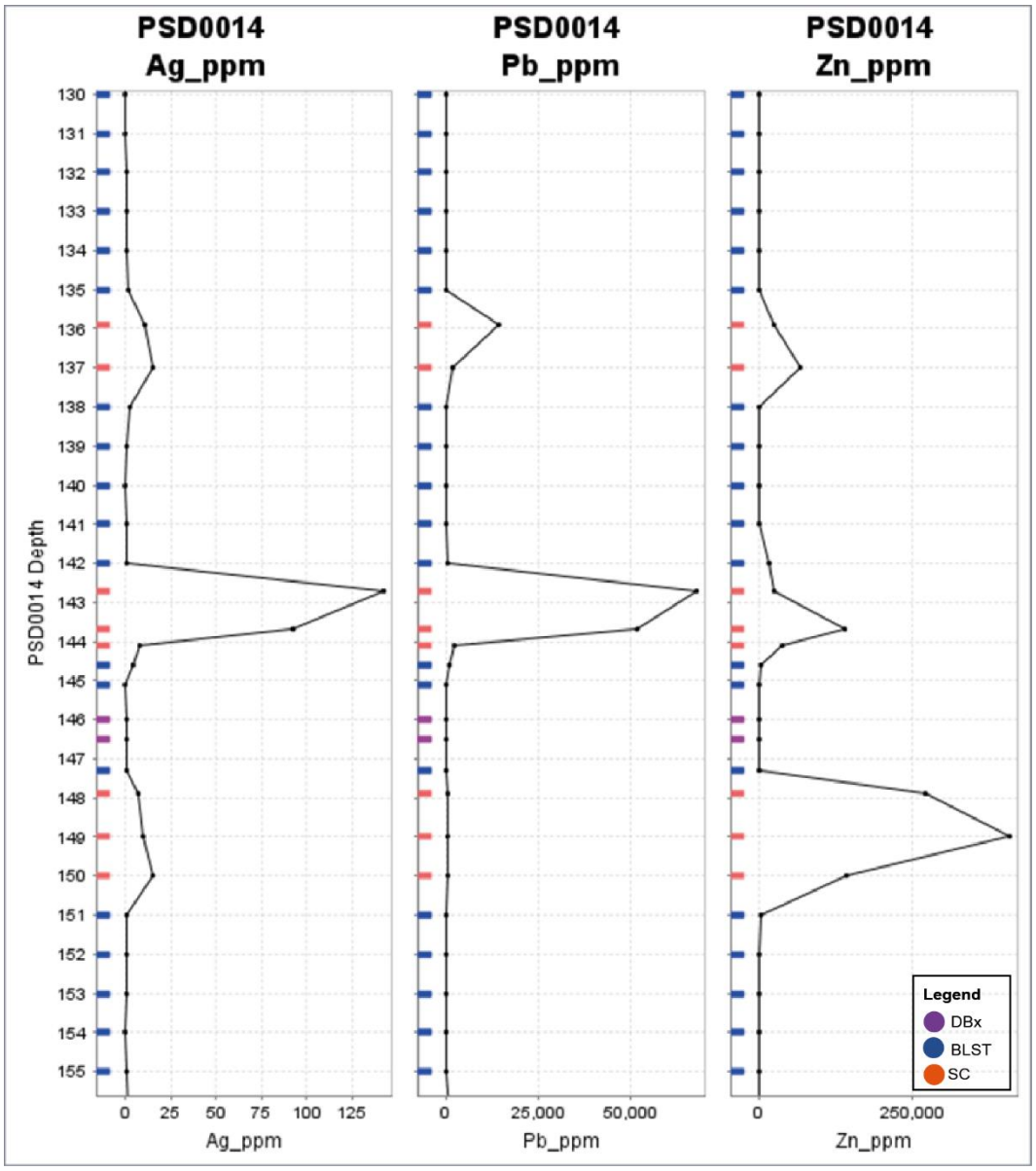


Figure 4.25. The downhole plot representing Ag (ppm), Pb (ppm), Zn (ppm) versus rock type and depth (SC: Silicified carbonate zone; DBx: Dolomite breccia; BLST: Black limestone).

Table 3. Significant intercepts of drill hole: PSD-14.

From (m)	To (m)	Intercept Length (m)	Ag (gpt)	Cu (ppm)	Pb (ppm)	Zn (ppm)
135.9	138	2.1	12.8	805	8333	44210
142.7	144.6	1.9	96.5	1958	47047	53200
147.9	151	3.1	10.5	1071	494	275293

The paragenetic sequence of carbonate replacement type alteration and mineralization at Çubuklu prospect is provided in Figure 4.26.

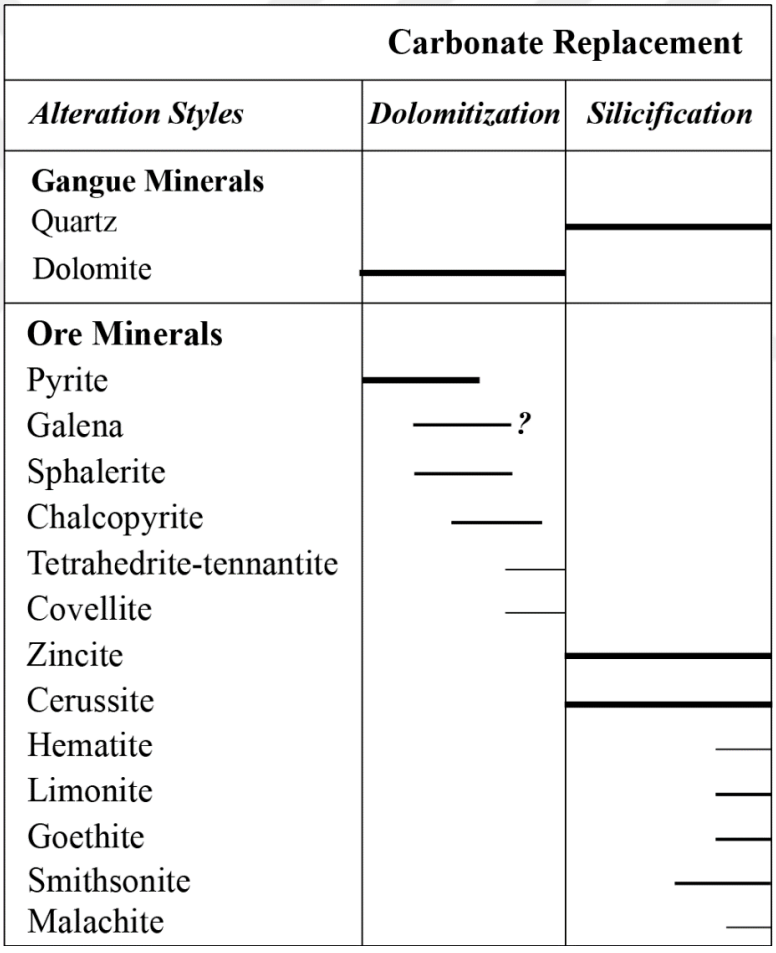


Figure 4.26. The paragenetic sequence of the Çubuklu carbonate replacement-type alteration and mineralization.

4.3 Porphyry-Style Alteration and Mineralization

A narrow zone of porphyry-style alteration and mineralization was encountered in the northeastern part of the Çubuklu license, where at surface, the Tauride carbonates standing at a relatively high topography transition into the flat-lying topographic low of the Sultansazlığı basin. Here, Centerra Gold completed a total of nine drill holes, but only one of these (PSD-8), which was drilled in the northeast direction, intersected porphyry mineralization underneath the young sedimentary cover (Figure 4.27). Drill hole PSD-8 was collared in an area of farmland, and as a result no surface geochemistry that could vector towards a potential porphyry system had been carried out prior to drilling at this location. Instead, drilling was aimed to test a significant magnetic high.

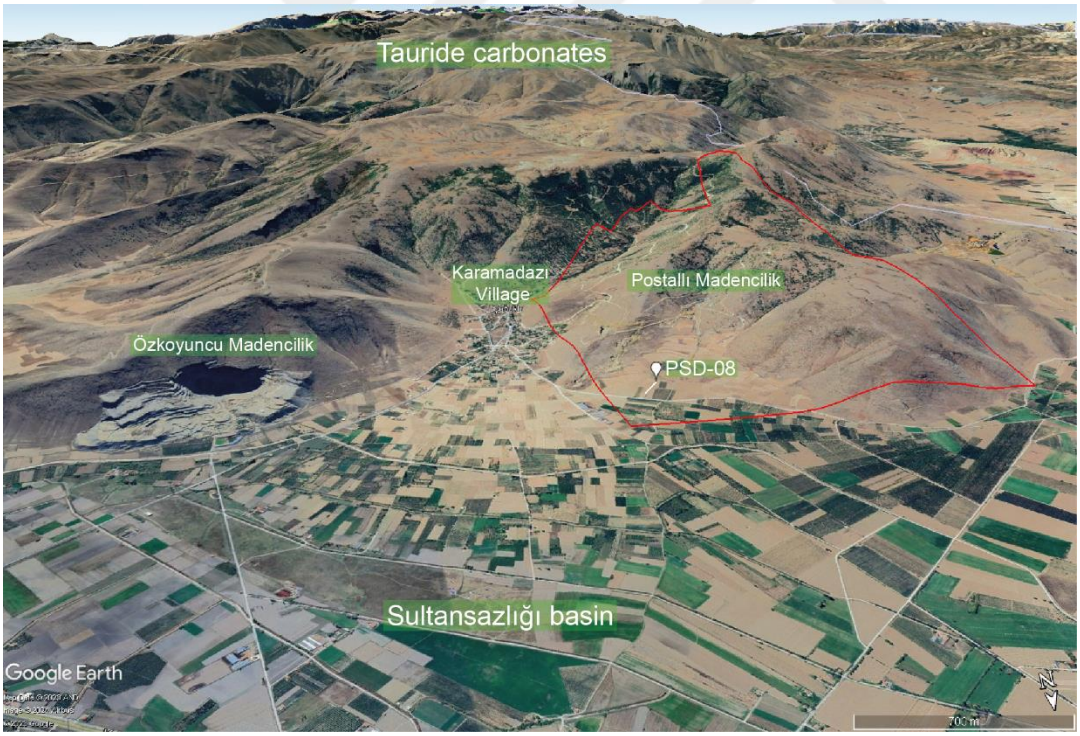


Figure 4.27. Location map showing drill hole: PSD-8 and its trace through the Sultansazlığı basin.

In drill hole PSD-8, a porphyry-altered granodiorite porphyry intrusive was encountered at depths of ~110 meters following the shallow alluvial cover rocks. Altered and mineralized drill core is quite weathered, likely due to the permeable nature of the overlying young sediments and also due to well-developed faults. However, it is not oxidized intensely as it still contains abundant sulfide minerals, and secondary oxide/hydroxide minerals are only restricted to narrow fractures.

Primary igneous minerals in granodiorite porphyry (Figure 4.28 a) include predominant plagioclase, hornblende, and biotite alongside lesser quartz phenocrysts (Figure 4.28 b). Within the rocks, selective potassic alteration resulted in almost complete replacement of igneous ferromagnesian phases (biotite and hornblende) by secondary biotite. Hydrothermal biotite occurs as fine-grained, anhedral to subhedral clusters (Figure 4.28 c-d), whereas relict primary biotite is generally subhedral to euhedral and coarser grained (Figure 4.28 e). Secondary K-feldspar is not well-developed and was only observed as a partial replacement mineral within some plagioclase phenocrysts (Figure 4.28 f). Most plagioclase can be still recognized in the sample. Hydrothermal quartz generally dominates the groundmass (Figure 4.28 b-d).

Potassic alteration has been overprinted by moderate-intensity sericite-chlorite-actinolite-epidote alteration. Chlorite and locally fibrous crystals of actinolite has replaced biotite of both igneous and hydrothermal origin, whereas very fine-grained flakes of sericite developed within plagioclase. This alteration is almost continuous along a ~55 meters-long interval, which was later followed by an approximately 20 meters-long interval of highly broken core with fault gouge that passes into actinolite-chlorite-magnetite-pyrite exoskarn (Figure 4.29).

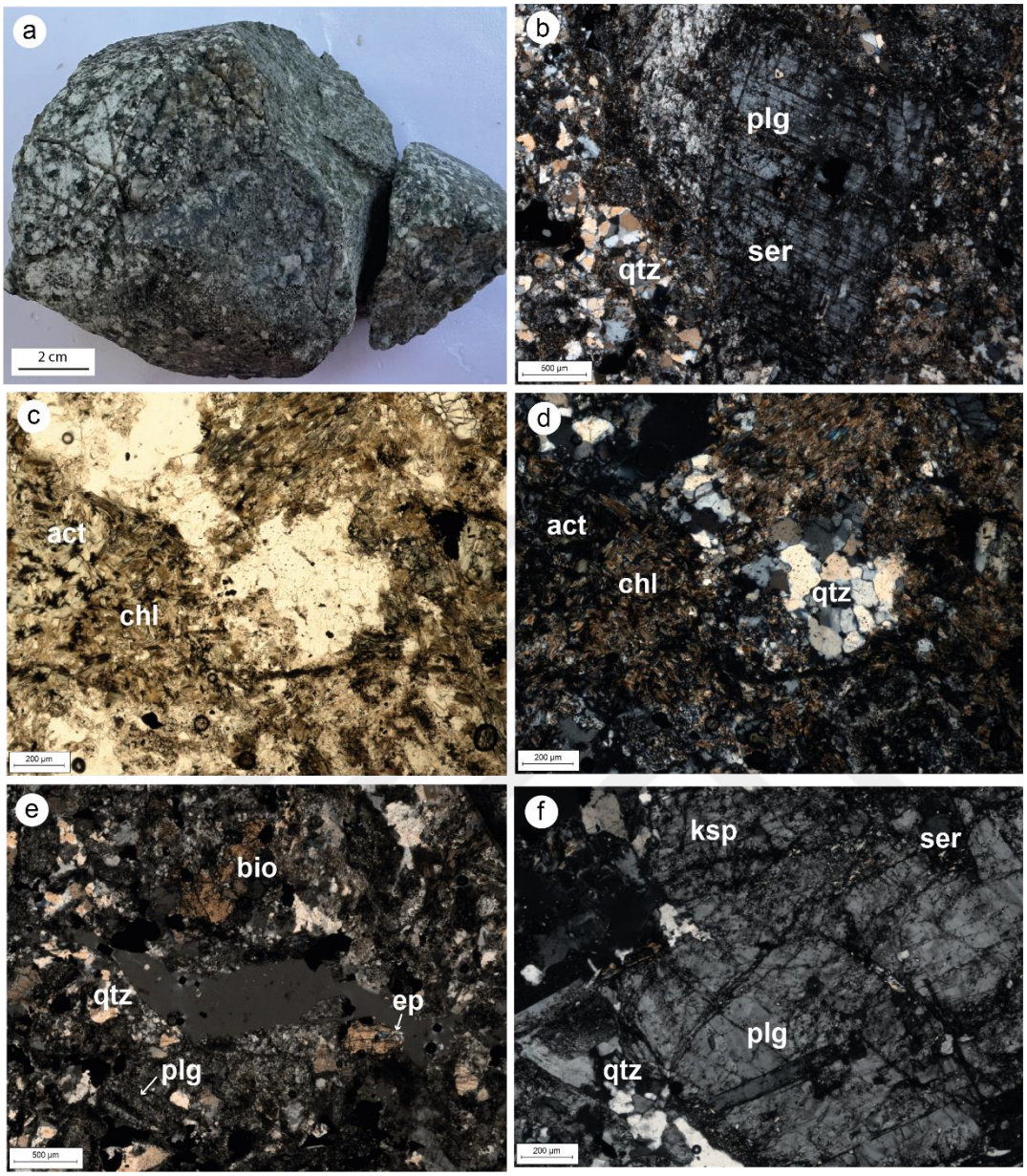


Figure 4.28. Hand specimen image (a) and photomicrographs (b–f) of porphyry-related alteration (drill hole PSD-8, 161.20 m). a) Fractured drill core sample of granodiorite porphyry with molybdenite coating, b) Sericite alteration on plagioclase phenocryst, surrounded by fine-grained hydrothermal quartz (XPL, TL image), c–d) Fine-grained aggregates of hydrothermal biotite, which was later altered into chlorite and actinolite (PPL and XPL images, respectively), e) Hydrothermal biotite, quartz, epidote, and relict plagioclase (XPL, TL image), f) Weakly sericitized plagioclase, along with possible K-feldspar domain (XPL, TL image). Abbreviations: act = actinolite, chl = chlorite, ep=epidote, qtz = quartz, ser = sericite, bio = biotite, plg =plagioclase, Ksp = K-feldspar, TL = transmitted light, XPL= cross-polarized light, PPL = plane-polarized light.

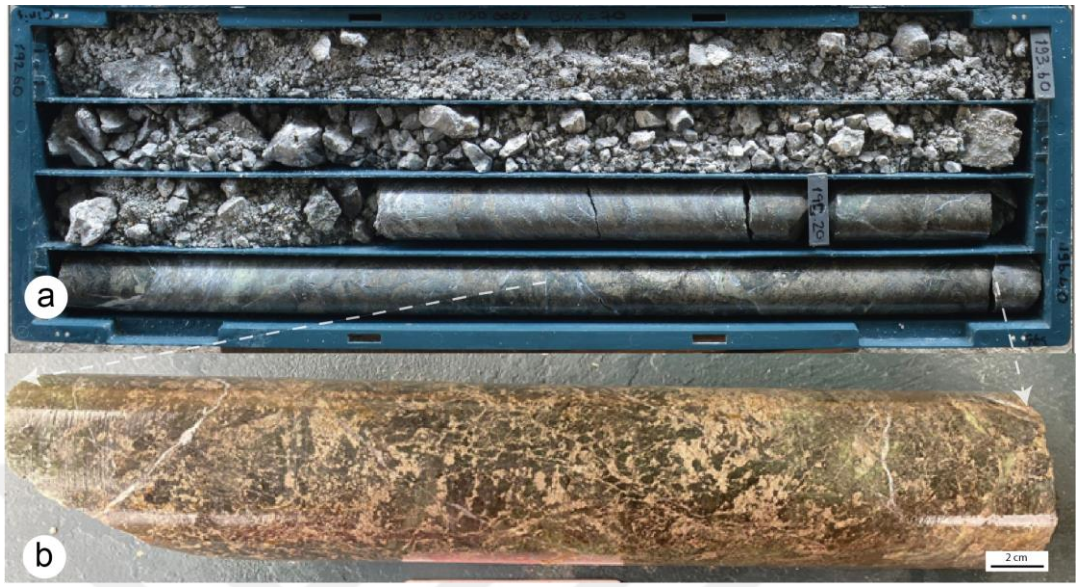


Figure 4.29. a) Core box showing 3.8 m-long section (drill hole: PSD-8, between 192.60 and 196.40 meters) of approximately 20 m-long faulted contact separating porphyry-altered granodiorite porphyry from Cu-Fe mineralized exoskarn, b) Drill core photograph showing representative Fe-Cu exoskarn zone.

Porphyry mineralization occurs either as weak disseminations of sulfides or along quartz-rich sulfide-bearing veins. Due to the weathered nature of rocks, most veins have been fragmented and not well-preserved. The existing veins appear to have up to 2 cm thickness. They are quartz-rich, planar, and often observed as sheeted veins. Sulfide minerals either form bands at the vein center or along vein walls. Consequently, these are classified as B-type veins (sensu Gustafson and Hunt, 1975). Both the disseminated ore and B-veins contain the same sulfide assemblage including pyrite, chalcopyrite, and molybdenite (Figures 4.30 and Figure 4.31).



Figure 4.30. Drill core photographs of granodiorite porphyry with a) B-type quartz-molybdenite vein (drill hole: PSD-8, from147.60 m), b) B-type quartz vein with sulfide-bearing centerline (drill hole: PSD-8, from 138.00 m).

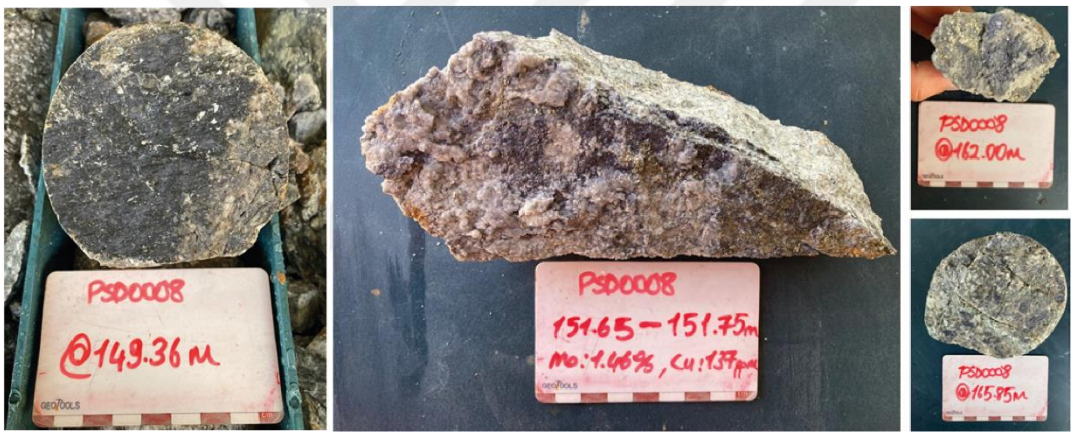


Figure 4.31. Drill core photographs showing fracture-coating of molybdenite ± pyrite ± chalcopyrite, at various depths in drill hole: PSD-8.

Pyrite is the most abundant sulfide phase and occurs as fine-grained crystals. In mineralized intervals its abundance reaches up to about 10% (Figure 4.32 c). Chalcopyrite (up to 5% of mineralized rock) was commonly identified as isolated crystals, but some occur as inclusions or as fracture-fill in deformed pyrite crystals (Figure 4.32 c). Molybdenite forms fine-grained, acicular crystals that often occur as aggregates in granodiorite porphyry (Figure 4.32 a-b). Fine-grained, granular disseminations of magnetite was also observed, which was partially oxidized into hematite (Figure 4.32 d). The paragenetic sequence of porphyry-style alteration and mineralization is provided in Figure 4.33.

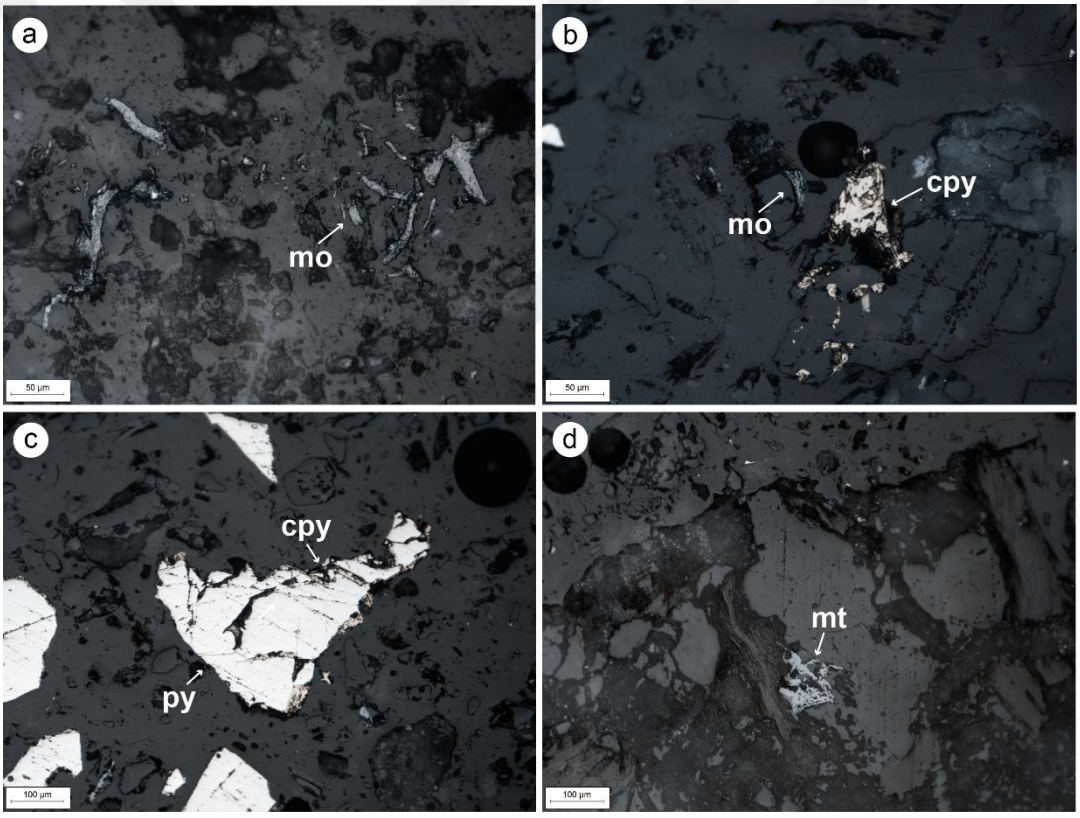


Figure 4.32. Representative microphotographs (XPL, RL image) of porphyry-mineralized samples. a) Cluster of fine-grained, acicular molybdenite in granodiorite porphyry, b) Disseminated chalcopyrite and molybdenite, c) Disseminated pyrite partially replaced by chalcopyrite along fractures, d) Fine-grained magnetite partially oxidized into hematite. All images from sample 161.20m (drill hole: PSD-8). Abbreviations: cpy = chalcopyrite, mo = molybdenite, py = pyrite, mt = magnetite, XPL = cross-polarized light, RL= reflected light.

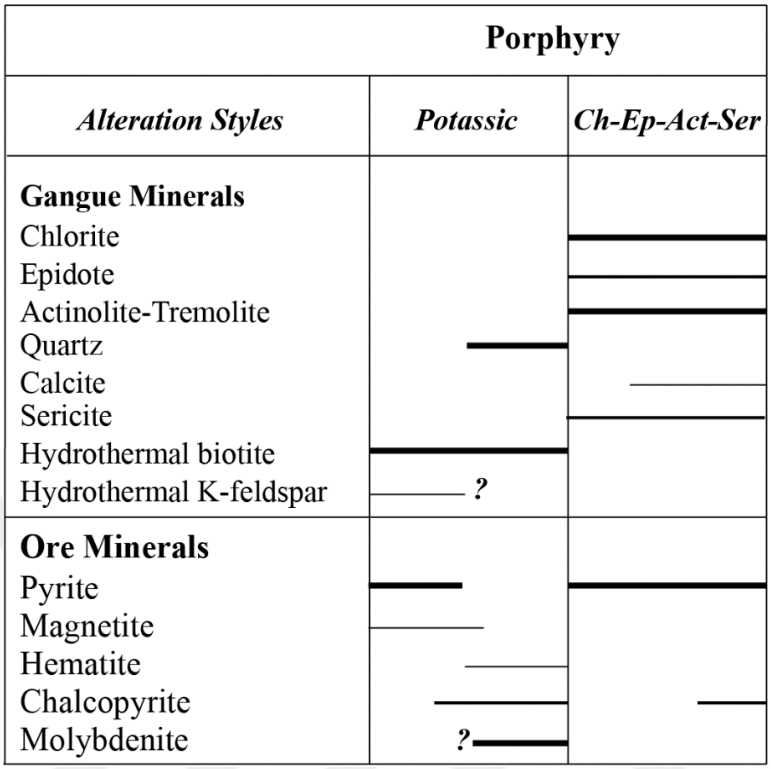


Figure 4.33. The paragenetic sequence of porphyry-style alteration and mineralization at Çubuklu prospect.

In the porphyry-mineralized granodiorite porphyry, the best intercept is 55 meters, grading 814 ppm copper and 357 ppm molybdenum, from 139 meters to 195 meters, including the highest-grade interval of 1090 ppm Mo and 3531 ppm Cu over one-meter-length intervals at depths of 178.1 m and 145.7 m, respectively (Table 4). Gold grades in the porphyry zone are quite low, consistently <0.05 gpt.

Table 4. Significant intercepts of drill hole: PSD-8.

HOLE ID	**From (m)**	**To (m)**	**Length (m)**	**Intercept (ppm)**
PSD-8	139	1945	55	Cu: 814
				Mo: 357

Variation of Cu and Mo grades as well as Fe contents with depth in porphyry mineralization is shown in Figure 4.34. The transition from vein-type molybdenite-chalcopyrite mineralized granodiorite porphyry to disseminated, banded, and massive magnetite-chalcopyrite mineralized skarn is illustrated through a downhole plot of molybdenum (ppm), copper (ppm), and iron (pct) grades versus associated rock type and depth of the representative drill hole (PSD-8).

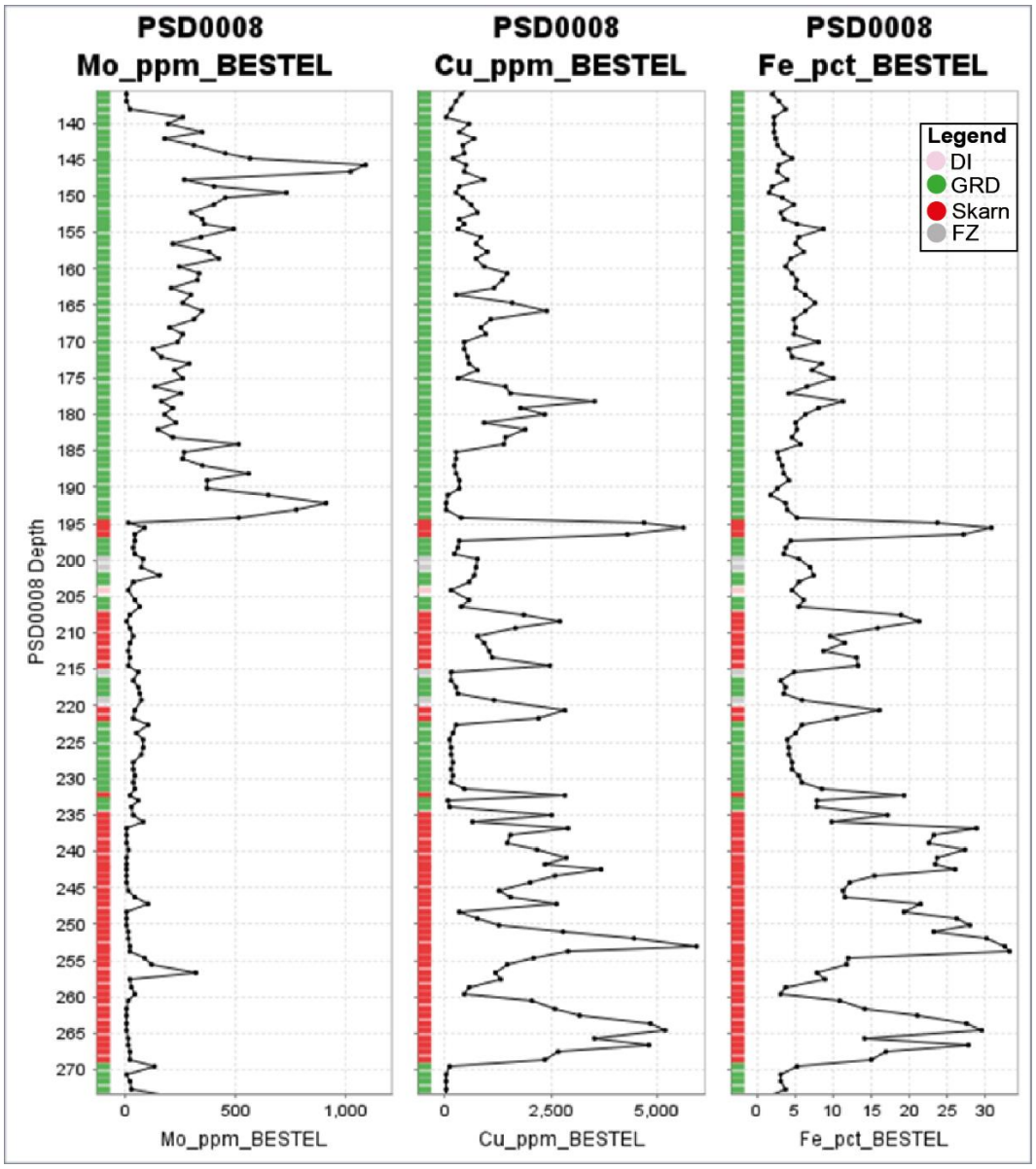


Figure 4.34. The downhole plot of drill hole PSD-08 showing the variation of Cu and Mo grades as well as Fe contents. Porphyry-mineralized granodiorite porphyry (GRD) interval ends at 174.80 meters, followed by a fault zone (FZ) and then Fe-Cu-mineralized skarn starting at 195 meters.

4.3.1 Re-Os Molybdenite Geochronology

To determine the timing of porphyry-style mineralization at the Çubuklu prospect, one molybdenite sample was analyzed through Re-Os geochronology. Molybdenite was obtained from a drill core of potassically-altered granodiorite porphyry. The sample is characterized by a molybdenite-chalcopyrite-quartz-bearing B-type vein within drill core PSD-8 at a depth of 166.70 meters. The result of the Re-Os age determinations is provided in Table 5.

Table 5. The result of the Re-Os geochronology (drill hole: PSD-8, from 166.70 m).

Re (ppm)	**±2σ**	**^{187}Re (ppm)**	**±2σ**	**^{187}Os (ppb)**	**±2σ**	**Model Age Ma**	**±2σ**
4.984	0.014	3.133	0.009	2.6053	0.0069	49.9	0.2

Analyzed molybdenite sample is characterized by low amounts of rhenium (Table 5). Re-Os geochronology reveals the timing of the porphyry-style alteration and mineralization as middle Eocene (49.9 ± 0.2 Ma), which correlates well with Eocene magmatism throughout the eastern and central Taurides. The obtained age of ~50 Ma is slightly older than the ^{40}Ar/^{39}Ar ages reported by Kuşcu et al. (2013). These ages obtained from hornblende and biotite separates from a granodiorite (48.74 ± 0.67 Ma) and a monzodiorite (46.58 ± 0.82 Ma) intrusions associated with Fe skarn mineralization to the east of Çubuklu. The older age of 48.74 ± 0.67 Ma does not overlap with the Re-Os molybdenite age. However, the slight difference between these two may reflect formation during cooling of the same intrusive body as Ar-Ar hornblende closure temperature (480–550°C; Richards and Noble, 1998) is significantly lower than the Re-Os molybdenite closure temperature (>700°C; Bingen and Stein, 2003). Another possibility is that the porphyry-mineralizing granodiorite at NE Çubuklu represents an older magmatic phase that has been identified in the Karamadazı Fe skarn mineralization. Regardless, the Re-Os molybdenite age reported here indicates a middle Eocene age for porphyry formation at Çubuklu.

CHAPTER 5

DISCUSSION AND CONCLUSION

5.1 Discussion

5.1.1 Formation of Skarn-Type Alteration and Mineralization

In the Çubuklu prospect, main mineralization occurs as Fe-Cu skarn and carbonate-replacement-type Pb-Zn±Cu mineralization. In the skarn zone relatively small zones of endoskarn developed in the granodiorite porphyry intrusion of the Karamadazı granitoid, whereas the more widespread exoskarn zones developed within the Paleozoic–Mesozoic sedimentary rocks, mainly comprising dolomitic carbonate units.

Exoskarn zones are dominated by a forsterite-serpentine-magnetite-chalcopyrite mineral assemblage, along with talc, chlorite, tremolite and calcite, which signifies the presence of a magnesian-rich dolomitic host rock. Petrographic studies have revealed that the magnesium silicate hydroxide member of serpentine group lizardite is a pseudomorph mineral substituting forsterite as a magnesium-rich end-member of the olivine mineral group. The occurrence of calcic exoskarn and associated ore mineralization is rare, where calc-silicate minerals such as grandite garnet and Ca-pyroxene are mostly found in relict form. Thus, the variable mineralogy of the skarn assemblages directly reflects the nature of the calcareous wall-rocks, which are primarily composed of dolomite rather than calcite.

The introduction of silicon, aluminum, and iron from magma into calcareous sedimentary rocks led to the formation of early hydrous skarn zones possibly within the temperature range of 600-400°C, while Ca, Mg, and CO2 are locally derived

(Burt, 1997; Robb, 2005). During early anhydrous stage, in limestone, this process resulted in the formation of garnet and pyroxene, while in dolomite, forsterite was formed (Burt, 1997). The prograde reaction (1) describes forsterite formation in magnesian skarns, where aqueous fluid including dissolved silica infiltrated into dolomitic carbonates during contact metamorphism and early metasomatism (Bucher-Nurminen, 1981; Bucher-Nurminen, 1982; Holness, 1997; Bucher, 1998; Ferry et al., 2011).

Reaction 1:

$2CaMg(CO_3)_2$ (s) + SiO2 (aq) = $MgSiO_2$ (s) + $2CaCO_3$ (s) + $2CO_2$ (g)

Dolomite Forsterite Calcite

During the retrograde stage, where early anhydrous skarn minerals are destroyed due to the meteoric fluid influx within a temperature range of 400–200°C, serpentine replaces forsterite, and other magnesian-skarn specific minerals such as humite ($Mg_7(SiO_4)_3F_2$), talc ($Mg_3Si_4O_{10}(OH)_2$), and brucite ($Mg(OH)_2$) form (Burt, 1997; Meinert et al, 2005).

The serpentine minerals forming with the introduction of H_2O as a result of olivine hydration (reactions 2 through 4) depends on the composition of aqueous fluid (Lafay et al, 2018, Pirajno, 2009). If CO_2 is absent, brucite may form as a result of hydration of forsterite along with serpentine (4), whereas presence of CO_2 and calcite let the carbonation reaction forming dolomite (5) (Lafay et al. 2018; Öngen, 2000).

Reaction 2:

$2Mg_2SiO_4$ (s) + H_2O (l) + $2H^+$ (aq) = $Mg_3Si_2O_5(OH)_4$ (s) + Mg^{2+} (aq)

Forsterite Serpentine

Reaction 3:

$3Mg_2SiO_4$ (s) + SiO_2 (aq) + $4H_2O$ (l) = $Mg_3Si_2O_5(OH)_4$

Forsterite Serpentine

Reaction 4:

$2Mg_2SiO_4$ (s) + $3H_2O$ (l) = $Mg_3Si_2O_5(OH)_4$ (s) + $Mg(OH)_2$ (s)

Forsterite Serpentine Brucite

Reaction 5:

$2Mg_2SiO_4$ (s) + $CaCO_3$ (s) + $2H_2O$ (l) + CO_2 (g) = $Mg_3Si_2O_5(OH)_4$ (s) + $CaMg(CO_3)_2$ (s)

Forsterite Calcite Serpentine Dolomite

The high magnetic anomaly revealed by ground magnetic survey in the northwest of the Çubuklu tenement has been confirmed drilling and petrographic examinations, because of magnetite mineralization, which is rarely observed in calcic exoskarn, more abundant in magnesium exoskarn zones of the Çubuklu prospect.

According to Hallof and Winniski (1971), Chermeninov (1988) and Meinert et al. (2005), the way to distinguish protolith in skarn deposit might be high magnetic signature. Metasomatism of dolomitic rocks commonly results in the abundant magnetite mineralization due to the lack of iron in the typical magnesian skarn minerals such as forsterite, talc, and serpentine. Hence the soluble iron present in the solution tends to form magnetite rather than andradite or hedenbergite (Meinert et al., 2005). At Çubuklu, subeconomic Fe-Cu skarn mineralization is primarily composed of magnetite, which commonly occurs as cm-scale layers, often together with pyrite and lesser chalcopyrite. The banded nature of magnetite and pyrite in these rocks possibly reflects the original sedimentary layers.

5.1.2 Metal Zonation

Intrusion-related ore systems, including skarn-type deposits as well as porphyry-centered magmatic-hydrothermal systems, mostly exhibit base metal zoning patterns that reflect temperature gradients. In porphyry systems this metal zonation is generally from a proximal Cu-Mo zone to a distal zone of Zn-Pb-Ag in an upward and outward direction extending laterally for variable distances of up to 8 kilometers (Sillitoe, 2010; Catchpole et al., 2015; Stoltnow et al., 2023). Metal transportation from hydrothermal fluid is controlled by temperature, pressure, pH, salinity, sulfur, and oxygen fugacity conditions affecting the solubility (Crerar, 1985; Einaudi et al. 2003).

In skarn systems, zonation of ore and gangue minerals is also pronounced due to abrupt changing physico-chemical conditions around plutonic bodies in relation to cooling and wall-rock reactions (Meinert et al., 2005). At Çubuklu, widespread retrograde overprint of the earlier high-temperature skarn minerals precludes identification of zonation within the typical skarn mineralogy including spatial changes in the relative proportions of garnet and pyroxene and also changes in the colors of these minerals. However, at the prospect-scale a zonation is apparent from a central and proximal Cu-Mo signature in the northeast transitioning first into Fe-Cu and then into Pb-Zn±Cu such towards southwest. This apparent metal zonation is most likely controlled by (1) a decrease in temperatures, and (2) an increase in magma–wall-rock interaction from NE to SW.

In addition to this, a temporal change in the fluid chemistry was also identified at Çubuklu, particularly in relation to the sulfidation states of the Cu-sulfide minerals observed within the carbonate-replacement zones. There, chalcopyrite (alongside pyrite and sphalerite) is early in the paragenesis and was later overprinted by tetrahedrite/tennantite and covellite, which possibly suggest a progressive increase in the sulfidation states of the mineralizing fluids. The relatively dark colors in sphalerite indicate that the early fluids carrying Pb-Zn-Cu are of intermediate-sulfidation state rather than being typical low-sulfidation state fluids (Einaudi et al.,

2003). In the carbonate-replacement zones, sulfide-rich mineralization shows a close spatial association to calcareous lithologies that are particularly rich in organic carbon (either as bitumen or graphite). Sulfide abundances (especially pyrite) in these ore levels locally reach up to 13 vol.%. This implies a strong control on variation in redox conditions in the carbonate-replacement zones, where a relatively oxidized fluid of probable magmatic origin interacts with an organic-rich reductant unit. The contrasting nature of these two fluids likely resulted in sudden precipitation of base metal sulfides in the basement Tauride carbonate succession.

Evolution of porphyry-related systems comprise high-sulfidation conditions forming Cu-Zn±Au ore mineral assemblages including covellite, Fe-poor sphalerite, that grading outwards to intermediate sulfidation assemblage of Zn-Pb-Ag including Fe (moderate to poor) sphalerite, galena, tennantite-tetrahedrite, chalcopyrite, and other Mn-Fe (±Zn) carbonates, where low sulfidation stage (350-220 °C) is characterized by pyrrhotite, pyrite, magnetite, chalcopyrite, galena and Fe-rich sphalerite ore mineral assemblage (Fontboté, 2020).

5.1.3 Regional Significance

The carbonate-dominated sequences of the Tauride belt host known porphyry, skarn and carbonate-replacement type mineralization associated with Eocene calc-alkaline magmatism, as well as carbonate hosted Pb-Zn mineralization (Kuşcu et al., 2001, 2007, 2010, 2011, 2013, and 2019; İmer et al., 2013 and 2016; Yıldırım et al., 2019; Hanilçi and Öztürk, 2019).

The Eocene intrusive systems of Karamadazı (Kayseri), Horoz (Niğde), and Doğanşehir (Malatya), along with the slightly younger middle Eocene systems of Çöpler-Kabataş (Erzincan) magmatic complex and Bizmişen (Erzincan) intrusions, constitute isolated, shallowly emplaced suites in the eastern and central Taurides, that are localized around regional-scale strike-slip faults (İmer et al., 2013; Kuşcu et al., 2013).

Among the many Eocene intrusive centers emplaced within the Tauride range, only a few of them contain porphyry-style mineralization, whereas skarn development (particularly Fe skarns) is relatively more common. There are two known Eocene porphyry systems; the Çöpler and Mavidere/Karakartal, both developed as part of the 48–44 Ma Çöpler-Kabataş Magmatic Complex in the eastern Taurides (İmer et al., 2013; Kuscu et al., 2013). The >9 Moz Çöpler Au deposit in Erzincan, situated ~320 km NE of the Çubuklu prospect comprises epithermal-porphyry Au-(Cu) mineralization centered around dioritic to granodioritic intrusions (~44 Ma) emplaced within a Late Paleozoic-Mesozoic metaclastic and carbonate succession (İmer et al., 2013 and 2016). At Çöpler most of the Au mineralization occurs along intermediate-sulfidation epithermal veins that overprint a marginally economic porphyry Cu-Au mineralization (İmer et al., 2016). Manto-type carbonate replacement Cu-Au zones and much smaller massive magnetite skarns are located at the periphery of porphyry-epithermal mineralization (İmer et al., 2016). The Mavidere/Karakartal porphyry Cu-Au prospect lies about 10 km to the south of Çöpler. Mavidere is slightly older (~48 Ma; Kuşcu et al., 2013), lacks epithermal-style veins as well as carbonate-replacement zones, and appears to be sub-economic, but is similar to the porphyry Cu-Au system at Çöpler in many other aspects including the basement lithologies, nature of causative intrusions, and broad tectonic setting (İmer et al., 2013). Mavidere prospect also contains small Fe skarn occurrences developed in close spatial association with the porphyry system.

Bizmişen is Fe-Cu skarn deposit, located approximately 300 km northeast of the Çubuklu prospect, in eastern central Anatolia. The currently operated Bizmişen deposit has a total reserve of 23.8 Mt at 53% Fe (Bozkaya et al., 2017). The intrusion of Middle Eocene quartz dioritic rocks into Triassic-Cretaceous limestones and Upper Cretaceous ophiolitic rocks resulted in the formation of endoskarn, ophiolite, and limestone-hosted exoskarn, along with lower-temperature clay alteration zones (Bozkaya et al., 2019). The ore mineral assemblages consist of magnetite, hematite, with subordinate pyrite, chalcopyrite, covelline, chalcocite, goethite, and limonite,

which are develop in skarn, vein/lens, replacement, and placer types (Bozkaya et al., 2017).

The Horoz Fe skarn deposit situated approximately 85 km southwest of the Çubuklu prospect, is located in the Bolkar Mountains of southern Türkiye (Niğde). The early Eocene Horoz granitoid intruded into the Late Paleozoic to early Mesozoic metamorphic rocks of the Central Tauride block, forming a small resource with 0.2 Mt at 50% Fe, composed of primarily magnetite with rare chalcopyrite and cobaltite (Kadıoğlu and Yıldırım, 2009; MTA, 1980; Kuşcu et al. 2013). Skarn-type mineralization and alteration occur as both endoskarn zones characterized by the chloritization of granodiorite, and exoskarn zones consisting of prograde garnet and retrograde epidote, occasionally accompanied by rare tremolite-actinolite (Özözlü, 2019). The hydrothermal stage mineral assemblage composed of quartz, calcite, chalcopyrite, and pyrite, and the supergene stage mineralization composed of probably arsenic bearing- iron oxides/hydroxides and rare malachite (Özözlü, 2019).

The Nevruztepe iron-copper skarn prospect is situated 6 km northwest of the Çubuklu prospect, nearby Yeşilhisar, Kayseri. According to Tiringa et al. (2020), the skarn mineralization is formed between Permian to Jurassic carbonate rocks intruded by the Eocene Yahyalı granitic pluton, where skarn zones are classified as endoskarn and exoskarn. Magmatic rocks comprising variable type of composition from gabbro porphyry to monzonite, altered into mostly and/or argillic assemblages. The exoskarn zones display both a prograde stage characterized by garnet and diopside, and retrograde stage with epidote mineralization. Magnetite, hematite, and chalcopyrite are the main ore minerals with variable thickness form few meters to 55 meters (Tiringa et al., 2020).

The Karamadazı Fe mine, operated by Özkoyuncu Madencilik, is situated approximately 3–4 km northeast of the Çubuklu prospect, in Yahyalı, Kayseri. The regionally important deposit comprises 6.4 Mt at 54% Fe (Oygür,1986). The skarn mineralogy and zonation of Karamadazı Fe mine were investigated and classified as a typical calcic skarn by Kuşcu et al. (2001). Endoskarn, ranging from 50 to 100

meters in width, display zonation from unaltered granite to exoskarn. 350 meters wide exoskarn zones display a zonation of pyroxene-garnet-epidote, and epidote-actinolite zonation, where main magnetite mineralization occurs as massive bodies (Kuşcu et al. 2001).

The Eastern Taurides host significant economic Cu-bearing Pb-Zn deposit closely associated with an Eocene granodioritic intrusion occurring in the Yahyalı and Siyah Aladağ Nappes known as Aladağlar-Zamantı Province (Hanilçi and Öztürk, 2011; Hanilçi et al., 2019). Ayraklı and Çadırkaya deposits within the Yahyalı Nappe, and the Suçatı and Delikkaya deposits in the Siyah Aladağ Nappe, comprise a total of 6.3 Mt, grading 30% Zn, with 3.5 Mt of measured reserves remaining (Hanilçi and Öztürk, 2011). The main alteration type is dolomitization and kaolinization of massive to recrystallized limestone, strata-bound, replacement type, karstic and vein type mineralization.

Çadırkaya Pb-Zn is located almost near east of Çubuklu prospect. Replacement and vein type ore mineralization is hosted by Upper Permian recrystallized limestone within kaolinized zones (Hanilçi and Öztürk, 2011).

Overall, it is apparent that the Eocene magmatism of eastern and central Taurides is productive in terms of Fe±Cu skarn mineralization (e.g., Horoz, Karamadazı, Nevruztepe). Most of these systems are characterized by well-developed calcic-skarn zones, and a few of them (Çöpler and Mavidere) also contain marginally- to sub-economic Cu-Au porphyry and carbonate replacement mineralization (Kadıoğlu and Yıldırım 2009; Özözlü, 2019; Tiringa et al., 2020; Kuşcu et al. 2001; Kuşcu et al., 2013; İmer et al., 2013 and 2016).

As one of the Eocene intrusion systems, the Çubuklu prospect is primarily dominated by magnesian exoskarn zones characterized by serpentine pseudomorphing early forsterite, which clearly differs from other Fe-skarn deposits, while ore mineralization of magnetite and chalcopyrite is common.

Even at the local scale, the comparison between Karamadazı Fe deposits and the Çubuklu prospect reveals differences in host and associated magmatic rocks, therefore the type and assemblage of ore mineralization. Karamadazı Fe-skarn is hosted by limestone produces calc-silicate minerals, whereas in Çubuklu, Paleozoic-Mesozoic sedimentary succession dominated by dolomite producing magnesian skarn characterized by serpentine, along with a low-intensity mineralized calcic exoskarn zone. Furthermore, associated magmatic rocks differ, with Karamadazı hosting granodiorite, diorite, granite, whereas the Çubuklu prospect comprises porphyritic rock. Massive bodies of magnetite and hematite reach up to 300 meters developed in actinolite-epidote exoskarn in Karamadazı, whereas in lens-like bodies of up to 50 meters of magnesium-rich exoskarn are found in the Çubuklu prospect.

In the southwestern central part of the Çubuklu prospect, carbonate hosted Pb-Zn type mineralization occurs as strata-bound type silicification and dolomitization of sedimentary sequence. Field mapping and soil geochemistry anomalies of Pb, and Zn indicate that the southwestern intrusive stock extends through the Çadırkaya Pb-Zn deposits (Figure 4.5). Based on the Hanilçi and Öztürk (2011) studies, in comparison to the Çubuklu prospect, there are differences in host rock, and ore type along with few ore mineral assemblage such arsenopyrite mineralization in Çadırkaya, tetrahedrite and tennantite mineralization in the Çubuklu prospect.

The Çubuklu prospect hosts Fe-Cu skarn-type and Zn-Pb carbonate replacement type and newly recognized porphyry-style alteration and mineralization, where B-type quartz-sulfide vein yielded a Re-Os age of 49.9 ± 0.2 Ma. The weak Fe-Cu mineralization of magnesian exoskarn exhibits local and regional differences on the basis of skarn minerology. Furthermore, porphyry-style alteration and mineralization are the first discovery for Karamadazı district which is explored under Sultansazlığı Basin at a depth of 120 meters. Although alignment of the porphyry is not predictable since intersected in one drill hole as a 55meters think narrow zone which is followed by a fault zone, potassic alteration, B-type veins and Mo-Cu signatures are revealed. Considering Karamadazı Fe-skarn, Nevruztepe Fe-Cu skarn prospect, Çadırkaya Pb-Zn, and numerous small irons, zinc, and lead mineralization in the Karamadazı

region as local scale, and further porphyry-epithermal, carbonate replacement and skarn complexes that Eocene magmatism produced such as Çöpler, the porphyry-style alteration and mineralization discovery in Çubuklu prospect indicating potential of fertility for district and Eocene magmatism.

A recent study by İmer et al. (2023) reported zircon trace element and Hf isotope data from numerous intrusions from the eastern and central Tauride range that range in age from Late Cretaceous to Late Miocene. They suggested that magma fertility for porphyry-style mineralization in the collided Southern Neotethys arc in the Tauride-Anatolide Block significantly increased starting from the middle Eocene through to Oligocene. According to their findings, middle Eocene Tauride magmatism has the potential to develop porphyry Cu-Mo-Au mineralization due to increased interaction between arc-related magmas and a thickened continental crust resulting an increase in magma oxygen fugacity and volatile contents. Despite this, porphyry development is relatively scarce along the belt in relation to middle Eocene magmatic activity (İmer et al., 2013 and 2023; Kuşcu et al., 2019). In particular, the area including the central part of the eastern Taurides and also the central Taurides, where the Karamadazı district is located in, was not known for any porphyry-style mineralization. Porphyry Cu-Mo mineralization intersected in the northeastern part of the Çubuklu prospect is therefore a significant discovery that suggests porphyry potential for this part of the Taurides. Although the extent of this mineralization type could not be well constrained due to the limited number of drill holes in NE Çubuklu, but it is possible that the intersected porphyry Cu-Mo mineralization is a part of a larger system now buried under the young alluvial cover of the Sultansazlığı basin. One striking feature of the porphyry mineralization at Çubuklu is that it contains Cu-Mo mineralization (as opposed to the Cu-Au signature of the Çöpler and Mavidere porphyries; Kuşcu et al., 2013; İmer et al., 2016), where Mo grades seem to be more significant and continuous along the intersected level.

Table 6. Summary of the Eocene magmatism associated deposits and prospects in Eastern and Central Anatolia.

Deposit/prospect	Type	Host Lithology/Age	Associated magmatic rock/host	Ore Minerals	Ore type	
Çöpler (Erzincan)	Porphyry-Epithermal Au-(Cu), Carbonate Replacement Cu-Au, Fe Skarn	Late Paleozoic -Mesozoic meta-carbonates	Diorite to granodioritic rocks	asp, py, cpy, ten/ttr, ga, sph, mar, orp	Stock, vein, manto type	1
Bizmişen (Erzincan)	Fe-Cu Skarn	Triaccis-Cretaceous limestone, Upper Cretaceous ophiolitic rocks	Quartz diorite, diorite porphyry	mt, cpy, py, cv, cc	Vein, lens, placer	2
Dedeyazı (Malatya)	Fe-Cu Skarn	Early Paleozoic -Mesozoic meta-carbonates	Tonalite to diorite	mt, cpy, py	Vein	3
Karamadazı (Kayseri)	Fe Skarn	Paleozoic metamorphics	Granodiorite, diorite, granite	mt, cpy, py	Massive to vein	4
Horoz (Niğde)	Fe Skarn	Paleozoic metamorphics and overlying Eocene volcano-sedimentary rocks	Granodiorite, diorite, granite	mt, cpy, co	Vein	5
Nevruzkaya (Kayseri)	Fe-Cu Skarn mineralization	Permian to Jurassic carbonate rocks	Gabbro porphyry to monzonite	mt, hm, cpy	Vein, massive	6
Çadırkaya (Kayseri)	Carbonate Hosted Pb-Zn	Upper Permian recrystallized limestone	Granodioritic rock	apy, py, mar, ga, sph, cpy, angl, cer, sm, hm-lm	Replacement type, vein	7
Ayraklı (Kayseri)	Carbonate Hosted Pb-Zn	Middle Devonian limestone, talc, schist	Granodioritic rock	py, mar, ga, sph, angl, cer, sm, hyc-zc, hm-lm	Starat-bound, vein, karstic	8
Delikkaya (Kayseri)	Carbonate Hosted Pb-Zn	Middle Jurassic massive limestone	Granodioritic rock	py, mar, ga, sph, cpy, angl, cer, beu, sm, hyc-zc, hm-lm	Replacement type, vein, and karstic	9
Suçatı (Kayseri)	Carbonate Hosted Pb-Zn	Massive limestone	Granodioritic rock	py, mar, ga, sph, angl, cer, sm, hyczc, hm-lm	Replacement type, karstic	10
Denizovası (Kayseri)	Carbonate Hosted Pb-Zn	Upper Permian Mizzia-bearing limestone	Granodioritic rock	-	Strata-bound, karstic, vein	11

Data sources : 1 = İmer et al. (2013 and 2016), Kuşcu et al. (2013); 2 = Bozkaya et al. (2017 and 2019); 3 = Kuşcu et al. (2013); 4 = Kadıoğlu and Yıldırım (2009), Kuşcu et al. (2013), Özözlü (2019); 5 = Oygür (1986), Kuşcu et al. (2001, 2013); 6 = Tiringa et al. (2020); 7, 8, 9, 10, and 11 = Hanilçi and Öztürk (2011 and 2019). *Abbreviations: angl=anglesite, asp=arsenopyrite, beu=beudantite, cc=chalcocite, cer=cerrusite, co=cobaltite, cv=covellite, cpy=chalcopyrite, ga=galena, gt=goethite, hm=hematite, hyczc=hydrozincite, lm=limonite, mar=marcasite, mt=magnetite, orp=orpiment, py=pyrite, sm=smithsonite, sph=sphalerite, ten=tennantite, ttr=tetrahedrite, zc=zincite.*

5.2 Conclusion

The Çubuklu prospect is situated in the Yahyalı Nappe in the Aladağ region, Central Anatolia. The emplacement of the Eocene Karamadazı Granitoid into Paleozoic-Mesozoic carbonate rocks, resulted in distinct intrusion-related system which are newly discovered porphyry-style, proximal skarn-type, and distal carbonate replacement-type alteration and mineralization.

Cu-Mo porphyry-style mineralization associated with granodiorite porphyry is a newly discovered narrow zone, located in the northeast part of the Çubuklu prospect. Porphyry-style alteration zone is characterized by selective potassic alteration of primary igneous ferromagnesian minerals into secondary biotite, and presence of lesser K-feldspar. B-type quartz-sulfide veinlets contain chalcopyrite, molybdenite, and pyrite, as well as weak dissemination. One molybdenite sample obtained from porphyry-style veins yielded a Re-Os age of 49.9 ± 0.2 Ma.

Fe-Cu skarn mineralization is situated proximal to the porphyry, extending farther towards the southwest along narrow dikes. Skarn zones occur between the irregular contact of Eocene Karamadazı granitoid and sequence of carbonate rocks, where both endoskarn and exoskarn are present. Endoskarn zones are mainly developed in granodiorite porphyry and are characterized by garnet-clinopyroxene-sericite-epidote-chlorite, and pyrite, rare chalcopyrite mineralization along with frequent calcite veinlets. Exoskarn zones are classified as calcic and magnesian exoskarn based on the skarn mineralogy. Rare zones of calcic exoskarn are characterized by garnet-chlorite-tremolite-calcite along with weak mineralization of pyrite-magnetite-chalcopyrite. As the most prevalent type, magnesian exoskarn rocks comprise mainly retrograde mineral assemblages of serpentine-chlorite-tremolite-calcite. The main ore mineralization of the Çubuklu prospect is developed in magnesium exoskarn rocks, which contain pyrite, magnetite, and chalcopyrite.

Zn-Pb±Cu carbonate replacement-style mineralization occurs in the southwestern part, within compositionally heterogeneous carbonate sequence. The alteration is characterized by dolomitization and silica replacement, mostly stratabound in nature, along with dissolution and hydrothermal brecciation. The ore minerals have been mostly oxidized into secondary Pb-Zn minerals, whereas rare sulfidic ore mineralization containing abundant pyrite alongside sphalerite, chalcopyrite, lesser tetrahedrite, covellite, and galena.

Porphyry Cu-Mo mineralization is associated with the core of the igneous complex in the northeast part of Çubuklu prospect, and transitions into proximal Fe-Cu skarn and later into stratabound Pb-Zn mineralization towards the southwest. Discovery of a porphyry-system and determination of mineralization timing (49.9 ± 0.2 Ma) by Re-Os method, significantly contributes to the porphyry prospectivity for the Karamadazı district, as well as potential porphyry fertility of other the Eocene magmatic systems in south Central Anatolia.

REFERENCES

Agard, P., Omrani, J., Jolivet, L., & Mouthereau, F. (2005). Convergence history across Zagros (Iran): constraints from collisional and earlier deformation. International Journal of Earth Sciences, 94, 401-419.

Aksay, A. (1980). Toroslar'da fasiyes yönünden farklı bir Alt Karbonifer istifi: Türkiye Jeol. Kur. Bült. 23(1), 193-199.

Allen, M. & Armstrong, H. (2008). Arabia-Eurasia collision and the forcing of mid-Cenozoic global cooling. Palaeogeography, Palaeoclimatology, Palaeoecology, 265(1-2), 52-58.

Ayhan, A. (1983). Aladağ yöresi karbonatlı kurşun-çinko-yataklarının kökeni: Türkiye Jeol.Kur. Bült., 26(2), 105-116.

Ayhan, A. & Erbayar, M. (1986). Bati zamanti (aladağlar-yahyali) karbonatli kurşun-çinko yataklarinin jeokimyasal prospeksiyonu. Türkiye Jeol.Kur. Bült., 105-106, 53-66.

Ayhan A., & Lengeranlı Y. (1986, April). Teetonostratigrapkical features of Aladag Region between Yahyalı and Demirkazık. Geological Engineering, 27, 31-45.

Babcock, R. C., Ballantyne, G. H., Phillips, C. H. (1995). Summary of the geology of the Bingham district, Utah. In: Porphyry Copper Deposits of the American Cordillera. Arizona Geological Society Digest 20, 316–335.

Ballato, P., C.E. Uba, A. Landgraf, M.R. Strecker, M. Sudo, D.F. Stockli, A. Friedrich, and S.H. Tabatabaei (2011), Arabia-Eurasia continental collision: insights from late Tertiary foreland-basin evolution in the Alborz mountains, northern Iran, Geol Soc. Am Bull, 123, 106–131.

Ballato, P., Parra, M., Schildgen, T. F., Dunkl, I., Yıldırım, C., Özsayın, E., Sobel, E. R., Echtler, H., & Strecker, M. R. (2018). Multiple exhumation phases in the Central Pontides (N Turkey): New temporal constraints on major geodynamic changes associated with the closure of the Neo-Tethys Ocean. Tectonics.

Beyarslan, M., & Bingöl A.F. (2000). Petrology of a supra-subduction zone ophiolite (Elazığ, Turkey). Canadian Journal of Earth Sciences, 37, 1411-1424.

Bingen B, Stein H (2003) Molybdenite Re–Os dating of biotite dehydration melting in the Rogaland high-temperature granulites, S Norway. Earth Planet Sci Lett 208:181–195

Blumenthal, M. M. (1941). Niğde ve Adana vilâyetleri dahilinde Torosların jeolojisine umumi bakış [A general overview of the geology of the Taurus Mountains within the provinces of Niğde and Adana]. Maden Tetkik Arama Enstitüsü, Ankara, No 8, 48 s.

Blumenthal, M. M. (1944). Bozkır güneyinde Toros sıradağlarının serisi ve yapısı [Series and structure of the Taurus Mountains south of Bozkır]. 1st. Univ. Fen Fak. Mec, Seri B, 9(2), 95-125.

Blumenthal, M. M. (1947). Belemedik Paleozoik penceresi ve bunun Mezozoik Kalker çerçevesi [The Belemedik Paleozoic window and its Mesozoic Limestone framework]. Maden Tetkik Arama Enstitüsü, Ankara, No 3, 39 s.

Blundell, D., Arndt, N., Cobbold, P.R., and Heinrich, C., 2005, Geodynamics and ore deposit evolution in Europe: Introduction: Ore Geology Reviews, v. 27, p. 5–11.

Bozkaya, G., Bozkaya, Ö., Yılmaz, H., & Banks, D. (2017). Fluid inclusion study of the Bizmisen skarn deposit related to Eocene intrusive rocks, East-Central Anatolia, Turkey. In Workshop on Subduction Related Ore Deposits (Vol. 1, pp. 16). Trabzon, Turkey

Bozkaya, Ö., Bozkaya, G., Yılmaz, H., Hozatlıoğlu, D., & Banks, D. A. (2019). The origin, age and duration of hydrothermal alteration associated with iron skarn mineralization determined from clay/phyllosilicate minerals, Bizmişen-Erzincan, East-Central Turkey. Ore Geology Reviews, 115, 103179.

Bozkurt, E., 2001, Neotectonics of Turkey—a synthesis: Geodinamica Acta, v. 14, p. 3–30.

Brown PE, Bowman JR, Kelly WC (1985) Petrologic and stable isotope constraints on the source and evolution of skarn-forming fluids at Pine Creek California. Econ Geol 80:72–95

Bucher-Nurminen, K. (1981). The formation of the metasomatic reaction veins in dolomitic marble roof pendants in the Bergell intrusion (Province Sondrio, northern Italy). American Journal of Science, 281, 1197-1222.

Bucher-Nurminen, K. (1982). On the mechanism of contact metamorphic aureole formation in dolomitic country rock by the Adamello intrusion (northern Italy). American Mineralogist, 67, 1101-1117.

Bucher, K. (1998). Growth mechanisms of metasomatic reaction veins in dolomite marbles from the Bergell Alps. Mineralogy and Petrology, 63, 151-171.

Burt, D. M. (1997). Mineralogy and petrology of skarn deposits. Societa Italiana di Mineralogia e Petrologia, 33(2), 859-873.

Camus, F., and Dilles, J.H., 2001, A special issue devoted to porphyry copper deposits of northern Chile—Preface: ECONOMIC GEOLOGY, v. 96, p.233–237.

Catchpole, H., Kouzmanov, K., Putlitz, B., Seo, J. H., Fontboté, L. (2015). Zoned base metal mineralization in a porphyry system: origin and evolution of mineralizing fluids in the Morococha district, Peru. Economic Geology, 110, 39–71.

Chermeninov, V. B. (1988). Mapping of hydrothermally altered rocks according to a borehole section. Soviet Geology and Geophysics, 29, 88-97.

Cooke, D. R., Hollings, P., & Walsh, J. L. (2005). Giant Porphyry Deposits: Characteristics, Distribution, and Tectonic Controls. Economic Geology, 100(4), 801-818.

Corbett, G.J. and Leach, T.M. (1998) Southwest Pacific Rim Gold–Copper Systems: Structure, Alteration and Mineralization. Special Publication 6. El Paso, TX: Society of Economic Geologists, 237 pp.

Crerar, D., Wood, S., Brantley, S., & Bocarsly, A. (1985). Chemical controls on solubility of ore-forming minerals in hydrothermal solutions. Canadian Mineralogist, 23, 333–352.

Darin, M. H., Umhoefer, P. J., & Thomson, S. N. (2018). Rapid late Eocene exhumation of the Sivas Basin (Central Anatolia) driven by initial Arabia-Eurasia collision. Tectonics, 37, 3805–3833.

Dewey, J., Hempton, M., Kidd, W., Saroğlu, F., & Şengör, A. (1986). Shortening of continental lithosphere: the neotectonics of Eastern Anatolia—a young collision zone. Geological Society, London, Special Publications, 19, 1-36.

Dilles, J. H., Einaudi, M. T. (1992). Wall-rock alteration and hydrothermal flow paths about the Ann-Mason porphyry copper deposit, Nevada; a 6-km vertical reconstruction. Econ. Geol. 87, 1963–2001.

DiPietro, J. A. (2013). Keys to the interpretation of geological history. In J. A. DiPietro (Ed.), Landscape Evolution in the United States (Chapter 20, pp. 327-344). Elsevier. ISBN 9780123977991.

Einaudi, M. T., Meinert, L. D., & Newberry, R. J. (1981). Skarn deposits: Economic Geology 75th Anniversary Volume, 317–391

Einaudi, M. T., & Burt, D. M. (1982). A special issue devoted to skarn deposits: Introduction. Economic Geology and the Bulletin of the Society of Economic Geologists, 77(4).

Einaudi, M. T., Hedenquist, J. W., & Inan, E. E. (2003). Sulfidation state of fluids in active and extinct hydrothermal systems: transitions from porphyry to epithermal environments. Society of Economic Geologists Special Publication, 10, 285–314.

Emmons, S. F. (1927). Geology and Ore Deposits of the Leadville Mining District. US Government Printing Office, Colorado.

Faccenna, C., Bellier, O., Martinod, J., Piromallo, C., & Regard, V. (2006). Slab detachment beneath eastern Anatolia: A possible cause for the formation of the North Anatolian fault. Earth and Planetary Science Letters, 242, 85–97.

Ferry, J. M., Ushikubo, T., & Valley, J. W. (2011). Formation of forsterite by silicification of dolomite during contact metamorphism. Journal of Petrology, 52(9), 1619-1640.

Fontboté, L. (2020). Systematic trends in the evolution of porphyry-related Zn-Pb-(Ag) deposits. Swiss Geoscience Meeting, Zurich, pp. 40-41.

Forster, D. B., Downes, P. M. (2008). Skarns in the Porphyry Copper-Gold Environment. PACRIM Congress.

Gençalioğlu Kuşcu, G., Göncüoğlu, M. C., & Kuşcu, İ. (2001). Post-collisional magmatism on the northern margin of the Taurides and its geological implications: Geology and petrology of the Yahyalı-Karamadazı granitoid. Turkish Journal of Earth Sciences, 10(3), Article 2.

Geological Survey of Turkey (MTA). (1980). Türkiye Maden Envanteri: Maden Tetkik ve Arama Enstitüsü Publ. No. 179. (571 p.).

Göğüş, O. H., & Pysklywec, R. N. (2008). Mantle lithosphere delamination driving plateau uplift and synconvergent extension in eastern Anatolia. Geology, 36, 723–726.

Gökten, E., & Floyd, P. A. (1987). Geochemistry and tectonic environment of the Şarkışla area volcanic rocks in Central Anatolia, Turkey. Mineralogical Magazine, 51, 553–559.

Gökten, E. (1993). Geology of the southern boundary of the Sivas Basin in the east of Ulaş (Sivas–Central Anatolia): Tectonic development related to the closure of inner Tauride Ocean. Turkish Association of Petroleum Geologists Bulletin, 5(1), 35–55.

Göncüoğlu, M. C., Toprak, V., Kuşcu, İ., Erler, A., & Olgun, E. (1991). Geology of the western part of the Central Anatolian Massif. In Turkish Petroleum Corporation Report.

Göncüoğlu, M.C. (1997). Distribution of Lower Paleozoic units in the Alpine Terranes of Turkey: paleogeographic constraints. In: Göncüoğlu MC, Derman AS, editors. Lower Paleozoic Evolution in Northwest Gondwana. Turkish Association of Petroleum Geologist Special Publications, 3, 1324.

Göncüoğlu, M. C. (2010). Introduction to the Geology of Turkey: Geodynamic Evolution of the Pre-Alpine and Alpine Terranes.

Göncüoğlu, M. C. (2012). An introduction to the Paleozoic of Anatolia with a NW Gondwanan perspective. In M. C. Göncüoğlu & N. Bozdoğan (Eds.), Guidebook Paleozoic of Eastern Taurides (pp. 1-15). Turkish Association of Petroleum Geologists, Special Publication, No:7, Ankara. ISBN: 978-975-95677-2-9.

Gürsu, S., Göncüoğlu, M. C., & Bayhan, H. (2004). Geology and petrology of the pre-Middle Cambrian rocks in Sandikli area: Implications for the Pan-African evolution in NW Gondwanaland. Gondwana Research, 7(4), 923-935.

Görür, N., Oktay, F., Seymen, Ü., & Şengör, A. M. C. (1984). Paleotectonic evolution of the Tuzgölü basin complex, central Turkey: sedimentary record of a Neo-Tethyan closure. In J. E. Dixon & A. H. F. Robertson (Eds.), The Geological Evolution of the Eastern Mediterranean (pp. 467–482). Geological Society, London, Special Publications, 17.

Görür, N., Tüysüz, O., & Celal Şengör, A. M. (1998). Tectonic evolution of the central Anatolian basins. International Geology Review, 40(9), 831-850.

Görür, N., & Tüysüz, O. (2001). Cretaceous to Miocene Palaeogeographic Evolution of Turkey: Implications for Hydrocarbon Potential. Journal of Petroleum Geology 24, 119-146.

Graciansky, P. Ch. de. (1968). Teke yarımadası (Likya) Torosları'nm üstüste gelmiş ünitelerinin stratigrafisi ve Dinaro-Toroslar'daki yeri [Stratigraphy of the superposed units of the Teke Peninsula (Lycia) Taurus Mountains and their position in the Dinaric-Taurus]: Maden Tetkik Arama Enstitüsü Dergisi, 71, 73-91.

Gustafson, L.B. (1978). Some major factors of porphyry copper genesis: Economic Geology, v. 73, p. 600−607.

Hallof, P. G., & Winniski, E. (1971). A geophysical case history of the Lakeshore ore body. Geophysics, 36, 1232-1249.

Hanilçi, N., & Öztürk, H. (2011). Geochemical/isotopic evolution of Pb–Zn deposits in the Central and Eastern Taurides, Turkey. International Geology Review, 53(13), 1478-1507.

Hanilçi, N., Öztürk, H., & Kasapçı, C. (2019). Carbonate-Hosted Pb-Zn Deposits of Turkey. Mineral Resources of Turkey, 497-533.

Hempton, M.R. (1987) Constraints on Arabian Plate Motion and Extensional History of the Red Sea. Tectonics, 6, 687-705.

Holness MB (ed.) (1997) The permeability of non-deformingrock. In: Deformation-enhanced Fluid Transport in the Earth's Crust and Mantle, pp. 9–39. Chapman and Hall, London.

Hüsing, S. K., Zachariasse, W. J., van Hinsbergen, D. J., Krijgsman, W., Inceöz, M., Harzhauser, M., Mandic, O., & Kroh, A. (2009). Oligocene–Miocene basin evolution in SE Anatolia, Turkey: constraints on the closure of the eastern Tethys gateway. Geological Society, London, Special Publications, 311, 107-132.

İmer, A., Richards, J. P., and Creaser, R. A. (2013). Age and tectonomagmatic setting of the Eocene Çöpler-Kabataş magmatic complex and porphyry-epithermal Au deposit, East Central Anatolia, Turkey. Mineralium Deposita, 48(5), 557‑583.

İmer, A., Richards, J. P., and Muehlenbachs, K. (2016). Hydrothermal evolution of the Çöpler porphyry-epithermal Au deposit, Erzincan Province, Central Eastern Turkey. Economic Geology, 111(7), 1619‑1658.

İmer A., Wang R., Sayıt K., Koralay O. E. (2023). Porphyry Cu fertility of Late Mesozoic-Cenozoic Magmatism along the East Anatolian Magmatic Belt based on zircon trace element compositions. Society of Economic Geologists Conference 2023: Resourcing the Green Transition, London, UK, 26–30 August 2023.

Jaffey, M., & Robertson, A. H. F. (2001). New sedimentological and structural data from the Ecemiş Fault Zone, southern Turkey: Implications for its timing and offset and the Cenozoic tectonic escape.

Jaffey, M., & Robertson, A. H. F. (2004). Non-marine sedimentation associated with Oligocene–Recent exhumation and uplift of the Central Taurus Mountains, S. Turkey. Sedimentary Geology, 173, 53–89.

Jolivet, L., and Faccenna, C. (2000 Mediterranean extension and the Africa-Eurasia collision: Tectonics, v. 19, p. 1095–1106.

Jones, B. K. (1992). Application of metal zoning to gold exploration in porphyry copper systems. Journal of Geochemical Exploration, 43, 127–155.

Kadıoğlu, Y. K. & Güleç, N. (1996). Mafic microgranular enclaves and interaction between felsic and mafic magmas in the Ağaçören Intrusive Suite: evidence for petrographic features and mineral chemistry. International Geological Review 38, 854-867.

Kadıoğlu YK, Dilek Y, Foland KA (2006). Slab break-off and syncollisional origin of the Late Cretaceous magmatism in the Central Anatolian Crystalline Complex, Turkey. In: Dilek Y, Pavlides S, editors. Postcollisional Tectonics and Magmatism in the Mediterranean Region and Asia. Boulder, CO, USA:Geological Society of America, pp. 381-415.

Kadıoğlu, Y., & Dilek, Y. (2009). Structure and geochemistry of the adakitic Horoz granitoid, Bolkar Mountains, south-central Turkey, and its tectonomagmatic evolution. International Geology Review, 52.

Kaymakcı, N., İnceöz, M., & Ertepınar, P. (2006) 3D-architecture and neogene evolution of the Malatya Basin: inferences for the kinematics of the Malatya and Ovacık fault zones. Turkish Journal of Earth Sciences, 15, 123–154.

Kaymakcı, N., & Kuşcu, İ. (2007). Late Cretaceous to recent kinematic evolution of Turkey. European Geosciences Union 2007, Geophysical Research Abstracts, 9, 05426, SRef-ID: 1607–7962/gra/ EGU2007-A-05426.

Kaymakcı, N., Özçelik, Y., White, S. H., & Van Dijk, P. M. (2009). Tectonostratigraphy of the Çankırı Basin: Late Cretaceous to early Miocene evolution of the Neotethyan suture zone in Turkey.

Keskin, M. (2003). Magma generation by slab steepening and breakoff beneath a subduction-accretion complex: An alternative model for collision-related volcanism in Eastern Anatolia.

Ketin, İ. (1966). Tectonic units of Anatolia. Maden Tetkik ve Arama Bulletin, 66, 23– 34.

Kirkham, R. V. (1971). Intermineral intrusions and their bearing on the origin of porphyry copper and molybdenum deposits. Economic Geology, 66, 1244−1249.

Koçak, K. (2008). Mineralogy, geochemistry, and Sr-Nd isotopes of the Cretaceous leucogranite from Karamadazı (Kayseri), central Turkey: Implications for their sources and geological setting. Canadian Journal of Earth Sciences, 45, 949-968.

Koçyiğit, A., & Beyhan, A. (1998). A new intracontinental transcurrent structure: the Central Anatolian Fault Zone, Turkey. Tectonophysics, 284, 317-336.

Köksal, S., Toksoy Köksal, F., & Göncüoğlu, M. C. (2013). Crustal source of the Late Cretaceous Satansari monzonite stock (central Anatolia - Turkey) and its significance for the Alpine geodynamic evolution. Journal of Geodynamics, 82–93.

Kuşcu, İ., Gençalioğlu Kuşcu, G., & Göncüoğlu, M. C. (2001). Skarn mineralogy and zoning patterns of Karamadan (Yahyalı-Kayseri) iron deposit. Geological Bulletin of Turkey, 44(3).

Kuşcu, İ., Gençalioğlu-Kuşcu, G., & Tosdal, R. M. (2007). Tectonomagmatic-metallogenic framework of mineralization events in the southern Neo-Tethyan arc, southeastern Turkey. In Proceedings of the 9th Biennial SGA Meeting, Society for Geology Applied to Mineral Deposits, Dublin, 20–23 August 2007 (pp. 853–856).

Kuşcu, İ., Gençalioğlu-Kuşcu G., Tosdal, R. M., Ullrich, T., & Friedman, R. (2010). Magmatism in the southeastern Anatolian orogenic belt: transition from arc to post-collisional setting in an evolving orogeny. In: Stephenson, R. A., Kaymakcı, N., Sosson, M., Starostenko, V., Bergerat, F. (Eds.) Sedimentary Basin Tectonics from the Black Sea and Caucasus to the Arabian Platform. Geological Society, London, Special Publications, 340, 437–460.

Kuşcu, İ., Yılmazer, E., Bayır, S., Sezerer-Kuru, G., Güleç, N., Demirela, G., Gençalioğlu-Kuşcu, G., Kaymakcı, N. (2011). U-Pb and Ar-Ar age dating and fluid inclusion constraints on the genesis of Hasançelebi iron oxide-copper-(gold) mineralizations, Malatya (Turkey). Econ Geol, 106, 261–288.

Kuşcu, I., Tosdal, R. M., Gençalioğlu-Kuşcu, G., Friedman, R., & Ullrich, T. D. (2013). Late Cretaceous to Middle Eocene Magmatism and Metallogeny of a Portion of the Southeastern Anatolian Orogenic Belt, East-Central Turkey. Society of Economic Geologists, Inc. Economic Geology, 108, 641-666.

Kuşcu İ., Tosdal R.M., Gençalioğlu-Kuşcu G. (2019). Porphyry-Cu Deposits ofTurkey. In: Pirajno F., Ünlü T., Dönmez C., Şahin M. (eds) Mineral Resources of Turkey. Modern Approaches in Solid Earth Sciences, vol 16. Springer, Cham, Switzerland.

Lafay, R., Montes-Hernandez, G., Renard, F., & Vonlanthen, P. (2018). Intracrystalline reaction-induced cracking in olivine evidenced by hydration and carbonation experiments. MDPI. Received: August 3, 2018; Accepted: September 14, 2018; Published: September 18, 2018.

Lang, J. R., Eastoe, C. J. (1988). Relationships between a porphyry Cu-Mo deposit, base and precious metal veins and Laramide intrusions, Mineral Park, Arizona. Econ. Geol. 83, 551–567.

Lei, J., & Zhao, D. (2007). Teleseismic evidence for a break-off subducting slab under Eastern Turkey. Earth and Planetary Science Letters, 257, 14–28.

Love, D. A., Clark, A. H., & Glover, J. K. (2004). The lithologic, stratigraphic, and structural setting of the giant Antamina copper-zinc skarn deposit, Ancash, Peru. Economic Geology, 99, 887-916.

Mackintosh, P. W., & Robertson, A. H. F. (2012). Late Devonian–Late Triassic sedimentary development of the central Taurides, S Turkey: Implications for the northern margin of Gondwana. Gondwana Research, 21(4).

Markey, R., et al. (2007). Standardizing Re-Os geochronology: A new molybdenite Reference Material (Henderson, USA) and the stoichiometry of Os salts. Chemical Geology, 244, 74-87.

McQuarrie, N., & van Hinsbergen, D. J. (2013). Retrodeforming the Arabia-Eurasia Collision zone: Age of collision versus magnitude of continental subduction. Geology, 41(3).

Meijers, M. J., Kaymakci, N., Van Hinsbergen, D. J., Langereis, C. G., Stephenson, R. A., & Hippolyte, J. C. (2010). Late Cretaceous to Paleocene oroclinal bending in the central Pontides (Turkey). Tectonics, 29, 1-21.

Meinert, L.D., (1992). Skarns and skarn deposits: Geoscience Canada, v. 19, p. 145–162.

Meinert, L. D., Dipple, G. M., Nicolescu, S., (2005). World skarn deposits. Econ. Geol. 100, 299–336.

Metag and Stolberg (1971) Zamantı Kurşun-Çinko Projesi Nihai Raporu, Maden Sahalarının Jeolojisi ve Paleontoloji [Final report of the Zamantı lead-zinc project, geology and paleontology of the mining licenced areas]. DPT Undersecretariat report, vol. IV, p 191 (in Turkish Unpublished)

Mitchell, A.H.G., (1992). Andesitic arcs, epithermal gold and porphyry-type mineralization in the western Pacific and eastern Europe: Transactions of the Institute of Mining and Metallurgy, Section B, Applied Earth Science, v. 101, p. 125–138.

Mineral Research and Exploration Institute of Turkey (MTA), 1989, Geologic map of Turkey: Ankara, Mineral Research and Exploration Institute of Turkey, scale 1:2,000,000, 1 sheet.

Moix, P., Beccaletto, L., Kozur, H. W., Hochard, C., Rosselet, F. & Stampfli, G. M. (2008). A new classification of the Turkish terranes and sutures and its implication for the paleotectonic history of the region. Tectonophysics, 451(1– 4), 7–39.

Ocakoğlu, F. (2002). Dikme Miyosen Havzasının (KD Aladağlar) Sedimantolojik İncelemesi [Sedimantary Analysis of the Miocene Dikme Basin (NE Aladağ Mnt.)]. Türkiye Jeoloji Bülteni. 45(1).

Okay, A. I. (1984). Distribution and characteristics of the northwest Turkish blueschists. In: The Geological Evolution of the Eastern Mediterranean (Eds. J. E. Dixon & A. H. F. Robertson), Geological Society Special Publication No. 17, 455- 466.

Okay, A. I. (1986). High pressure/low temperature metamorphic rocks of Turkey. In: Blueschists and Eclogites (Eds. B.W. Evans & E. H. Brown), Geological Society of America Memoir No. 164, 333-348.

Okay, A. I., and Tüysüz, O. (1999). Tethyan sutures of northern Turkey Major continental blocks of Turkey. The Mediterranean Basins: Tertiary Extension within the Alpine Orogen., 475–515.

Okay, A. I. (2008). Geology of Turkey: A synopsis. Anschnitt, 21, 19-42.

Okay, A. İ., Zattin, M., & Cavazza, W. (2010). Apatite fission-track data for the Miocene Arabia- Eurasia collision. Geology, 38, 35-38.

Oygür, V., Yurt, M. Z., Yurt, F., ve Sarı, İ. (1978). Kayseri Yahyalı - Karamadazı ve Kovalı yöresi demir madenleri jeoloji raporu : MTA Rap., 1626, 159 s., yayınlanmamış.

Oygür, V. (1986). Karamadazı (Yahyalı-Kayseri) Kontak Metazomatik Manyetit Yatağının Jeolojisi ve Oluşumu, Jeo. Müh. Dergisi 27, 1-9.

Öngen, S. (2000). Relationship between magnesian skarns and ore deposits at Dereköy, NW Turkey. Yer Bilimleri Dergisi, 13(1-2), 63-75.

Özgül, N. (1971). Orta Torosların kuzey kesiminin yapısal gelişiminde blok hareketlerin önemi [The importance of block movements in the structural development of the northern part of the Central Taurus]: Türkiye Jeoloji Kurumu Bülteni, 14, 75-87.

Özgül, N. (1976). Some geological aspects of the Taurus orogenic belt (Turkey). Geological Society Turkey Bulletin, 19, 65-78 (in Turkish).

Özgül, N. (1984). Stratigraphy and tectonic evolution of the Central Taurides. In O. Tekeli and M. C. Göncüoğlu (Eds.), International Symposium on the Geology of Taurus Belt, Ankara, 77-90.

Özözlü, A. M. (2019). Ulukışla (Niğde) Havzasındaki Esendemir Tepe Skarn ve Horoz Skarn Mineralizasyonlarının Karşılaştırmalı İncelemesi [master's thesis, Dokuz Eylül Üniversitesi, Fen Bilimleri Enstitüsü, Jeoloji Mühendisliği Anabilim Dalı, Ekonomik Jeoloji Programı].

Park et al. (2017). Oscillatory zoning in skarn garnet: Implications for tungsten ore exploration.

Parlak, O., Karaoğlan, F., Rizaoglu, T., Klötzli, U., Koller, F., & Billor, Z. (2013). U-Pb and Ar-40-Ar-39 geochronology of the ophiolites and granitoids from the Tauride belt: Implications for the evolution of the Inner Tauride suture. Journal of Geodynamics, 65, 22-37.

Parlak, O. (2016). Subduction initiation, metamorphic sole formation, and rollback processes for genesis and emplacement of Tethyan ophiolites in Turkey. GeoTirol2016 (pp. 258).

Pearce, J. A., Bender, J. F., De Long, S. E., Kidd, W. S. F., Low, P. J., Güner, Y., Şaroğlu, F., Yılmaz, Y., Moorbath, S., & Mitchell, J. G. (1990). Genesis of collision volcanism in Eastern Anatolia, Turkey. Journal of Volcanology and Geothermal Research, 44, 189–229.

Pirajno, F. (2009) Hydrothermal Mineral Deposits, Principles and Fundamental Concepts for the Exploration Geologist. 1992 Edition, Springer, p. 706.

Poisson, A. M., Guezou, J. C., Ozturk, A., Inan, S., Temiz, H., Gürsöy, H., Kavak, K. S., and Özden, S. (1996). Tectonic Setting and Evolution of the Sivas Basin, Central Anatolia, Turkey. International Geology Review, 38(9), 838-853.

Pourteau, A., Candan, O., & Oberhänsli, R. (2010). High pressure metasediments in central Turkey: Constraints on the Neotethyan closure history. Tectonics, 29, TC5004.

Radwany, M., Whitney, D. L., Brocard, G., Umhoefer, P. J., & Teyssier, C. (2017). Ophiolite gabbro from source to sink: A record of tectonic and surface processes in Central Anatolia. Geosphere, 13(5), 1329–1358.

Reilinger, R., McClusky, S., Vernant, P., et al. (2006). GPS constraints on continental deformation in the Africa–Arabia–Eurasia continental collision zone and implications for the dynamics of plate interactions. Journal of Geophysical Research, 111(B5), V05411.

Rızaoğlu, T., Parlak, O., Höck, V., Koller, F., Hames, W.E. & Billor, Z. (2009). Andean-type active margin formation in the eastern Taurides: Geochemical and geochronogical evidence from the Baskil granitoid (Elazığ, SE Turkey). Tectonophysics, 473, 188–207.

Richards, J. P. & Noble, S. R. (1998). Application of radiogenic isotope systems to the timing and origin of hydrothermal processes: Reviews in Economic Geology 10: 195-233.

Richards, J. P. (2003). Tectono-magmatic precursors for porphyry Cu-(Mo-Au) deposit formation. Econ. Geol. 98, 1515–1533.

Richards, J.P., (2005). Cumulative factors in the generation of giant calc-alkaline porphyry Cu deposits. In: Porter, T.M. (Ed.), Super Porphyry Copper and Gold Deposits: A Global Perspective, 1. Porter Geoscience Consulting Publishing, Linden Park, South Australia, pp. 7–25.

Richards, J.P., (2011). Magmatic to hydrothermal metal fluxes in convergent and collided margins: Ore Geology Reviews, v. 40, p. 1–26, https:// doi .org /10 .1016 /j .oregeorev .2011 .05 .006

Ricou, L.E. (1994). Tethys Reconstructed: Plates Continental Fragments and Their Boundaries Since 260 Ma from Central America to South-Eastern Asia. Geodinamica Acta, 7, 169-218.

Robb, L. J. (2005). Introduction to Ore-Forming Processes. Blackwell Science Ltd.

Robertson, A. H. F., Ustaömer, T., Parlak, O., Ünlügenç, U. C., Taşlı, K., İnan, N. (2005). Late Cretaceous– Early Tertiary tectonic evolution of south-Neotethys in SE Turkey: evidence from the Tauride thrust belt in SE Turkey (Binboğa-Engizek segment). Journal of Asian Earth Sciences, https://doi. org/10.1016/j.jseaes.2005.02.004.

Robertson, A. H. F., Ustaoğmer, T., Parlak, O., Ünlügenc, U. C., Taşlıd, K., & İnan, N. (2006). The Berit transect of the Tauride thrust belt, S Turkey: Late Cretaceous–Early Cenozoic accretionary/collisional processes related to closure of the Southern Neotethys. Journal of Asian Earth Sciences, 27, 108–145.

Robertson, A. H. F., Parlak, O., Rizaoğlu, T., Ünlügenç, Ü., İnan, N., Tasli, K., & Ustaömer, T. (2007). Tectonic evolution of the South Tethyan ocean: evidence from the Eastern Taurus Mountains (Elazığ region, SE Turkey): Geological Society, London, Special Publications, 272, 231-270.

Robertson, A., Parlak, O., & Ustaömer, T. (2009). Melange genesis and ophiolite emplacement related to subduction of the northern margin of the Tauride-Anatolide continent, central and western Turkey. Geological Society of London Special Publications, 311, 966.

Robertson, A. H. F., Parlak, O., & Ustaömer, T. (2012). Overview of the Palaeozoic–Neogene evolution of Neotethys in the Eastern Mediterranean region (Southern Turkey, Cyprus, Syria). Petroleum Geoscience, 18(4), 381–404.

Robertson, A. H. F., Parlak O. & Ünlügenç, U. C. (Eds.). (2013). Geological Development of Anatolia and the Easternmost Mediterranean Region. Geological Society of London, Special Publication no. 372. ISBN 978-1-862 39-353-0.

Rolland, Y., Perinçek, D., Kaymakcı, N., Sosson, M., Barrier, E., Avagyan, A. (2012). Evidence for 80–75 Ma subduction jump during Anatolide–Tauride–Armenian block accretion and 48 Ma Arabia–Eurasia collision in Lesser Caucasus–East Anatolia. Journal of Geodynamics.

Rush, P. M., & Seegers, H. J. (1990). Ok Tedi copper-gold deposits. Australasian Institute of Mining and Metallurgy Monograph, 14(2), 1747-1754.

Seedorff, E., Dilles, J. H., Proffett, J. M., Einaudi, M. T., Zurcher, L., Stavast, W., Johnson, D. A., Barton, M. D. (2005). Porphyry deposits: characteristics and origin of hypogene features. Econ. Geol. 100th Anniversary Volume, 251–298.

Selby, D., Creaser, R. A., & Feely, M. (2004). Accurate and precise Re–Os molybdenite dates from the Galway Granite, Ireland: Critical comment on 'Disturbance of the Re–Os chronometer of molybdenites from the late Caledonian Galway Granite, Ireland, by hydrothermal fluid circulation' by Suzuki et al. Geochemical Journal, 35, 29–35. Geochemical Journal, 38, 291–294.

Selby D., Creaser R.A. and Fowler M.G. (2007) Re–Os elemental and isotopic systematics in crude oils.Geochem. Cosmochim. Acta. 71,378–386.

Seward, T.M., and Barnes, H.L., (1997). Metal transport by hydrothermal ore fluids, in Barnes, H.L., ed., Geochemistry of hydrothermal ore deposits, New York, John Wiley and Sons, p. 435−486.

Shafiei, B., Haschke, M., and Shahabpour, J., (2009). Recycling of orogenic arc crust triggers porphyry Cu mineralization in Kerman Cenozoic arc rocks, southeastern Iran: Mineralium Deposita, v. 44, p. 265–283.

Sillitoe, R. H. (1973). The tops and bottoms of porphyry copper deposits. Econ. Geol. 68, 799–815.

Sillitoe, R.H. (1995). Exploration of porphyry copper lithocaps: Australasian Institute of Mining and Metallurgy Publication Series No. 9/95, 527-532.

Sillitoe, R.H. (1999). Styles of high-sulphidation gold, silver, and copper mineralization in the porphyry and epithet-ma1 environments: Pacrim ‘99, Bali, Indonesia, l0-13 October, Proceedings, 29-44.

Sillitoe, R.H. (2000). Gold-Rich Porphyry Deposits: Descriptive and Genetic Models and Their Role in Exploration and Discovery, Gold in 2000. Reviews in Economic Geology, 13.

Sillitoe, R. H. (2010). Porphyry copper systems. Econ. Geol. 105, 3–41.

Sinclair, W. D. (2007). Porphyry Deposits. Geological Survey of Canada.

Stampfli, G. M., Marcoux, J., & Baud, A. (1991). Tethyan margins in space and time. In: Channell, J. E. T., Winterer, E. L., Jansa, L. F. (Eds.), Paleogeography and paleoceanography of Tethys. Elsevier, Amsterdam, 373–409, Netherlands.

Stampfli, G.M. (2000). Tethyan oceans. In: Bozkurt, E., Winchester, J.A., Piper, J.D.A. (Eds.), Tectonics and Magmatism in Turkey and the Surrounding Area. Geological Society London, Special Publication No. 173, 1–23.

Stoltnow, M., Weis, P., & Korges, M. (2023). Hydrological controls on base metal precipitation and zoning at the porphyry-epithermal transition constrained by numerical modeling. Scientific Reports 13, 3786.

Şengör, A. M. C. & Kidd, W. S. F. (1979). Post-collisional tectonics of the Turkish-Iranian plateau and a comparison with Tibet. Tectonophysics, 55, 361-376.

Şengör, A. M. C. & Yilmaz, Y. (1981). Tethyan evolution of Turkey: A plate tectonic approach. Tectonophysics, 75(3–4).

Şengör, A. M. C. (1982). The classical theories of orogenesis. In: Miyashiro, A., Aki, K., Şengör, A. M. C. (Eds.), Orogeny. John Wiley and sons, Chichester, 1–48.

Şengör, A.M.C. (1984). The Cimmeride Orogenic System and the Tectonics of Eurasia: Geological Society of America Special Paper 195, 82 p.

Şengör, A.M.C., Görür, N. & Şaroğlu, F. (1985). Strike-slip deformation basin formation and sedimentation. In: Biddle, K.T. & Christie-Blick, N. (eds) Strike-slip Deformation, Basin Formation and Sedimentation. Society of Economic Palaeontologists and Mineralogists Special Publications, 37, 227–264.

Şengör, A. M. C. (1987). Cross-faults and differential stretching of hanging walls in regions of low-angle normal faults: examples from western Turkey.

Şengör, A. M. C., Özeren, M. S., Genç, T., & Zor, E. (2003). East Anatolian high plateau as a mantle-supported, north-south shortened domal structure. Geophysical Research Letters, 30, 8045. doi:10.1029/2003GL017858

Tablacı, A., & Akyıldız, M. (2012). Bizmişen-Çaltı (Kemaliye-Erzincan) Yöresindeki Fe'lere Bağlı Cu-Au-Ag ve Ni Cevherleşmeleri [Copper-Gold-

Silver and Nickel Occurrences Associated with Bizmişen-Çaltı Iron Oxide Deposits]. Ç. Ü. Fen ve Mühendislik Dergisi, 27(4), 142.

Tatar, O., Gürsoy, H., & Piper, J. D. A. (2002). Differential neotectonic rotations in Anatolia and the Tauride Arc: Palaeomagnetic investigation of the Erenlerdag Volcanic Complex and Isparta volcanic district, south-central Turkey. Journal of the Geological Society, London, 159, 281–294.

Tekeli, O. (1980), Toroslarda Aladağların yapısal evrimi. Türkiye Jeoloji Kurumu Bülteni, 23(1), 11-14.

Tekeli, O., Aksay, A., Evren-Ertan, İ., Işık, A., & Ürgün, B. M. (1981). Toros ofiyolit projeleri, Aladağ projesi: MTA Derleme, 6976, 132. yayınlanmamış.

Tekeli, O., Aksay, A., Ürgün, B. M., & Işık, A. (1984). Geology of the Aladağ Mountains.

Till, D. A. Foster, & J. C. Sample (Eds.), Exhumation associated with Continental Strike-Slip Fault Systems (pp. 35–57). Geological Society of America, Special Papers, 434.

Tiringa, D., Ateşçi, B., Çelik, Y., Demirkıran, G., Dönmez, C., Türkel, A., & Ünlü, T. (2020). Geology and formation of Nevruztepe Fe-Cu skarn mineralization (Kayseri-Turkey). Bulletin of Mineral Research and Exploration, 161, 101-119.

Ulakoğlu, S. (1983). Karamadazı graniti ve çevresinin jeolojisi [Geology of the Karamadazı granite and its surroundings]. Jeoloji Mühendisliği Dergisi, 17, 69-78.

Umhoefer, P. J., Whitney, D. L., Teyssier, C., Fayon, A. K., Casale, G., & Heizler, M. T. (2007). Yo-yo tectonics in a wrench zone, Central Anatolian fault zone, Turkey. In S. M. Roeske, A. B.

Van Hinsbergen, D. J. J., Edwards, M. A., & Govers, R. (2009). Chapter Title. In D. J. J. Van Hinsbergen, M. A. Edwards, & R. Govers (Eds.), Collision and

Collapse at the Africa-Arabia-Eurasia Subduction Zone (pp. 67–106). Geological Society of London Special Publication 311.

Yaliniz, M. K., Floyd, P. A. & Göncüoglu, M. C. (2000). Geochemistry of volcanic rocks from the Çiçekdag ophiolite, central Anatolia, Turkey, and their inferred tectonic setting within the northern branch of Neotethyan ocean. In E. Bozkurt, J. A. Winchester, and J. D. A. Piper (Eds.), Tectonics and magmatism in Turkey and the surrounding area. (Geological Society of London, Special Publication, no. 173, pp. 203-218).

Yazgan, E., Chessex, R., (1991). Geology and tectonic evolution of southeastern Taurus in the region of Malatya. Turkish Association of Petroleum Geologists Bulletin, 3, 1-42.

Yıldırım, E., Yıldırım, N., Dönmez, C., Koh, S. M., & Günay, K. (2019). Mineralogy, rare earth elements geochemistry and genesis of the Keban-West Euphrates (Cu-Mo)-Pb-Zn skarn deposit (Eastern Taurus metallogenic belt, E Turkey). Ore Geology Reviews, 114, 103102.

Yılmaz, Y., Yiğitbaş, E. & Genç, S. C. (1993). Ophiolitic and metamorphic assemblages of Southeast Anatolia and their significance in the geological evolution of the orogenic belt. Tectonics, 12, 1280–1297.

Yılmaz, Y., Tüysüz, O., Yiğitbaş, E., Genç, S. C. & Şengör, A. M. C. (1997). Geology and tectonic evolution of the Pontides. In A. G. Robinson (Ed.), Regional and Petroleum Geology of the Black Sea and Surrounding Region (American Association of Petroleum Geologists Memoir, 68, pp. 183-266.)

Yiğit, O. (2009). Mineral deposits of Turkey in relation to Tethyan metallogeny: implications for future mineral exploration. Economic Geology 104, 19–51.

Yiğitbaş¸, E. & Yılmaz, Y. 1996. Post-late Cretaceous strike-slip tectonics and its implications on the Southeast Anatolian orogen – Turkey. International Geology Review, 38, 818–831.